



# Energy optimisation of a solar vehicle for South African conditions

Christiaan C. Oosthuizen

## ► To cite this version:

Christiaan C. Oosthuizen. Energy optimisation of a solar vehicle for South African conditions. Other. Université Paris-Saclay; Tshwane University of Technology, 2020. English. NNT : 2020UPASG003 . tel-03150589

**HAL Id: tel-03150589**

**<https://theses.hal.science/tel-03150589>**

Submitted on 23 Feb 2021

**HAL** is a multi-disciplinary open access archive for the deposit and dissemination of scientific research documents, whether they are published or not. The documents may come from teaching and research institutions in France or abroad, or from public or private research centers.

L'archive ouverte pluridisciplinaire **HAL**, est destinée au dépôt et à la diffusion de documents scientifiques de niveau recherche, publiés ou non, émanant des établissements d'enseignement et de recherche français ou étrangers, des laboratoires publics ou privés.

# Optimisation énergétique pour une voiture solaire dans les conditions de l'Afrique du Sud

**Thèse de doctorat de l'université Paris-Saclay et de  
Tshwane University of Technology**

École doctorale n°580: Sciences et technologies de l'information et de  
la communication (STIC)  
Spécialité de doctorat: Mathématiques et Informatique  
Unité de recherche : Université Paris-Saclay, UVSQ, LISV, 78124, Vélizy -  
Villacoublay, France  
Réfèrent : Université de Versailles -Saint-Quentin-en-Yvelines

**Thèse présentée et soutenue à Pretoria le 06/10/2020**

**Christiaan C. OOSTHUIZEN**

## Composition du Jury

**François ROCARIES**

Professeur, Tshwane University of Technology

**Dong ENZENG**

Professeur, Tianjin University of Technology

**Patrick HENAFF**

Professeur, Ecole des Mines de Nancy

**Anish KURIEN**

Professeur, Tshwane University of Technology

**Fadila MAROTEAUX**

Professeur, Université de Versailles Saint-Quentin

**Yasser ALAYLI**

Professeur, Université Paris-Saclay

**Barend VAN WYK**

Professeur, Tshwane University of Technology

**Yskandar HAMAM**

Professeur, Université de Versailles Saint-Quentin

**Dawood DESAI**

Chargé de recherche, Tshwane University of Technology

Président

Rapporteur & Examineur

Rapporteur & Examineur

Examineur

Examinatrice

Directeur de thèse

Directeur de thèse

Co-Encadrant & Examineur

Invité

**Titre :** Optimisation énergétique pour une voiture solaire dans les conditions de l'Afrique du Sud

**Mots clés :** gestion de l'énergie, modélisation mathématique, Sasol Solar Challenge, simulation, irradiation solaire, véhicule solaire

**Résumé :** Les batteries généralement utilisées dans les véhicules électriques ont un rapport énergie-poids jusqu'à cent fois plus faible (pouvoir calorifique net, Wh / kg) que la plupart des combustibles fossiles utilisés dans les moteurs à combustion interne. De plus, les véhicules électriques à énergie solaire dépendent principalement de la récupération de l'énergie provenant de l'irradiation solaire (émise par le soleil) qui dépend des conditions météorologiques. La nécessité d'optimiser la consommation d'énergie des véhicules électriques à batterie fonctionnant à l'énergie solaire est cruciale pour maximiser la portée d'un tel véhicule. Si la distance est fixe, les conditions météorologiques constantes et la topographie plate, on peut approximativement optimiser la consommation d'énergie d'une voiture solaire en trouvant la vitesse, qui optimise en moyenne la consommation d'énergie sur tout un trajet. Une telle approche fournit une bonne estimation par exemple pour le Bridgestone World Solar Challenge (BWSC) en Australie (qui se déroule principalement dans les régions arides de l'arrière-pays) où la topographie est principalement plate et les conditions météorologiques sont relativement constantes et donc très prévisibles. En revanche, la route Sasol Solar Challenge (SSC) en Afrique du Sud contient une topographie complexe, qui comprend diverses régions montagneuses avec des pentes abruptes et des changements fréquents dans le gradient de la route. En

Les premiers chapitres de l'ouvrage jettent les bases sur l'état actuel de la technique lors de l'examen de la modélisation des véhicules et de l'interprétation des prévisions météorologiques. Un modèle détaillé d'énergie solaire de voiture est conçu et des statistiques de sortie de modèle (MOS) sont utilisées pour améliorer la précision et l'intervalle de confiance des prévisions météorologiques locales requises par le modèle énergétique. De vastes expériences dans le monde réel ont validé la robustesse et la précision du modèle énergétique. Le problème d'optimisation est formulé comme un problème d'optimisation à deux niveaux qui utilise des techniques de solveur de programmation quadratique séquentielle (SQP) et de programmation dynamique (DP). Le problème d'optimisation à deux niveaux est mis en œuvre sous la forme d'une interface utilisateur (UI) pour une facilité d'utilisation par le gestionnaire d'énergie.

La nouvelle technique d'optimisation à deux niveaux à distance variable a été mise en œuvre pendant les huit jours du Sasol Solar Challenge 2018. Elle a fourni à l'équipe automobile solaire de TUT l'avantage technologique nécessaire pour obtenir une 1ère place locale ainsi qu'une 4ème place au classement général (international). La mise en œuvre a mis en évidence la supériorité de la technique à deux niveaux par rapport aux techniques classiques de gestion de l'énergie à diverses occasions, en particulier dans des conditions météorologiques extrêmes.

outre, des événements tels que le BWSC sont des itinéraires à distance fixe, alors que le SSC est un itinéraire à distance variable.

Diverses méthodes pour optimiser l'utilisation d'énergie d'une voiture solaire dans un environnement BWSC ont été proposées. Cependant, aucune de ces méthodes ne convient au contexte SSC. Ce travail est consacré à la fois à la recherche théorique et aux nouvelles applications des techniques d'optimisation à deux niveaux, pour minimiser la consommation d'énergie et maximiser la distance parcourue par une voiture solaire participant à un événement SSC en Afrique du Sud.

La précision et les performances de la technique d'optimisation à deux niveaux ont été soigneusement évaluées et analysées. Il a été constaté qu'en moyenne, 94% de la variation de l'erreur de simulation énergétique (état de charge) peut s'expliquer par les variables contenues dans le modèle énergétique dérivé. La variation restante de 6% de l'erreur de simulation énergétique peut être due à la petite dynamique non modélisée du véhicule (y compris les forces de Coriolis), à la non-linéarité des cycles de charge et de décharge de la batterie et aux effets de la température.

**Title :** Energy optimisation of a solar vehicle for South African conditions

**Keywords :** energy management, mathematical modelling, Sasol Solar Challenge, simulation, solar irradiation, solar vehicle

**Abstract :** Batteries typically used in electric vehicles have up to one hundred times lower energy-to-weight ratios (net calorific value, Wh/kg) than most fossil fuels used in internal combustion engines. Furthermore, solar-powered electric vehicles rely mostly on harvesting energy from solar irradiation (emitted by the sun) which is weather dependant. The need to optimise the energy usage of battery assisted solar-powered electric vehicles is crucial to maximise the range of such a vehicle. If the distance is fixed, weather conditions constant, and the topography flat, one can approximately optimise the energy usage of a solar car by finding the speed, which on average optimises energy usage over an entire journey. Such an approach provides a good guestimate for example for the Bridgestone World Solar

The early chapters of the work create a foundation in terms of the current state-of-the-art when considering vehicle modelling and interpretation of weather forecasts. A detailed solar car energy model is devised, and Model Output Statistics (MOS) are employed to improve the accuracy and confidence interval of local weather forecasts required by the energy model. Extensive real-world experiments validated the robustness and accuracy of the energy model. The optimisation problem is formulated as a bi-level optimisation problem which makes use of Sequential Quadratic Programming (SQP) and Dynamic Programming (DP) solver techniques. The bi-level optimisation problem is implemented in the form of a User Interface (UI) for ease of use by the energy manager.

Challenge (BWSC) in Australia (taking place primarily in the desolate outback regions) where the topography is predominantly flat, and the weather conditions are relatively constant and therefore very predictable. Contrastingly, the Sasol Solar Challenge (SSC) route in South Africa contains complex topography, which includes various mountainous regions with steep slopes and frequent changes in the gradient of the road. Also, events such as the BWSC, are fixed distance routes, where the SSC is a variable distance route.

Various methods to optimise the energy usage of a solar car in a BWSC setting have been proposed. However, none of these methods are not suitable for the SSC context. This work is devoted to both theoretical research and novel applications of bi-level optimisation techniques to minimise energy usage and maximise distance travelled by a solar car participating in an SSC event in South Africa.

The novel variable distance bi-level optimisation technique was implemented during the eight days of the Sasol Solar Challenge 2018. It provided the solar car team from TUT with the technological advantage required to obtain a local 1st place as well as a 4th place overall (internationally). The implementation highlighted the superiority of the bi-level technique when compared to conventional energy management techniques on various occasions, especially during extreme weather conditions.

The accuracy and performance of the bi-level optimisation technique was thoroughly assessed and analysed. It was found that on average, 94 % of the variation in the energy simulation (State of Charge) error can be explained by the variables contained within the derived energy model. The remaining 6 % variation in the energy simulation error may be as a result of small un-modelled vehicle dynamics (including Coriolis forces), non-linearity of the charge and discharge cycles of the battery and temperature effects.

## TABLE OF CONTENTS

BIOGRAPHICAL INFORMATION .....	IV
LIST OF FIGURES.....	V
LIST OF TABLES .....	VIII
LIST OF ACRONYMS AND ABBREVIATIONS.....	X
ABSTRACT .....	XII
ACKNOWLEDGEMENT .....	XIV
I. RESEARCH OBJECTIVE AND PROJECT OVERVIEW .....	16
PROJECT CONTEXT .....	16
THE SASOL SOLAR CHALLENGE IN SOUTH AFRICA.....	16
IMPORTANCE AND BENEFIT OF THE STUDY .....	18
THE RESEARCH OBJECTIVE.....	18
RESEARCH QUESTIONS.....	18
RESEARCH METHODOLOGY, FRAMEWORK AND STRATEGY .....	20
Methodology .....	20
Strategy.....	20
Scope and delimitations .....	22
Form and nature of results .....	23
OVERVIEW OF THE CHAPTERS.....	24
SCIENTIFIC CONTRIBUTIONS TO THIS WORK.....	25
II. LITERATURE REVIEW.....	26
SOLAR VEHICLE MODELLING .....	26
Mechanical factors .....	28
Electrical factors.....	33
Environmental factors .....	35

Miscellaneous factors.....	36
Summary of energy parameters.....	38
WEATHER VARIABLES.....	39
SOLAR ELECTRIC VEHICLE CHALLENGES .....	43
LITERATURE SHORTFALL SUMMARY .....	47
III. MODELLING .....	49
ENERGY EQUATIONS .....	49
MODEL VALIDATION.....	61
Experimental equipment used.....	63
Experimental procedure .....	63
Experimental results and discussion .....	65
Modelling conclusion.....	70
IV. ENVIRONMENTAL CONDITIONS .....	72
EXPERIMENTAL EQUIPMENT AND PROCEDURE .....	73
EXPERIMENTAL RESULTS AND DISCUSSION.....	75
EXPERIMENTAL CONCLUSIONS.....	81
FORECAST BIAS CORRECTION .....	82
MODEL OUTPUT STATISTICS.....	87
Experimental equipment and procedure .....	87
Experimental results and discussion .....	89
Experimental conclusion .....	97
V. OPTIMISATION .....	99
UPPER-LEVEL: PROBLEM FORMULATION .....	102
LOWER-LEVEL: PROBLEM FORMULATION.....	104
BI-LEVEL OPTIMISATION: PROBLEM FORMULATION.....	106
SOLUTION METHODS .....	107

IMPLEMENTATION.....	111
Main UI.....	113
Lower-level optimisation function workflow .....	118
Upper-level optimisation function workflow .....	120
Weather API function .....	123
FIELD TEST SETUP .....	124
VI.    CASE STUDY RESULTS .....	126
PERFORMANCE METRICS.....	127
CASE STUDY SUMMARY .....	129
Detailed case study of Day 1 .....	138
Detailed case study of day 7 .....	142
Detailed case study of day 8 .....	147
CASE STUDY CONCLUSION .....	151
VII.   CONCLUSIONS, RECOMMENDATIONS AND FUTURE WORK.....	152
RESEARCH QUESTIONS.....	152
SIGNIFICANCE OF THE FINDINGS .....	154
FUTURE WORK AND RECOMMENDATIONS .....	154
LIST OF REFERENCES .....	156
ANNEXURE A: CODE VARIABLES.....	165
ANNEXURE B: CODE SPECIFICATIONS.....	169



## **BIOGRAPHICAL INFORMATION**

Full title: Energy Optimisation of a Solar Vehicle for South African Conditions

Submitted by: Christiaan Coenrad Oosthuizen

Supervisors: Prof B. Van Wyk, Prof Y. Alayli, Prof Y. Hamam, Dr. D. Desai

For the degree of: TUT - Doctor of Engineering: DENG17  
UVSQ - Doctor of Mathematics and Computer Science

Department: Department of Mechanical and Mechatronics Engineering, the French South African Institute of Technology (F'SATI) and, Versailles Systems Engineering Laboratory (LISV, France)

Faculty: Faculty of Engineering and the Built Environment (TUT) and Information and Communication Sciences and Technologies (STIC, UVSQ)

University: Tshwane University of Technology (TUT, South Africa) and Université Paris-Saclay in collaboration with Université de Versailles Saint-Quentin-en-Yvelines (UVSQ, France)

# LIST OF FIGURES

Figure 1: Sasol Solar Challenge 2018 route.....	17
Figure 2: Research strategy flow diagram.....	20
Figure 3: Energy model parameter summary .....	38
Figure 4: Coefficient of aerodynamic drag of SCIII (wind tunnel) .....	52
Figure 5: SCIII prototype, wind tunnel test model – rear view .....	53
Figure 6: SCIII prototype, wind tunnel test model – fluorescent surface flow .....	54
Figure 7: Coefficient of aerodynamic drag of SCIII prototype (ANSYS®).....	55
Figure 8: PMSM efficiency plot.....	56
Figure 9: Solar array - temperature vs efficiency.....	57
Figure 10: Top: SSC2016, SCII and support vehicle.....	62
Figure 11: SSC2016 Day 1, <i>SoC</i> comparison.....	65
Figure 12: SSC2016 Day 2, <i>SoC</i> comparison .....	66
Figure 13: SSC2016 Day 3, <i>SoC</i> comparison.....	66
Figure 14: SSC2016 Day 4, <i>SoC</i> comparison.....	67
Figure 15: SSC2016 Day 7, <i>SoC</i> comparison.....	67
Figure 16: SSC2016 Day 8, <i>SoC</i> comparison.....	68
Figure 17: QQ plot of <i>GHI</i> forecast data.....	78
Figure 18: Normal vs t-distribution .....	78
Figure 19: <i>GHI</i> confidence intervals .....	81
Figure 20: Forecast bias.....	83
Figure 21: <i>GHI</i> Confidence intervals (Forecast bias compensated) .....	85
Figure 22: Cloudy days summary (GMOS) .....	90
Figure 23: Standard deviation improvement (GMOS) .....	92
Figure 24: SSC2018 Day 1, <i>SoC</i> comparison (GMOS).....	95

Figure 25: SSC2018 Day 6, <i>SoC</i> comparison (GMOS).....	96
Figure 26: SSC2018 Day 8, <i>SoC</i> comparison (GMOS).....	96
Figure 27: Implementation: Main UI Part I & II - flow diagram .....	117
Figure 28: Implementation: Main UI Part III - flow diagram .....	118
Figure 29: Implementation: lower-level optimisation - flow diagram .....	119
Figure 30: Implementation: upper-level optimisation - flow diagram .....	122
Figure 31: Implementation: weather API - flow diagram.....	123
Figure 32: Top: Support vehicle with IoT, radio and weather sensors.....	125
Figure 33: SSC2018, Sun Chaser III solar vehicle .....	126
Figure 34: SSC2018 Day 1, <i>SoC</i> comparison.....	130
Figure 35: SSC2018 Day 6, <i>SoC</i> comparison.....	130
Figure 36: SSC2018 Day 1, wind comparison.....	131
Figure 37: SSC2018 Day 6, wind comparison.....	132
Figure 38: SSC2018 Day 4, <i>SoC</i> comparison .....	132
Figure 39: SSC2018 Day 7, <i>SoC</i> comparison .....	133
Figure 40: SSC2018 Day 4, speed profile comparison.....	133
Figure 41: SSC2018 Day 4, solar power comparison.....	134
Figure 42: SSC2018 Day 4, wind comparison.....	135
Figure 43: SSC2018 Day 8, <i>SoC</i> comparison.....	136
Figure 44: SSC2018 Day 1, official results.....	138
Figure 45: SSC2018 Day 1, route elevation .....	139
Figure 46: SSC2018 Day 1, speed profile comparison.....	140
Figure 47: SSC2018 Day 1, solar power comparison.....	140
Figure 48: SSC2018 Day 7, official results.....	142
Figure 49: SSC2018 Day 7, weather conditions.....	143
Figure 50: SSC2018 Day 7, speed profile comparison.....	144

Figure 51: SSC2018 Day 7, route elevation .....	144
Figure 52: SSC2018 Day 7, <i>SoC</i> comparison .....	145
Figure 53: SSC2018 Day 7, solar power comparison.....	146
Figure 54: SSC2018 Day 8, official results.....	147
Figure 55: SSC2018 Day 8, weather conditions.....	148
Figure 56: SSC2018 Day 8, solar power comparison.....	149
Figure 57: SSC2018 Day 8, route elevation .....	149
Figure 58: SSC2018 Day 8, <i>SoC</i> comparison .....	150

# LIST OF TABLES

Table 1: Research questions.....	19
Table 2: Coefficients of rolling resistance.....	29
Table 3: Coefficients of aerodynamic drag.....	31
Table 4: GFS/ECMWF specifications.....	39
Table 5: <i>GHI</i> EFP.....	40
Table 6: EFP summary.....	42
Table 7: Sun Chaser III model parameters.....	50
Table 8: Experiment route summary (SSC2016).....	68
Table 9: Model performance metrics.....	69
Table 10: Forecasted weather variables from Meteomatics AG.....	73
Table 11: Forecast Bias error.....	76
Table 12: Mean Absolute Error.....	76
Table 13: Root Mean Squared Error.....	76
Table 14: Standard deviation assuming a normal distribution.....	77
Table 15: T-distribution upper bounds (forecast confidence).....	79
Table 16: T-distribution lower bounds (forecast confidence).....	80
Table 17: Upper bounds (Forecast Bias compensated).....	84
Table 18: Lower bounds (Forecast Bias compensated).....	84
Table 19: <i>RMSE</i> comparison.....	86
Table 20: Standard deviation comparison, Pretoria.....	90
Table 21: Standard deviation comparison, Bloemfontein.....	91
Table 22: Standard deviation comparison, Port Elizabeth.....	91
Table 23: Standard deviation comparison, Stellenbosch.....	92
Table 24: Standard deviation comparison, an average of all sites.....	93

Table 25: SSC2018, SCIII results (Day 1,6,8) .....	95
Table 26: GMOS performance results.....	97
Table 27: GMOS vs MOS performance results .....	98
Table 28: Acceptable range for constraint variables .....	104
Table 29: SSC2018, SCIII results (all days) .....	127
Table 30: SSC2018, optimisation performance metrics .....	128
Table 31: SSC2018, energy prediction summary .....	129

# LIST OF ACRONYMS AND ABBREVIATIONS

AC	Alternating Current
ASC	American Solar Challenge
BLDC	Brushless Direct Current
BMS	Battery Management System
BWSC	Bridgestone World Solar Challenge
CAN BUS	Controller Area Network Communication Bus
DC	Direct Current
DHI	Diffuse Horizontal Irradiance
DNI	Direct Normal Irradiance
ECMWF-IFS	European Centre for Medium-Range Weather Forecasts Integrated Forecasting System
EFP	Expected Forecast Performance
EV	Electric Vehicle
FB	Forecast Bias
FOC	Field Oriented Control
GFS	Global Forecast System
GHI	Global Horizontal Irradiance
ICEV	Internal Combustion Engine Vehicles
IoT	Internet of Things
Li-Ion	Lithium-Ion
LQR	Linear Quadratic Regulator
MAE	Mean Absolute Error
MBE	Mean Bias Error
MPPT	Maximum Power Point Tracker
PAIRS	Physical Analytics Integrated Data Repository
PI	Proportional-Integral
PMF	Probability Mass Function
PMSM	Permanent Magnet Synchronous Motor
RMSE	Root Mean Squared error
SCII	Sun Chaser II
SCIII	Sun Chaser III

SESC	Somabay Egyptian Solar Challenge
SoC	State of Charge
SPEV	Solar-Powered Electric Vehicle
SQP	Sequential Quadratic Programming
SRM	Switched Reluctance Motor
SSC	Sasol Solar Challenge
TCC	Total Cloud Cover
TUT	Tshwane University of Technology
UI	User Interface
4IR	Fourth Industrial Revolution (Industry 4.0)



# ABSTRACT

Batteries typically used in electric vehicles have up to one hundred times lower energy-to-weight ratios (net calorific value, Wh/kg) than most fossil fuels used in internal combustion engines. Furthermore, solar-powered electric vehicles rely mostly on harvesting energy from solar irradiation (emitted by the sun) which is weather dependant. The need to optimise the energy usage of battery assisted solar-powered electric vehicles is crucial to maximise the range of such a vehicle. If the distance is fixed, weather conditions constant, and the topography flat, one can approximately optimise the energy usage of a solar car by finding the speed, which on average optimises energy usage over an entire journey. Such an approach provides a good guestimate for example for the Bridgestone World Solar Challenge (BWSC) in Australia (taking place primarily in the desolate outback regions) where the topography is predominantly flat, and the weather conditions are relatively constant and therefore very predictable. Contrastingly, the Sasol Solar Challenge (SSC) route in South Africa contains complex topography, which includes various mountainous regions with steep slopes and frequent changes in the gradient of the road. Also, events such as the BWSC, are fixed distance routes, where the SSC is a variable distance route.

Various methods to optimise the energy usage of a solar car in a BWSC setting have been proposed. However, none of these methods are not suitable for the SSC context. This work is devoted to both theoretical research and novel applications of bi-level optimisation techniques to minimise energy usage and maximise distance travelled by a solar car participating in an SSC event in South Africa.

The early chapters of the work create a foundation in terms of the current state-of-the-art when considering vehicle modelling and interpretation of weather forecasts. A detailed solar car energy model is devised, and Model Output Statistics (MOS) are employed to improve the accuracy and confidence interval of local weather forecasts required by the energy model. Extensive real-world experiments validated the robustness and accuracy of the energy model. The optimisation problem is formulated as a bi-level optimisation problem which makes use of Sequential Quadratic Programming (SQP) and Dynamic Programming (DP) solver techniques. The bi-level optimisation problem is implemented in the form of a User Interface (UI) for ease of use by the energy manager.

The novel variable distance bi-level optimisation technique was implemented during the eight days of the Sasol Solar Challenge 2018. It provided the solar car team from TUT with the technological advantage required to obtain a local 1<sup>st</sup> place as well as a 4<sup>th</sup> place overall (internationally). The implementation highlighted the superiority of the bi-level technique when compared to conventional energy management techniques on various occasions, especially during extreme weather conditions.

The accuracy and performance of the bi-level optimisation technique was thoroughly assessed and analysed. It was found that on average, 94 % of the variation in the energy simulation (State of Charge) error can be explained by the variables contained within the derived energy model. The remaining 6 % variation in the energy simulation error may be as a result of small un-modelled vehicle dynamics (including Coriolis forces), non-linearity of the charge and discharge cycles of the battery and temperature effects.

**Keywords:** energy management, mathematical modelling, Sasol Solar Challenge, simulation, solar irradiation, solar vehicle, stochastic optimisation, weather prediction

# ACKNOWLEDGEMENT

The following chapters are based on peer-reviewed published work from the same primary author and are hereby acknowledged:

*"In reference to IEEE copyrighted material which is used with permission in this thesis, the IEEE does not endorse any of Tshwane University of Technology or the Université Paris-Saclay products or services. Internal or personal use of this material is permitted. If interested in reprinting/republishing IEEE copyrighted material for advertising or promotional purposes or for creating new collective works for resale or redistribution, please go to [http://www.ieee.org/publications\\_standards/publications/rights/rights\\_link.html](http://www.ieee.org/publications_standards/publications/rights/rights_link.html) to learn how to obtain a License from RightsLink. If applicable, University Microfilms and/or ProQuest Library, or the Archives of Canada may supply single copies of the dissertation."*

## Chapter III - MODELLING

© 2018 IEEE. Reprinted, with permission, from:

C. Oosthuizen, B. van Wyk and Y. Hamam, *"Modelling and simulation of the South African designed Sun Chaser II solar vehicle,"* 2017 IEEE AFRICON, Cape Town, 2017, pp. 1149-1154.

DOI: 10.1109/AFRCON.2017.8095644

URL: <http://ieeexplore.ieee.org/stamp/stamp.jsp?tp=&arnumber=8095644&isnumber=8095433>

## Chapter IV - ENVIRONMENTAL CONDITIONS

© 2020 IEEE. Reprinted, with permission, from:

C. Oosthuizen, B. van Wyk, Y. Hamam, Y. Alayli and D. Desai, *"Development of Solar Irradiance Forecast Confidence Intervals for Solar Electric Vehicle Energy Simulations,"* IEEE SAUPEC 2020, Cape Town, 2020, pp. 56-61.

DOI: <https://doi.org/10.1109/SAUPEC/RobMech/PRASA48453.2020.9041019>

URL: <https://ieeexplore.ieee.org/document/9041019>

## **Chapter IV - ENVIRONMENTAL CONDITIONS**

© 2020 by the authors. Reprinted with permission, from:

C. Oosthuizen, B. van Wyk, Y. Hamam, Y. Alayli and D. Desai, " *The Use of Gridded Model Output Statistics (GMOS) in Energy Forecasting of a Solar Car*," MDPI Energies, vol. 13.

DOI: <https://doi.org/10.3390/en13081984>

URL: <https://www.mdpi.com/1996-1073/13/8/1984>

## **Chapter V - OPTIMISATION**

© 2019 IEEE. Reprinted, with permission, from:

C. Oosthuizen, B. Van Wyk, Y. Hamam, D. Desai, Y. Alayli and R. Lot, " *Solar Electric Vehicle Energy Optimisation for the Sasol Solar Challenge 2018*," in IEEE Access, vol. 7, pp. 175143-175158, 2019.

DOI: 10.1109/ACCESS.2019.2957056

URL: <http://ieeexplore.ieee.org/stamp/stamp.jsp?tp=&arnumber=8918287&isnumber=8600701>

The author would also like to acknowledge Meteomatics AG for supplying accurate and reliable weather forecasts used in this work. Lastly, the author would like to recognise The merSETA (The Manufacturing, Engineering and Related Services Sector Education and Training Authority) & TUT Chair in Intelligent Manufacturing, the Versailles Systems Engineering Laboratory (LISV, France) and finally the Embassy of France in South Africa for their financial support.

Finally, glory to God for His favour during this research journey!

# **I. RESEARCH OBJECTIVE AND PROJECT OVERVIEW**

## **PROJECT CONTEXT**

Recent developments in solar-powered electric vehicles are increasingly becoming more relevant and accessible as natural resources diminish and the exploration of alternative forms of energy becomes essential. These forms of energy can contribute to lowering the carbon footprint of various energy applications, especially vehicles. Various solar-powered electric vehicles are currently in existence, commercially, but may still be financially unrealistic for, and not yet trusted by the majority of the population. Broader economic awareness and exposure to the benefits of such vehicles could encourage funding contributions and other forms of financial support, making further research and development possible in the field of solar-powered electric vehicles. Furthermore, by creating awareness the demand for these vehicles will increase, encouraging large scale production and finally lowering the unit cost per “green” (renewable energy reliant) car, thereby benefitting the economy.

Around the world, industry and academia set up engineering challenges to encourage graduates and industry partners to invest time, research capacity and resources in solar-powered electric vehicles. These challenges were founded in order to spark enthusiasm as well as create awareness among the general public. The challenges include the Shell Eco-marathon (worldwide) and the Formula Student Germany Electric (Europe) as well as the Bridgestone World Solar Challenge (Australia) and the Sasol Solar Challenge (South Africa) to name but a few.

## **THE SASOL SOLAR CHALLENGE IN SOUTH AFRICA**

Among the many international solar challenges, the South African based Sasol Solar Challenge (SSC) is one of the most demanding (after the Australian Bridgestone World Solar Challenge (BWSC)). The SSC route offers unique and difficult geographical characteristics as well as an exclusive race structure, where the aim is to cover the longest distance possible in eight days, rather than the shortest time between two points of fixed distance, which seems to be the norm for solar challenges across the world. The SSC requires teams to design, build, manage and race their solar cars from

Pretoria across South Africa towards Stellenbosch (near Cape Town). Along the route teams will have to do careful planning as the landscape varies from vast, barren areas of flat topography to mountainous regions that ascend and descend by hundreds of meters at a time, and everything in between. The route also offers a broad spectrum of weather conditions as teams near the coastal towns; the challenge sees at least a day or two of rain, including some cloudy and very windy route locations. The SSC has various categories, two of which are the most prominent: Challenger and Cruiser class. Challenger is the most popular, requiring teams to design lightweight, streamlined solar vehicles carrying just one person and completing the challenge by solely using the sun *en-route*. On the other hand, the Cruiser class aims to bridge the gap between solar-powered cars and the commercial market by allowing multiple passengers, larger capacity battery packs and the ability to charge batteries not just from the sun alone, but also from a grid-tied power source. The typical route for the Sasol Solar Challenge is shown in Figure 1; this was the mandatory route for the 2018 event in South Africa.



Figure 1: Sasol Solar Challenge 2018 route

## **IMPORTANCE AND BENEFIT OF THE STUDY**

Tshwane University of Technology (TUT) participates in the bi-annual Sasol Solar Challenge and is in the process of designing a next-generation Challenger class solar-powered vehicle for future challenges. During the 2016 Sasol Solar Challenge, the TUT team analysed the recorded solar vehicle data with a unique long-range telemetry system over the eight days of the challenge to better understand where to improve the design and energy management strategy. Based on the information obtained from the recorded data, it became evident that there was a need for better energy management in the form of informed driving speeds as well as aid in decision making, based on changing weather conditions. No framework to incorporate weather data in mission-critical decisions existed which was in reach of the TUT solar car team.

The need to simulate the entire race in order to refine the informed energy management decisions became a priority. Similar recent studies do exist, but these are mostly based on international events that are more concerned with managing and optimising driving time as opposed to maximum distance covered by a solar vehicle confined to a set of constraints.

## **THE RESEARCH OBJECTIVE**

The objective of this research was to improve the energy management strategy of a solar vehicle operating in the South African environment by characterising a prototype vehicle, predicting the environmental conditions and developing a suitable optimisation technique to minimise the energy used for travelling variable distances. The principal aim was to optimise the energy-use of a solar electric car driving the route of a Sasol Solar Challenge in South Africa.

## **RESEARCH QUESTIONS**

Table 1 lists the core questions as well as the sub-questions of this research work.

**Table 1: Research questions**

No	CORE QUESTIONS	SUB-QUESTIONS
1	To derive a conceptual model to use for optimisation, based on vehicle characteristics and dynamics, solar car design methods, preliminary evaluation of logged vehicle data and other related literature and models.	Which dependent, independent, and moderating variables need to be considered for the model?
		How can statistical variation in environmental and other variables be modelled?
		Are there any profound vehicle or environmental variables arising as a result of the South African context that might influence the type of optimisation method and which we need to consider?
2	Based on the literature on optimisation algorithms, solar car design constraints and preliminary research, which optimisation algorithms are feasible to consider when managing the energy usage of a solar car; and what can we learn about the effectiveness of existing optimisation approaches and identified vehicle characteristics as well as environmental conditions when evaluating the approaches for use with a solar car operating under South African conditions?	Which optimisation strategies will be best suited to solving the problem?
		Which simulation methodologies, will be best suited to solving the problem?
3	Based on the effectiveness of existing algorithms and the use of certain characteristic combinations when evaluating their suitability for real-world constrained implementation, what possible contributions and recommendations can be made regarding suitable optimisation algorithms and the selection of the appropriate vehicle and environmental conditions for energy optimisation of a solar car operating in South African conditions?	What can be recommended to the South African solar vehicle team regarding choice of vehicle and environmental factors to consider, to ensure accurate characterisation of the solar vehicle and its environment?
		What can be recommended to the South African solar vehicle team regarding real-time updates when minimising the energy usage of a solar vehicle travelling a variable distance under South African conditions?



## RESEARCH METHODOLOGY, FRAMEWORK AND STRATEGY

### Methodology

This work is mostly quantitative but contains some qualitative elements. This research project was undertaken in South Africa and considered the specific conditions of the South African roads and the varying impacts of the weather and the influence of these conditions on a locally designed and built solar car competing in a Sasol Solar Challenge event. Unlike Australia, Egypt and many parts of North America, South African weather conditions can vary considerably across the country.

The non-uniformity of South African roads offer a variety of conditions such as flat terrain, steep inclines/declines and mountain roads that have many tight bends and blind turns in them, all of which may all be encountered on the same day of driving along the prescribed routes in a Sasol Solar Challenge event. In contrast, Australia, Egypt and even some American Solar Challenges (ASC), the gradient of the road is mostly flat with long winding curves, in many cases, the road seems wholly straight and flat as far as the eye can see. The weather, especially in Australia and Egypt, is somewhat predictable (mostly clear sky) which significantly simplifies energy management and planning.

### Strategy

This research uses the 2016 and 2018 TUT solar car as a case study for modelling, energy simulations, application of optimisation techniques and field testing.

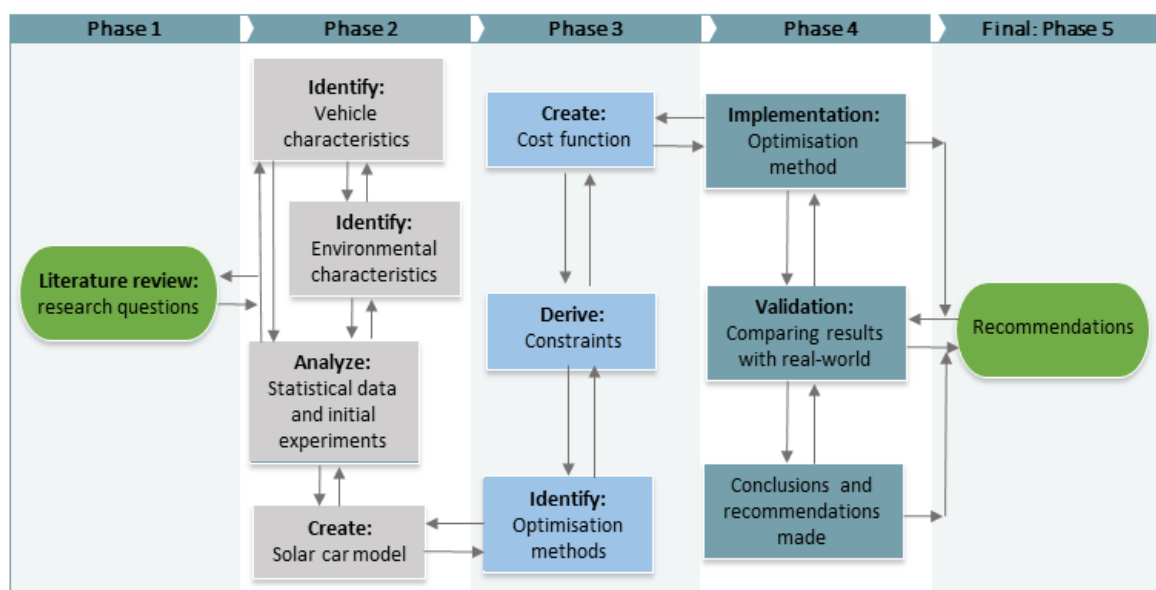


Figure 2: Research strategy flow diagram

The research strategy was structured as follows:

Phase 1: The research was initiated with a systematic and chronological approach and focused on information relevant to the context of the study. The literature was consulted to identify appropriate techniques that then formed part of the literature review. This in turn, assisted in the iterative formulation of the research's central and sub- questions.

Phase 2: The identified literature was used to establish the vehicle and environmental factors relevant by suitably characterising the behaviour of the car and its operating environment. Furthermore, an evaluation of historically recorded data, from previous Sasol Solar Challenges in South Africa, and experiments were used to help identify the more prominent factors that had to be considered, explicitly based on the South African context. A suitable model (in which non-linear components may be linearised around operational points) that describes the behaviour of the solar car on South African roads was developed. Some of the characteristics of the vehicle were also validated by the use of wind tunnel tests, simulations and experiments.

Phase 3: a) Optimisation strategies suited to the Sasol Solar Challenge Challenger category were used as a guideline to set up the constraints for the optimisation problems. A suitable objective function based on the Sasol Solar Challenge rules and regulations (including national road rules) was derived by considering the model obtained in Phase 2. In addition, the identified constraints aided in deriving the cost function.

b) The weather and other environmental variables were modelled and incorporated into the optimisation technique.

Phase 4: Subsequently, the optimisation strategy derived in Phase 3, in conjunction with the model of Phase 2, was used to simulate the SSC route to obtain the optimised speed profile for the solar car. Various experimental performance validations were performed by remotely recording (Internet of Things, IoT) drive data (big data) from the solar car and comparing it with that of the optimisation simulation

recommendations. Conclusions were then drawn and appropriate recommendations and contributions were made to the TUT solar car team in terms of a more effective energy management strategy.

Phase 5: Work and associated results were then documented. Although the research framework follows a seemingly chronological order, the research was an iterative process allowing for bi-directional movement between the different phases. Future work recommendations were made.

## **Scope and delimitations**

### Solar vehicle modelling

- Existing characteristics of the 2016 and 2018 TUT solar car (Sun Chaser II and Sun Chaser III) and historical weather data was used to mathematically describe the solar vehicle so as to create the analytical mathematical model.
- The aim of this research was not to develop a new vehicle, but rather to find the most prominent primary and secondary contributing variables that describe the car and its environment and identify these characteristics through analytics, measurements, tests and experiments. It was foreseen that the results would lead to better designs for the car developed in 2020 and beyond.
- The analytical model used for this research was based on the characteristics of an existing solar vehicle.

### Environmental characterisation

- All significant weather forecast variables identified in the literature were considered in this work; however, only the solar irradiance forecast received specific improvement and conditioning.

### Optimisation techniques and constraints

- Just those optimisation techniques were explored that allowed for non-linear finite horizon systems to be used.

- The South African Sasol Solar Challenge context was used as a framework for testing the optimisation techniques.
- The optimisation constraints were specifically formulated for a vehicle competing in the Sasol Solar Challenge on South African roads.

#### Nature of the contribution and recommendations

- The recommendations regarding the solar vehicle were not of an improved design nature, but rather focused on choosing good, relevant characteristics for modelling purposes and highlighting the major contributing features. That said, the results from this work might contribute to the improvement of future designs of the solar car.
- The recommendation regarding the energy management strategy improvement of the solar vehicle were in the form of a user interface (UI). The Sasol Solar Challenge participants from TUT used the UI to help them plan, manage and predict their energy usage by providing them with an optimal speed profile to drive at throughout the planned trip. The software interface (UI) would need to factor in the vehicle's physical characteristics in order to display the desired route distance for the day to be travelled, the time allowed for travel, the predicted weather forecast and various other parameters. The UI then used the parameters and mathematical equations describing the vehicle dynamics to simulate and minimise the energy usage for the route. This then enabled the UI to display advice for the drivers on the optimal speed to drive at, updating this as frequently as for every 1 km travelled.

#### **Form and nature of results**

The results of this study are presented in the form of optimal speed recommendations aimed at assisting the TUT solar team in making better energy management decisions while competing in a Sasol Solar Challenge in South Africa. The mentioned recommendation itself is in a User Interface (UI) format that allows the team to input their vehicle particulars and route data and extract weather data from on-line sources (IoT). The UI is able to simulate an energy model of the solar car. The optimisation

technique then provides the user with the required optimal speed profile at which the car has to travel along the entire route. In addition, the UI also provides the energy user with information on how to maximise distance travelled during a Sasol Solar Challenge event.

## **OVERVIEW OF THE CHAPTERS**

Chapter I introduced the research strategy, established the context of the work, provided a project overview and emphasised the importance and benefits of the work. The literature review in Chapter II provides a summary of the current knowledge on vehicle modelling, weather forecasting techniques and an overview of solar electric vehicle challenges worldwide. The chapter then concludes with a summary underlining the current research deficiencies in the identified areas. Chapter III contains details on the mathematical energy model of a solar car, including a section validating the model in real-world conditions. The environmental conditions and forecast improvements are detailed in Chapter IV. Here the author details how weather forecast performance can be improved and tailored to the niche area of solar vehicle energy predictions and simulations. Chapter V focusses on the optimisation techniques used to minimise energy usage while maximising distance travelled of a solar electric vehicle competing in the SSC event in South Africa. Chapter VI is an in-depth, real-world case study which validates the mathematical models and optimisation techniques as well as providing comprehensive performance characteristics. The concluding chapter (Chapter VII) wraps up the work by linking the research questions to the chapter content and illuminating how these questions were addressed and answered throughout the document. The references to the consulted literature follow Chapter VII. The work is concluded with an annexures section.

## SCIENTIFIC CONTRIBUTIONS TO THIS WORK

C. Oosthuizen, B. van Wyk and Y. Hamam, "*Modelling and simulation of the South African designed Sun Chaser II solar vehicle*," 2017 IEEE AFRICON, Cape Town, 2017, pp. 1149-1154.

DOI: 10.1109/AFRCON.2017.8095644

URL: <http://ieeexplore.ieee.org/stamp/stamp.jsp?tp=&arnumber=8095644&isnumber=8095433>

C. Oosthuizen, B. Van Wyk, Y. Hamam, D. Desai, Y. Alayli and R. Lot, "*Solar Electric Vehicle Energy Optimisation for the Sasol Solar Challenge 2018*," in IEEE Access, vol. 7, pp. 175143-175158, 2019.

DOI: 10.1109/ACCESS.2019.2957056

URL: <http://ieeexplore.ieee.org/stamp/stamp.jsp?tp=&arnumber=8918287&isnumber=8600701>

C. Oosthuizen, B. van Wyk, Y. Hamam, Y. Alayli and D. Desai, "*Development of Solar Irradiance Forecast Confidence Intervals for Solar Electric Vehicle Energy Simulations*," IEEE SAUPEC 2020, Cape Town, 2020, pp. 56-61.

DOI: <https://doi.org/10.1109/SAUPEC/RobMech/PRASA48453.2020.9041019>

URL: <https://ieeexplore.ieee.org/document/9041019>

C. Oosthuizen, B. van Wyk, Y. Hamam, Y. Alayli and D. Desai, "*The Use of Gridded Model Output Statistics (GMOS) in Energy Forecasting of a Solar Car*," MDPI Energies, vol. 13.

DOI: <https://doi.org/10.3390/en13081984>

URL: <https://www.mdpi.com/1996-1073/13/8/1984>

## **II. LITERATURE REVIEW**

Although this research concerns solar vehicles, the physical nature of a solar car is very similar to that of an electric vehicle or even a conventional fuel or self-powered vehicle. Therefore, this literature review consists mainly of research published in the domain of electric cars and where possible, makes reference to studies focussed explicitly on solar vehicle research.

### **SOLAR VEHICLE MODELLING**

Mathematical models can help us understand observed systems or phenomena by providing us with the means of being able to predict their reactions (output) based on specific actions (input stimulus) [1]. It also enables us to manipulate the world around us. Historically, to achieve this objective, we have used several mathematical methods: numbers, algebra, geometry, calculus, including differential equations, statistics, dynamic systems and chaos theory as well as more complicated systems. Mathematical modelling is used to create a mathematical description of the observed phenomenon which is generally too complicated to be fully described [2]. Mathematical modelling provides us with a recipe for simplifying the observed phenomenon and arriving at a computationally tractable description. We need to keep in mind that the model is merely a simplification of reality. There is always a possibility that the model's simulation output results will deviate from the actual results.

It is a commonly known fact that models very often have to be numerically expressed to allow its interpretation to be processed by a computer. From this, it is simple to recognise that among all instruments used to define, predict and manipulate natural phenomena, mathematical modelling plays an essential role. Mathematical modelling is, in many cases, the only possible way to comprehend or experience a phenomenon.

Typically, there are two distinct major methods of modelling: analytical modelling and statistical modelling. Both types are widely used, with the former commonly applied in the exact sciences and physics domains and the latter applied in economic, financial and biological fields. This does, however not mean that statistical modelling is not seen in the field of physics and mathematics. An example might be machine learning or an artificial intelligence which frequently relies heavily on statistically driven models or

mixed models. Mathematical modelling always starts by understanding the system in question, including its surroundings and the effect its surroundings have on it. Being able to understand these factors and system or phenomena characteristics is the first step in creating an analytical model. For this work, we focussed mainly on analytical modelling; whereas statistical models [3] use a different approach.

An Electric Vehicle (EV) is surprisingly similar in physical and other characteristics to a regular car [4]. The list below points out the common similarities (focussing on physical aspects which might affect energy usage) when comparing an EV to a traditional internal combustion engine vehicle [5-9]:

- Four wheels in contact with the road surface
- Mechanical transmission system
- Substantial vehicle mass
- Brake booster system and power steering
- Climate control
- Energy storage medium
- Safety equipment
- Auxiliary electrical equipment

The mechanical transmission system of a traditional vehicle has significant losses, mainly due to friction and heat. Similarly, in an EV, transmission losses play a vital role in energy consumption. However, the need for energy efficiency in EVs as a result of inferior battery technology tends to drive designs in the direction of direct drive motors which cuts out the transmission losses completely. In contrast, the Tesla Model 3 EV, for example, still makes use of an automatic transmission system, although it is quite efficiently designed and well suited for its purpose. Vehicles such as the newly launched commercial solar car Lightyear One, however, uses direct-drive in-hub motors to eliminate transmission losses.

A similar comparison is that of the various energy storage mediums used. Traditional vehicles typically use some fossil fuel as their energy storage medium whereas EVs usually make use of batteries for energy storage (typically, some Li-Ion variation). Extracting the stored energy from these various mediums requires certain transfer efficiencies, which is considered a type of energy loss. The reason for pointing out the



similarities is to show that modelling an EV is more general than one might initially have thought. In the same way that there are some similarities between traditional cars and EVs, there are also some differences that are discussed in this chapter.

## **Mechanical factors**

### Mass and gravity

The weight of an object has a massive impact on the energy required to displace an object from one place to another on a horizontal as well as a non-horizontal surface. This apparent parameter importance is emphasised by the inclusion [10] of mass in both the kinetic and the potential energy equations.

$$E_p = mg(h_1 - h_0) \quad (1)$$

$$E_k = \frac{1}{2}m(v_1^2 - v_0^2) \quad (2)$$

where  $m$  is the mass of the vehicle,  $g$  is gravitational acceleration,  $h$  is the altitude of the location and  $v$  is the speed of the vehicle.

The route gradient significantly affects the gravitational component of a vehicle and is aggravated by its independent variable, mass [11]. The effect can be positive or negative, depending on the state of the gradient and the magnitude of the mass. Increasing the number of occupants and luggage in a vehicle further increases the overall weight, which in turn also increases the effects of the route gradient on the energy consumption of an EV.

### Friction or rolling resistance

This is a result of two surfaces in contact (the wheel and the road) which deform slightly at the point of contact and do not recover their shape completely. Therefore, the contact involves a loss of elastic energy. Usually, the rolling friction is an order of magnitude less than the traction when solid surfaces are involved. Nonetheless, as in the case of most vehicle scenarios, the rolling friction is not negligible with a pliable rubber wheel on hard tar. Some independent variables affect the magnitude of rolling resistance [12]: road gradient, tyre material, tyre pressure, road surface conditions, bearing friction and wheel alignment. A coefficient of rolling resistance ( $C_r$ , can

summarise most of these independent variables) which can be calculated, but is mostly experimentally determined due to the complexity of the calculation [13]. The experimental method is commonly referred to as the “coast down method” [14]. The wheel alignment is vitally important as this is normally not included in the coefficient of rolling resistance. Incorrect Toe, Camber and Wheel Alignment settings of a vehicle can increase rolling resistance, not to mention cause uneven tyre wear and unsafe driving conditions. Rolling resistance is described by [15]:

$$F_r = C_r mg \cos(\theta) \quad (3)$$

where  $\theta$  is the gradient of the road. The following table (Table 2) presents typical (averaged)  $C_r$  values for some common applications [16].

**Table 2: Coefficients of rolling resistance**

Contact surfaces	$C_r$
railroad steel wheels on steel rails	0.001 - 0.002
low resistance tubeless tyres	0.002 - 0.005
bicycle tyre on concrete	0.002
bicycle tyre on asphalt road	0.004
truck tyre on asphalt	0.006 - 0.01
bicycle tyre on roughly paved road	0.008
ordinary car tyres on concrete, new asphalt	0.01 - 0.015
car tyres on tar or asphalt	0.02
car tyres on gravel - rolled new	0.02
car tyres on cobbles - large worn	0.03
car tyre on solid sand, gravel loose worn, soil medium-hard	0.04 - 0.08
car tyre on loose sand	0.2 - 0.4

The following equation shows a simple relationship between  $C_r$ , the tyre pressure and vehicle speed [17]:

$$C_r = 0.005 + \frac{1}{pt} \left( 0.01 + 0.0095 \left( \frac{v}{100} \right)^2 \right) \quad (4)$$

where  $pt$  is the tyre pressure and  $v$  is the vehicle speed.

It is important to note that the  $C_r$  coefficient is not completely independent of vehicle speed as can be seen in Equation (4). However, an increase in the tyre pressure ( $pt$ ) decreases the quadratic relationship effect that  $v$  has on the  $C_r$  coefficient and the relationship becomes more linear.

### Aerodynamic losses

A vehicle has three main sets of aerodynamic forces acting upon it, namely longitudinal forces, aerodynamic lift or down forces, and forces induced by crosswinds.

Consider first the longitudinal force: the EV's aerodynamic shape directly impacts the energy required to move forward and displace the air surrounding it [18]. Furthermore, wind speed and wind direction are critical considerations for calculating the real aerodynamic drag energy. For an accurate calculation, it is necessary to take into account the vector component of the wind [19], which directly affects the vehicle from the front or the rear. Other independent variables are air density, vehicle speed, the frontal surface area of the car as well as the coefficient of aerodynamic drag. The relationship is given by [20]:

$$F_a = \frac{1}{2} p A C_d (v + v_w)^2 \quad (5)$$

where  $p$  is the air density,  $A$  is the frontal area of the vehicle,  $C_d$  is the coefficient of aerodynamic drag and  $v_w$  is the frontal wind speed.

The losses due to aerodynamic drag also exhibit a quadratic speed relationship. It can, therefore, be said that the faster the vehicle is moving, the more prominent the aerodynamic forces become. The coefficient of aerodynamic drag ( $C_d$ ) is a measure of the performance of a streamlined aerodynamic shape which moves through the surrounding air. A low drag coefficient means that the streamlined shape of the vehicle's body is such that it can move effortlessly through the surrounding viscous air with minimal resistance. On the other hand, a high drag coefficient is produced by insufficient streamlining of the body profile, so that when the car is in motion there is elevated air resistance. In many cases, moving parts are added to performance vehicles to induce high aerodynamic drag (increasing the frontal area as well as the coefficient of aerodynamic drag) and aerodynamic downforce for short periods to allow

for high-speed cornering and improved manoeuvrability at high speeds without losing traction [21]. The following table (Table 3) provides typical  $C_d$  values for vehicle types:

**Table 3: Coefficients of aerodynamic drag**

Vehicle type	$C_d$
Motorcycle and rider	1.5
Typical F1 racing vehicle with dynamic rear wing for increased drag and downforce	1.2
A modern car like Toyota Prius	0.26
Tesla Model 3 EV	0.23
Convertible, open top	0.6 - 0.7
Bus	0.6 - 0.8
Old Car like a T-ford	0.7 - 0.9
Solar electric prototype car competing in Bridgestone World Solar Challenge or Sasol Solar Challenge	0.09 - 0.22

Typically, turbulent airflow at the tail of a vehicle is coupled with a high coefficient of aerodynamic drag. In the same way, laminar flow from the rear of a car is usually coupled with a low coefficient of aerodynamic drag [22].

The second component of the aerodynamic forces is that of aerodynamic lift or downforce. This is of particular importance to vehicles designed for high speed, such as Formula 1, NASCAR and in many cases, rally cars. If the car possesses positive lift, this means that the normal force on the tyres become less with the increase in speed, which in turn results in less traction with reduced cornering and evasive manoeuvring abilities. The goal for energy-efficient vehicles such as solar cars, is generally a neutral (zero) coefficient of aerodynamic lift [23].

The third component of aerodynamic force is that force which is induced by crosswinds. The second and third components are less important when considering ordinary everyday vehicles and are mainly relevant to high-performance cars or endurance cars such as solar cars.

These three aerodynamic coefficients are usually found employing computer simulation, wind tunnel experiments or other tests.

### Transmission losses

These are significant losses in Internal Combustion Engine Vehicles (ICEV) from where the power or torque is produced (the engine) to where it is applied to the shafts at the wheels [24]. These include components such as the transmission, transfer case, differentials, constant velocity joints, and universal joints. Generally, with an EV, these losses are minimised by reducing the distance between the power production unit (electric motor) and the shafts of the wheels as well as reducing the number of mechanical linkages [25]. Transmission losses can be eliminated by situating the electric motor directly into the wheel hubs to bypass all potential transmission losses. The latter is popularly applied by various EV manufacturers today. The transmission losses can typically be described by a simple constant-coefficient and are typically found through experimentation and measurement [26].

### Acceleration forces

When a vehicle is in motion, the energy it expends to accelerate between two known speeds can be calculated by the change in kinetic energy [27] as shown in Equation (2).

This equation shows us that energy due to ideal acceleration is not time-dependent, as the variable  $t$  does not appear in it. However, in the case of an EV, the limitation on acceleration is a combination of the maximum discharge rate of the battery pack and the safe operational regions of the electric motor/s [28]. Another consideration is that most electrical motors used in EVs are complex 3-phase machines and typically vary in efficiency with a variation in torque required [29]. Luckily, with most of these special 3-phase machines, the efficiency increases with an increase in torque demand [30] (limited to a specific r/min range of course). Therefore, pulling away rapidly (rapid acceleration) with an EV to reach a set speed will most likely use less energy than acceleration over a longer period of time (due to the relationship between torque and efficiency). Different behaviours are observed in fossil fuel cars as it has been proven that slower acceleration generally saves fuel.

### Deceleration forces (regenerative braking)

Vehicles in motion possess a lot of kinetic energy, and all this kinetic energy has to go somewhere when brakes are applied to slow the car down [31]. Brakes are traditionally based exclusively on friction and transform the vehicle's kinetic energy into waste heat and friction to decelerate a vehicle. Almost all of that energy is simply lost to heat and friction during a traditional braking cycle. Regenerative braking utilises the motor of an EV as a generator to transform much of the kinetic energy back into stored electrical energy when decelerating [32]. The next time the car accelerates, it utilises much of the energy stored earlier from the regenerative braking. Although the efficiency of regenerative braking is such that it may merely add 11-22 % in driving range [33], this is still much better than simply losing all of that energy to heat and friction as happens in traditional braking systems.

### **Electrical factors**

#### Motor and inverter

Some of the most essential components of EVs, such as drive motors, enjoy much attention in terms of improvement, and rightfully so. EV motors are available and range in efficiency from 35 % to 82 % [34] for DC motors and up to 97 % [35] for other technology motors, such as Permanent Magnet Synchronous Motors (PMSM). The efficiency also has some correlation with the technology used. Most EV motors are PMSM, Brushless DC (BLDC) or Switch Reluctance Motor (SRM) machines, which mostly boast high efficiencies. Older 3-phase AC and DC motors have lower efficiencies in general. The electric motor, however, cannot be more efficient than the drive or controller behind it. Typical methods such as square wave, trapezoidal and vector-based commutation methods are used. All three mentioned commutation methods or algorithms could drive popular motor technologies (PMSM, BLDC, and SRM). More advanced algorithms, such as Field Oriented Control (FOC, vector-based) [36] are closed-loop and perform at superior efficiencies, compared to other less expensive and less sophisticated commutation methods. As mentioned earlier, the motor and controller efficiencies usually are not constants, but rather a function of the torque (load) and r/min (vehicle speed) required [37].

### Climate control, power steering and electrical peripherals

Climate control might be one of the more prominent (up to 30 % of the total energy expended) electrical consumers of regular vehicles as well as on EVs [38]. Luckily, the climate control function is not always active and intelligent sensing within the vehicle cabin ensures minimum usage of climate control to achieve maximum thermal results.

### Vehicle communication, entertainment systems and control systems

All modern vehicles have internal communication systems and state of the art control systems as well as integrated entertainment systems [39]. These vary according to the manufacturer and the specific model, and their power consumption can be estimated or measured to arrive at a suitable constant.

### Battery characteristics

The most prominent battery technology used in modern EVs is Li-Ion chemistry. These cells have charge and discharge efficiencies as well as other capacity characterising parameters that influence their performance to convert stored energy into usable electrical energy. The specific battery efficiencies, energy density and weight to energy ratio of Li-Ion are relatively superior to many of its counterparts and therefore, a favourite in the EV industry [40, 41]. Many complex battery models exist; however, it has been shown that a simple constant coefficient can yield acceptable results in describing the efficiency and performance of a Li-Ion cell [42].

### Solar panels

Many EVs and even regular internal combustion vehicle manufacturers are leaning towards renewable energies and the application of these in their vehicles. Silicon-based solar panels typically have an efficiency of between 16 % and 25 % [43], depending mainly on the quality of the cells, the encapsulation materials as well as the manufacturing process. Gallium and multi-junction based cells can reach efficiencies of up to 47 %, but are known to be very expensive [44]. Car manufacturers usually opt for making use of the silicon-based cells, except for certain prototype solar electric

vehicles [45] where some gallium and multi-junction technologies are incorporated in their solar panel arrays. The cloud cover conditions, very high temperatures and the accumulation of dust all decrease the output efficiency of solar panels.

## **Environmental factors**

### Condition of the air

The air temperature, humidity, pressure and dew point temperature all affect the air density, which in turn directly affects all three components of the aerodynamic drag forces. The air density at a ground surface level can be seen to vary by up to a few percentiles [46] and must, therefore, be considered when modelling a vehicle.

### Wind

The wind speed and direction affect the aerodynamic component, as explained before. These wind components need to be evaluated and included in the energy model of a vehicle to make the model more realistic. Wind gusts are challenging to predict and therefore, the average wind speed and direction for any specific hour is used to evaluate the forces brought to bear on a vehicle body.

### Solar irradiance (*GHI*)

EVs fitted with solar panels will see a change in input power based on the amount of solar irradiation they receive from the sun. Solar irradiance can be divided [47] into three main categories: Direct Normal Irradiance (*DNI*), Diffuse Horizontal Irradiance (*DHI*), and Global Horizontal Irradiance (*GHI*). Equation (6) shows the relationship between the components where ( $\sigma$ ) is the angle between the normal (horizontal) surface of the earth and the sun.

$$GHI = DNI \cos \sigma + DHI \quad (6)$$

If a surface is held normal to the angle of the incoming sun rays, the amount of solar radiation received here is called the *DNI*. The application of solar photovoltaic installations and other installations that track the position of the sun has particular interest to this quantity. The *DHI*, on the other hand, is the amount of indirect solar



irradiance which arrives on a surface due to the scattering of molecules and particles in the atmosphere and is observed equally from all directions. The most useful is the *GHI* component as this describes what a horizontal surface on the ground might experience in terms of solar irradiance, which includes the effects from both the *DNI* and the *DHI* components. The *GHI* component [48] is often used to evaluate the available solar energy of a fixed solar installation. The same applies to a typical EV, hybrid or solar-powered vehicle, as in most cases they expose their integrated solar panels horizontally to the sun (roof, bonnet/hood and boot/trunk areas).

### Clouds

Although current *GHI* forecast attempts to account for the cloud effect, the presence of clouds decreases the confidence interval of the *GHI* prediction [49, 50]. The amount of Total Cloud Cover (*TCC*) was historically measured in Octas; however, recent forecasts can supply an intuitive percentage scale to describe the *TCC*. While cloud conditions can be described by high level, low level and other cloud parameters, *TCC* however, provides a holistic description of the cloudy conditions [51] and is popularly used in combination with *GHI* forecasts to sharpen results.

### Rain

The presence of rain might affect parameters such as traction [52], and when heavy rainfall is present while driving at high speeds, the rain may add resistive force to the front of the vehicle; possibly producing a similar effect to when the air density increases. This means that the car will have to exert more force to move through its surrounding air [53]. Heavy rain is mostly isolated and is therefore not very prominent when modelling a vehicle.

## **Miscellaneous factors**

### Driving behaviour and traffic

Each driver will have a unique style of driving, which will directly impact the energy consumption of a vehicle. Findings from a study in Thailand demonstrated that the fuel consumption of an internal combustion vehicle varied by up to 30 % [54] based on

comparisons of the most fuel-economic driving style measured and the most uneconomical driving style measured. Some studies have been done on the driving behaviour of EVs, but as general driving behaviour (not including following a strict speed profile) is a delimitation of this study, it is of less importance to discuss those results. In principle, the kinetic energy equation is not dependent on time, which technically means that if one accelerated harshly or slowly, one would use a similar amount of energy to do so. However, the ICEV engine or EV motor would be operating at different operational efficiencies (coupled to r/min and load). This means one first has to understand the vehicles' power plant and transmission to appreciate what impact the driving behaviour will have on a car. In general, the type of electric motors used on EVs operate at a higher efficiency under high torque, which is not always the case with ICEVs. The traffic component adds some variation to the driver's behaviour and does not necessarily decrease efficiency. Traffic does, however, affect ICEVs more than it does EVs as the ICEV still has to maintain a state of idle, which consumes energy. When the EV is stationary in traffic, it will be the auxiliary equipment alone that will be consuming a small amount of energy.

## Summary of energy parameters

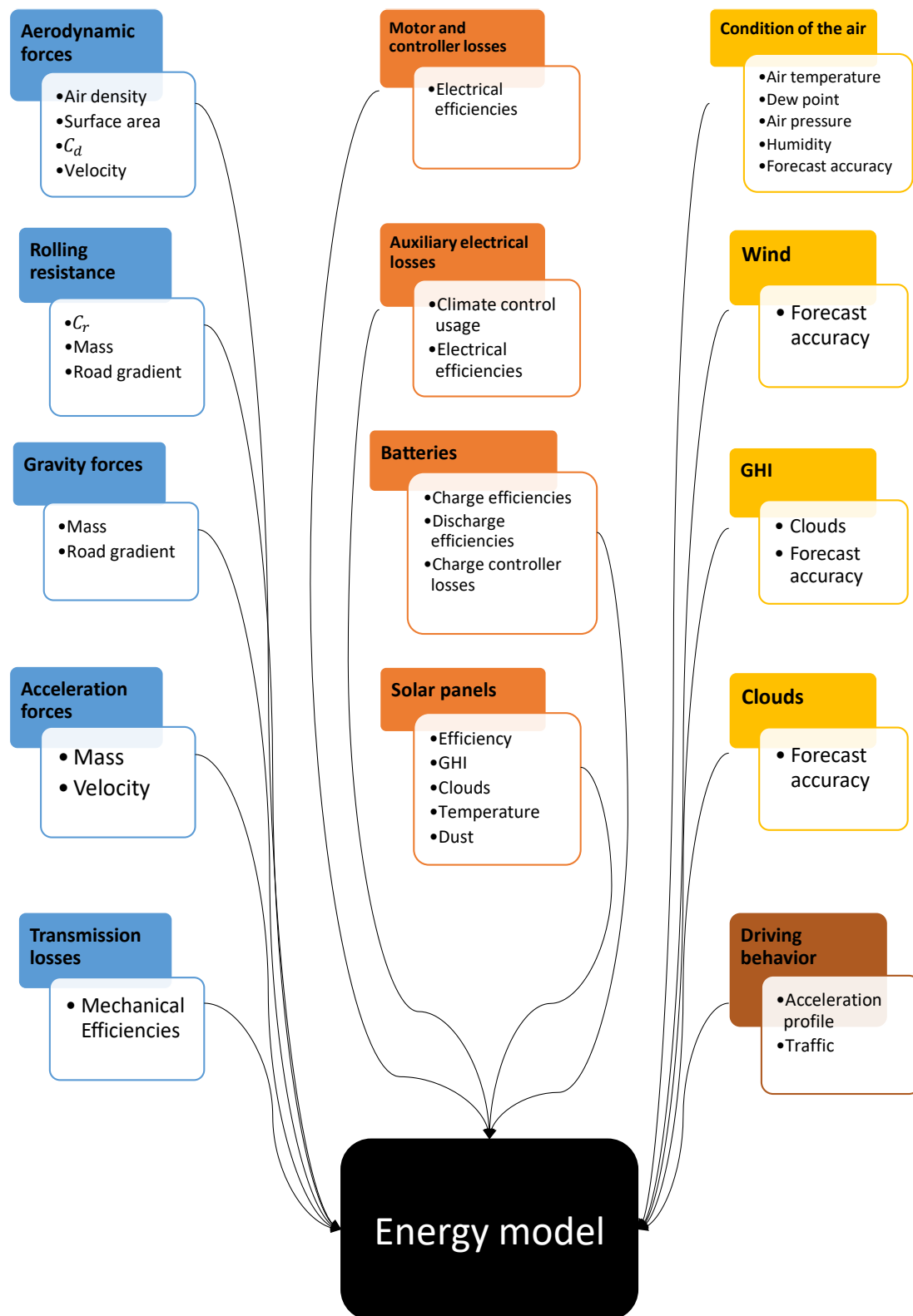


Figure 3: Energy model parameter summary

## WEATHER VARIABLES

An integral part of ensuring an accurate energy model (specifically for solar electric-powered vehicles) is by including relevant weather conditions to the energy variable set. Knowing what the weather conditions might be before travelling a particular route will be beneficial to be able to plan it effectively. For instance, a driver might be planning to drive the following morning to a town 300 km away from his current location (assuming the range of this solar vehicle is 300 km with good sunshine when travelling at 120 km/h). He does not know that the weather forecast until 1 pm the following day predicts fully overcast conditions (which would force the driver to drive slower to conserve energy). The driver will become frustrated when departing early, while having to drive slowly rather than leaving after lunch and being able to drive at a good pace. One can then argue that if the driver had watched the weather channel the previous night, he would have been able to make the necessary adjustments to the trip. However, when you have to consider the clouds, wind speed and direction, the air density, the solar irradiance forecast (such as *GHI*) and the variability of these parameters, it quickly becomes apparent and somewhat necessary to make the weather forecasts more accurate, refined and used in context to become more useful for a vehicle energy model used by a potential energy manager (user).

Two prominent databases are available which supply these forecasts to the public for use on a global scale. These are the European Centre for Medium-Range Weather Forecasts Integrated Forecasting System (ECMWF-IFS) [55] and the Global Forecast System (GFS) [56] produced by the National Centres for Environmental Prediction. These two global databases provide a wide range of meteorological forecasts. Table 4 displays the forecast specifications of each of these systems.

**Table 4: GFS/ECMWF specifications**

	Global spatial resolution (km)	Forecast resolution (hours)	Forecast horizon (days)
ECMWF-IFS	9	3	10
GFS	27	1	10

Although these forecast providers provide reliable and readily available data, a need arose for intermediary services which take data from these sources and apply certain techniques to improve the accuracy and reliability even further. Several of these intermediary weather services now exist [57] and are used by energy managers for solar installations and wind installations as well as by diverse professionals and ordinary citizens, including meteorologists, sailors, farmers, weather enthusiasts and many more. Recently, the data provided by these intermediary services has also become important to participants of solar electric powered vehicle teams in events such as the BWSC in Australia and the SSC in South Africa. Many researchers are now using this intermediary forecast data and fine-tuning the team's performance by combining the data with some historical data, creating forecast ensembles and applying some regression methods. This is done with the aim of making the forecast data even more useful for specialised applications in a variety of areas [58].

To establish a baseline for reference purposes, the following sections briefly summarise the Expected Forecast Performance (EFP) of some critical weather variables as seen from the primary data sources (ECMWF-IFS and GFS, but ECMWF in particular) or intermediary data sources.

### GHI

The University of California has done an extensive study [59] where they set out to evaluate the performance of the *GHI* forecast from the GFS as well as ECMWF models. They made use of seven weather stations across the Americas for validation. They evaluated the Mean Bias Error (*MBE*) or Forecast Bias (*FB*) and the Root Mean Squared Error (*RMSE*) of the *GHI* forecasts to establish a baseline for the performance of these forecasts. Table 5 records the results they obtained.

**Table 5: *GHI* EFP**

	<b>GFS</b>	<b>ECMWF</b>
<b><i>MBE</i> (W.m<sup>-2</sup>)</b>	5.2	0.5
<b><i>RMSE</i> (W.m<sup>-2</sup>)</b>	84.6	106.2

Although these results are based on a one-day forecast evaluation, they still provide a baseline for the *GHI* forecast accuracy, and under normal circumstances, one would expect that the accuracy would be similar or worse for forecasts with a broader time horizon.

### Wind

The ECMWF published a wind speed verification document [60], which made use of 633 stations across Europe for verification of the 10 m wind speed forecast with a horizon of up to six days. The mean *RMSE* values (as seen by over 90 % of the stations) were found to be 2.1 m/s for one day ahead forecast, and 2.4 m/s for six-day ahead forecasts. The *RMSE* values ranged between a minimum of 1.1 m/s and a maximum of 5.2 m/s.

### Air density

The air density is calculated by using dew point temperature, surface air temperature, and air pressure by making use of a polynomial method [46]. The air density itself does not have a unique forecast, probably due to its predictability when referring to the previously mentioned variables. Secondly, the air density variation is highly dependent on the temperature, and the typical density variation with air at 5 °C and 30 °C is around 8 %. Although this relationship is not linear, when considering ideal operational points of 5 °C to 30 °C the relationship is approximately linear [61], which makes estimation relatively easy, which reduces the need for such a forecast (air density forecast).

### Clouds

The cloudiness of the sky is commonly expressed as *TCC*, which is a percentage between zero and 100 %. Cloudiness is one of the more challenging weather parameters to predict. It is evident in the accuracy of the *TCC* forecast from the ECMWF model [50], which ranges from an *MAE* of 25 % for the same day forecast up to an *MAE* of 36 % for a six-day forecast. This weather parameter is by far the most unpredictable when compared to the *GHI*, wind and air density.

In summary, Table 6 indicates the EFP range for the significant weather variables contributing to the energy model of a vehicle for a six-day forecast.

**Table 6: EFP summary**

	<i>MAE</i>	<i>MBE</i>	<i>RMSE</i>
<i>GHI</i> ( $\text{W.m}^{-2}$ )	-	0.5	106.2
Wind (m/s)	-	-	1.1 - 5.2
Air density (%)	8	-	-
Clouds ( <i>TCC</i> , %)	25 - 36	-	-

### Improving local weather forecasts

An extensive forecasting technique comparison has been made [62], and the best forecast techniques were found to be the Artificial Neural Network (ANN) based methods. This work, however, simply shows results for one day ahead forecasting and the process of training the ANN is relatively lengthy and intricate and requires seven other weather variables apart from *GHI* and *TCC*, too. Furthermore, the work does not apply the forecasting techniques to a real-world application to illustrate how improved accuracy can lead to an increase in application performance. Other techniques, such as Model Output Statistics (MOS) have been used since 1972 [63] for site-specific forecasts. MOS is a post-processing forecast method that uses data of some predictors (such as the *GHI* forecast) and relates this to some historical statistical data of some other predictors (such as *GHI* and *TCC*). Gridded MOS [63, 64] or GMOS is a type of MOS which is evaluated for a whole network of ground observation stations (site-specific) to create a forecast model for a larger area. The more ground observation stations in the grid, the better the performance of the GMOS model will be.

The improvement of the *GHI* forecast component is essential for route and speed planning, especially with cars such as Lightyear One and the single-seater solar cars designed by teams competing in the BWSC and the SSC, relying heavily on solar power. With a better understanding of the risk associated with the available *GHI* forecast, the car user and energy manager will be able to make better and more energy-conscious decisions. In the current literature, there is no mention of how a

GMOS model can benefit the design teams in a SSC event in terms of energy management.

## **SOLAR ELECTRIC VEHICLE CHALLENGES**

Energy management or even energy optimisation of a solar car travelling on the desired route has various apparent benefits to the user. Therefore, the application of energy management is increasingly being applied in this context. In a solar endurance challenge, however, energy management or energy optimisation is not only beneficial, but it is also crucial in most cases. Although a super light chassis, good aerodynamic design, low rolling resistance tyres and super-efficient electronics are essential, a good energy management strategy is necessary. In an endurance challenge, a lower-ranked solar car with a better energy management strategy can beat a better-designed, more expensive solar vehicle.

To encourage young academic graduates (mostly engineering graduates) as well as industry partners to invest time, research capacity and resources in electric and especially solar vehicles, various international engineering challenges were created to spark enthusiasm and awareness among the general public. As previously mentioned, some of these challenges include the Shell Eco-marathon (worldwide), Formula Student Germany Electric (Europe) and solar vehicle challenges such as the Bridgestone World Solar Challenge (BWSC, Australia), the American Solar Challenge (ASC, America), the Somabay Egyptian Solar Challenge (SESC, Egypt), the Sasol Solar Challenge (SSC, South Africa) and many more.

In the Sasol Solar Challenge 2018 (SSC2018, held in South Africa over eight days in September), teams enrolled in the Challenger [65] category were allowed to compete in a long-distance engineering endurance challenge on national roads. The objective was to cover the mandatory daily distances between Pretoria and Stellenbosch in addition to being able to drive an unspecified number of additional route sections daily (adding variable daily distances).

On each day, the first stage started at 08:00, followed by the number of loops (additional route sections) desired by the team, including a thirty-minute mandatory stop during the day. Finally, the last stage for that day saw the car navigated through to the terminus by 17:00. These distances were covered by the single-seater solar



electric-powered vehicles that the diverse international teams had designed. Competing vehicles were allowed to enter the challenge with a fully charged battery restricted to a maximum of 20 kg of Li-Ion, about 18 MJ (5000 Wh), and 4 m<sup>2</sup> of a silicon-based solar array and were required to manage this energy throughout the eight days in order to maximise their distance. Although many solar challenges exist worldwide, the South African based Sasol Solar Challenge is notoriously challenging as it provides a variety of extreme landscape topographies such as severe road gradients as well as varying weather conditions along the entire route.

It is not uncommon to see the more experienced teams (despite them originating from different corners of the world) designing solar vehicles with very similar vehicle characteristics. Therefore, the need to optimise the race strategy as well as energy management has become just as or even more important, than the design of the vehicle itself. Usually, these top-ranking teams cover anything up to nine loops per day in the SSC and even the smallest energy mismanagement or strategy mistake may cost them the title. Typically, basic energy predictions of the solar vehicle are simulated by creating a mathematical model of the car, knowing the route profile (gradients and distances) and the average solar power available from the sun for the specific day of travel. Top and medium ranking teams often incorporate more advanced energy predictions by including additional factors such as models of the battery and motor systems, acceleration losses, traffic conditions and advanced weather variables such as the wind speed and direction, cloud cover and air density.

The BWSC held bi-annually in Australia possibly receives the highest number of single-seater solar vehicle entries for any such challenge worldwide. The BWSC is different from the SSC in that the distance is fixed and the aim is to cover the mandatory distance in the shortest time. Appropriately so, there have been various publications on energy optimisation techniques for these specific route conditions at the BWSC. Although the BWSC is arguably the largest of its kind in the world, the general route gradient is somewhat flat with fairly predictable (predominantly sunny) weather conditions.

As early as 1997, research on the optimal driving speed of a solar car on a level road (referring to the rather flat topography of the BWSC route) was published [23]. The authors were able to predict the average optimal speed of the vehicle within 12 km/h

of the actual sustainable average speed by making use of classic non-linear programming techniques. A simplified model for the car was used, in which just gravity, aerodynamic forces and rolling resistance were considered and the model assumes perfect mechanical efficiency. The same authors published more work in 2002 [66], including a more realistic model of the battery and removing the restriction of an average optimal speed strategy. Good results were obtained, although no acceleration forces were considered. In 2006, a master's thesis was published [67] in which the researcher used dynamic programming to solve the optimal speed profile. The work uses a fairly comprehensive mathematical model that considers battery and some motor characteristics, but neglects acceleration forces. The results are, however, only simulative and no real-world data was used.

In 2008, a review [68] of an energy management system for a vehicle competing in the BWSC highlighted some noteworthy findings in regard to existing energy management systems. While their model does not consider acceleration forces, it does recognise the three primary force components as well as the electrical motor, solar array and battery characteristics. Researchers from Istanbul Technical University determined that a theoretical Big Bang-Big Crunch optimisation approach [69] is realistic for use at the BWSC. Although the results are satisfactory, the methods were of a purely simulative nature alone. The authors of [70] used a relatively in-depth model of the electrical parts of the solar car (again disregarding acceleration). They introduced a multi-level optimisation technique customised for the BWSC by making use of a high-level long term (future driving days) planning strategy for the days ahead followed by a continuous optimal control problem for the short term (current day) solved through pseudo-spectral methods in MATLAB®. No real-world implementation was done. Nevertheless, the simulation results proved robust and reliable.

Another multi-level optimisation technique was demonstrated by [71] in 2016, by making use of an exciting model which compensates for the angle of incidence of the sun and the effect of this angle on the solar irradiance. Acceleration forces have been disregarded. This time, however, the high-level long term planning was merely based on the users' anticipation of the route difficulties (gradients) for each day, while the short term planning was done with classic non-linear programming techniques in MATLAB®. Only simulations were presented, and the authors did not take any weather variables, other than the solar irradiance into consideration. Very recent work has been

published by [72] in regard to a case study done on the University of Michigan Solar Car Team at the BWSC2015 in Australia and the ASC2016. The work makes use of a very similar energy model as described in this paper except for not considering the acceleration forces and using only raw weather forecasts (non-refined). The authors made use of genetic programming and machine learning techniques to search for optimised driving speeds along the route; these minimise the total race time. Here they treated the whole race (multiple days) as one problem instead of two different problems as has been adopted by various other authors. The authors demonstrated their success by implementing their systems on the solar vehicle. It is important to note that none of the abovementioned research can work for a solar challenge route where variable distance is of concern, such as in the case of the Sasol Solar Challenge route.

Much research has been undertaken in the domain of speed optimisation of electric and solar cars. This is not necessarily linked to a specific route and therefore the analysis is more generalised. The authors of [73] demonstrated the importance of route planning by considering the possible shading areas on a specific route as a result of natural occurrences, such as mountains and artificial objects, like buildings. Here, the objective of the speed optimisation was aimed at relieving what is known as 'range anxiety' of the drivers when planning a trip, rather than maximising the distance travelled or minimising the time travelled on pre-defined routes such as the routes of the BWSC and the SSC. The optimal speed profile was found by using dynamic programming on multiple routes (the route with the least amount of shading was usually the preferred route). Intending to eradicate the environmental pollution crisis caused by global warming, the authors of [74] focused on a dynamic programming optimisation algorithm to create an energy management system to find the best speed trajectory with minimal energy consumption for a pre-defined route. The influence of the weather conditions on energy consumption has not been considered, although some real-world data was used to substantiate their theoretical findings.

Another study [75] considered real-time traffic conditions when determining an optimal speed profile for an electric vehicle. This was accomplished by solving a multi-stage optimal control problem utilising a new proposed approximation model, which reduces the number of decision variables and expedites the processing. Field tests verified high computational efficiency and a reduction in energy consumption without incurring additional journey time.

At the time of this research, just two sets of work have been published that focus on an energy management strategy or speed optimisation of solar-powered vehicles competing in the Sasol Solar Challenge event. In 2013, the authors of [8] developed an energy model for their solar car and used Google Maps to retrieve the route data and ultimately, Mathematica®, to find the highest average speed maintainable. However, the method allows for the computation of just a single day and not multiple days (the SSC is usually an eight-day challenge). Furthermore, the air density variation and acceleration forces were not considered. In addition, a simple constant motor efficiency coefficient was used with no consideration of electrical and auxiliary losses. The other study mentioned was conducted by [15] and focused on the SSC making use of a model that considered the auxiliary electrical losses and a variety of efficiency coefficients. Acceleration, however, was not recognised. The authors introduced a fundamental energy management strategy (negating wind and other weather variables other than solar irradiance) to find the best average speed to drive at. Although this method could merely be calculated for a single day and made use of diverse averaged variables, the results proved reliable when implemented on non-windy days, but inefficient on days where considerable wind and other weather variations were present.

## **LITERATURE SHORTFALL SUMMARY**

Authors very often merely estimate or use non-verified mechanical and electrical coefficients as part of the mathematical energy model. This introduces inaccuracies, mainly when the energy simulation is done for a significant time horizon. The variable nature of major weather parameters are rarely seen to be incorporated into energy models. Instead, weather constants or weather assumptions are widely adopted as a result of the difficulty of acquiring real-time weather data, the processing requirement thereof as well as the usability due to the variable nature of these forecasts. Furthermore, it has been recognised that weather parameters are commonly treated as deterministic, which disregards the importance of the inherently variable nature of the weather. Some research has shown to improve local forecasting, but no such previous work has applied the forecast improvement to a solar electric vehicle application in the South African region.

Many researchers opted for an averaged type speed optimisation method and not an incremental higher resolution optimal speed profile. Averaging often results in misleading results with decreased accuracy. Moreover, most researchers' outcomes were solely based on simulations, thereby failing to deliver extensive real-world application comparative results. While it is correct that some researchers did develop methods of producing incremental higher resolution optimal speed profiles, none of them demonstrated their techniques as being capable of optimising speed over a multi-day, variable distance route. Their methods failed to involve maximising distance by introducing additional daily route sections to be driven (variable distance).

For these reasons, this work undertook to satisfy the current research shortfalls by developing and validating a comprehensive energy model and evaluating the statistical forecast error variation of the significant weather parameters to improve the forecast accuracy. To achieve this, the research made use of optimisation techniques capable of incremental high-resolution output by extensively evaluating and determining the performance of the fully integrated system through a large-scale real-world implementation.

### III. MODELLING

The energy behaviour, or mathematical model of a solar car, can be expressed by an analytical relationship, inferring some characteristics from statistical data or a combination of both. This chapter explains each of the components, which, when combined, form a comprehensive mathematical energy model for a typical solar vehicle. Throughout this chapter, specific reference is made to the parameters for the mathematical energy model created either for Sun Chaser II (SCII) which competed in the SSC2016 or Sun Chaser III (SCIII) which competed in the SSC2018.

#### ENERGY EQUATIONS

Chapter II described the aerodynamic, rolling resistance and gravitation forces acting on the car. This chapter refers to them by the symbols  $F_1$ ,  $F_2$  and  $F_3$  and these forces account for the majority of forces acting on the solar vehicle while it is in motion. The Equations (7) to (10) describe the aerodynamic forces ( $F_1$ ), rolling resistance ( $F_2$ ) and gravitational forces ( $F_3$ ) due to the gradient of the road acting on the vehicle in parallel to the vehicle's movement along the route.

In the three equations  $k$  indicates the discrete interval over which the individual forces are calculated for the entire route to be driven; the interval is typically to 1 km resolution. In Chapter V the discussion details how the optimisation algorithm produces a single optimal speed for each discrete interval  $k$ . Typically, the higher the resolution of  $k$ , the more accurate the results, but the resolution must be constrained by the increase in computation intensity.

$P_{aux}$  contains the constant (approximated) electrical power consumption of the auxiliary electrical components in the vehicle. Such ancillary equipment includes, but is not limited to:

- Motor controller
- Battery Management System (BMS)
- Contactors, relays and other power circuitry
- Cockpit display screen
- Wireless telemetry hardware
- DC to DC conversion losses (high voltage to low voltage for sub-systems)

- Microcontrollers, regulators and other electronic circuits and sensors
- Controller Area Network communications bus (CAN bus)
- Reverse camera and brake lights/indicators
- Resistive heat losses in the cabling

Simple theoretical calculations can produce suitable values for the various auxiliary components; with the aid of laboratory and field experiments under real-world conditions, it is possible to verify and calibrate these calculated values.

$P_{loss(k)}$  describes the driving power loss (negative) or gained power (positive) at any one of the discrete-time sampling periods.  $P_{loss(k)}$  can only be positive when force  $F_3$  (effect due to gradient of a significant downward slope) is larger than the sum of  $F_1$  and  $F_2$  or, when a fierce wind is blowing in the same direction of movement, and this results in  $F_1$  being more significant than the sum of  $F_2$  and  $F_3$ . The former case typically occurs more often than the latter.  $P_{loss(k)}$  is described by Equation (10) where  $v_k$  is the speed of the car in m/s at each optimal speed interval  $k$ .

$$F_{1(k)} = \frac{1}{2} \rho A_{car} C_d (v + v_w)^2 \quad (7)$$

$$F_{2(k)} = C_r m g \cos(\theta) \quad (8)$$

$$F_{3(k)} = m g \sin(\theta) \quad (9)$$

$$P_{loss(k)} = \frac{v_k}{\eta_{motor}} [F_1 + F_2 + F_3] + P_{aux} \quad (10)$$

Table 7 describes all the variables used in (7) to (10) including some additional variables used later in this chapter.

**Table 7: Sun Chaser III model parameters**

Symbol	Parameter	Value	Units
$m$	Mass (including 80 kg driver)	268	kg
$C_r$	Coefficient of rolling resistance	$\approx 0.0085$ at 60km/h (Equation (4))	-
$C_d$	Coefficient of aerodynamic drag	0.162	-
$A_{car}$	Frontal surface area	1.03	m <sup>2</sup>
$A_{pv}$	Solar array size	4	m <sup>2</sup>

$\eta_{motor}$	Motor and controller efficiency	0.3 – 0.938 (range for typical operational conditions)	-
$\eta_{elec}$	The combined solar array, Maximum Power Point Tracker (MPPT), battery and charging circuit efficiency	0.242 (at 25 °C solar array temperature)	-
$P_{aux}$	Auxiliary electrical losses	13	W
$e_{cap}$	Battery storage capacity	17.8 (4942)	MJ (Wh)
$v_w$	Wind speed	Variable	m/s
$p$	Air density	Variable	kg/m <sup>3</sup>
$\theta$	Theta, road gradient	Variable (pre-determined from the chosen route)	radians

### Coefficient of drag and rolling resistance

The coefficient of aerodynamic drag ( $C_d$ ) in Equation (7) should be as accurate as possible. Normally, calculating the  $C_d$  component accurately for an arbitrary shape (such as the SCIII solar car, which represents the shape of a catamaran sailboat when viewed from the front) can be cumbersome and often results in unnecessarily complex mathematical equations. Modern methods include wind tunnel experiments or computer simulation.

Gaining access to large wind tunnels is a further challenge and therefore scaled models are used. The typical operational speeds of the solar car in South Africa would never exceed 120 km/h, and consequently, the importance of the Mach number (object speed to speed of sound ratio) is not of concern. When scaling the model, however, it is vital to understand the fundamental Reynolds number relationship, which is equal to the product of the speed of the fluid (air) and the characteristic length (chord length) divided by the kinematic viscosity of the fluid (air). The Reynolds number needs to stay constant for the scaled model results to be comparable with those of the full-size object. As the kinematic viscosity of air is constant, and the chord length is easily measurable on the physical scaled model, the sole variable which needs to be adapted is the speed of the fluid or airspeed in our case. This means that if the scale model chord length is 1 m and the full-size object is 3 m, then the speed of the fluid (air) over the scaled model has to be three times larger (360 km/h in this case) to ensure the



Reynolds number stays constant. Although the solar car might be travelling at real-world speeds of 120 km/h, the wind tunnel measurements typically reach a steady state at much lower rates and therefore does not always require the wind tunnel experiments to be conducted at maximum speed. Another critical factor to consider is that a rolling road should be present in the wind tunnel to ensure airflow characteristics underneath the vehicle are appropriately accounted for.

Using the wind tunnel effectively typically requires the operator to run a series of tests in the wind tunnel, initially without the actual model, but with all the mounting hardware in place, which is also exposed to the flowing air when the trial takes place with the model present. This allows the user to arrive at a baseline to calibrate the wind tunnel before introducing the actual model. After this calibration has been verified, the model is introduced, and all the data is recorded step-wise, while increasing the airspeed in small intervals. These tests are conducted until an acceptable steady state (less than 5 % output variation is observed over time) has been reached, which then signifies the aerodynamic drag constant,  $C_d$ . If a valid steady state has been achieved at a particular airspeed and continues to remain within this steady-state even with the increase of airspeed, there is no need to increase the airspeed further, even though the operational speed of the object might be at a higher actual speed. Figure 4 depicts the  $C_d$  wind tunnel results of a half-scale model of SCIII.

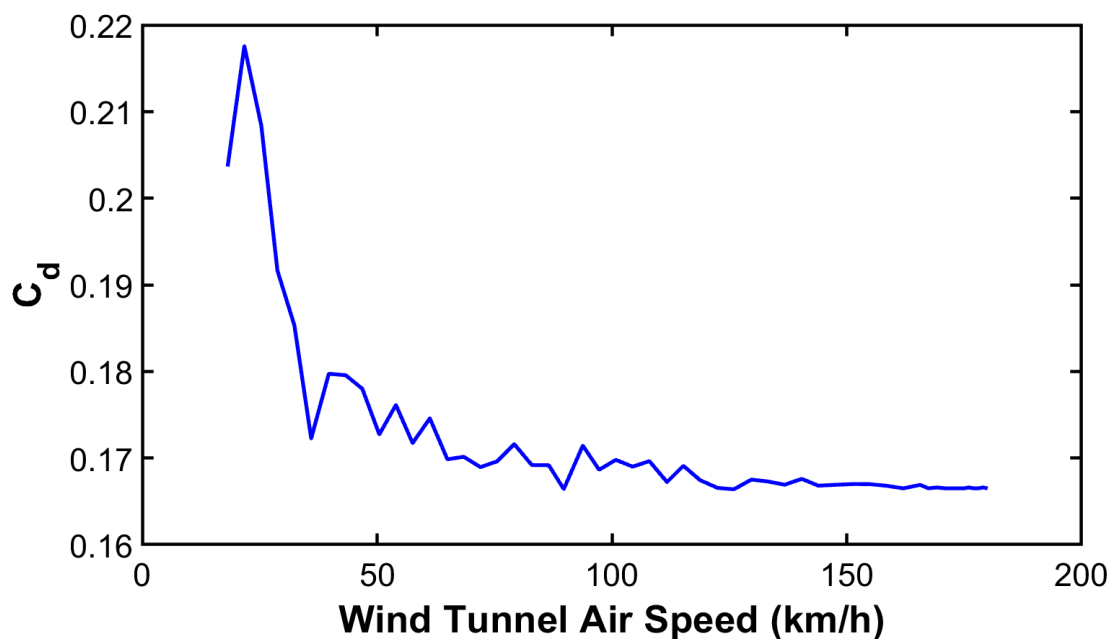
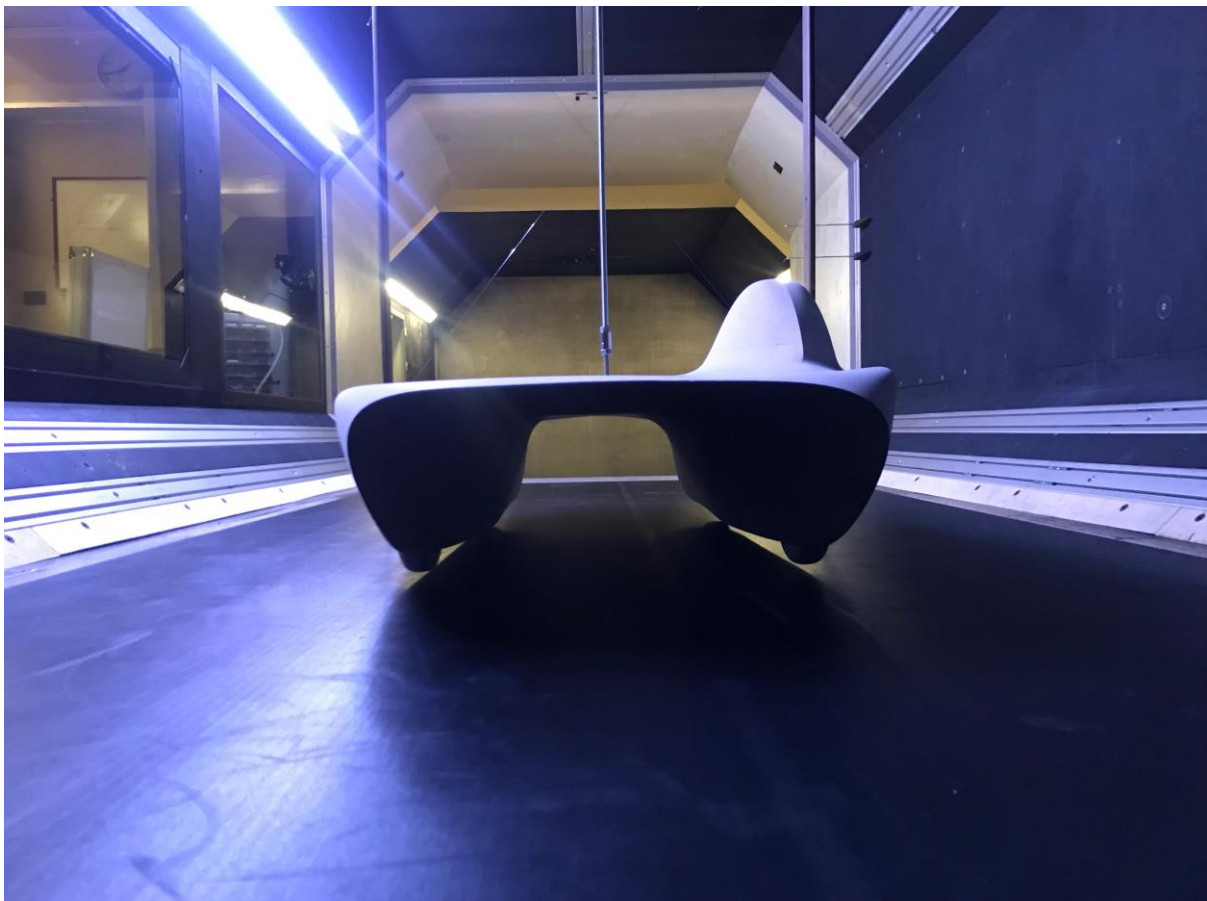
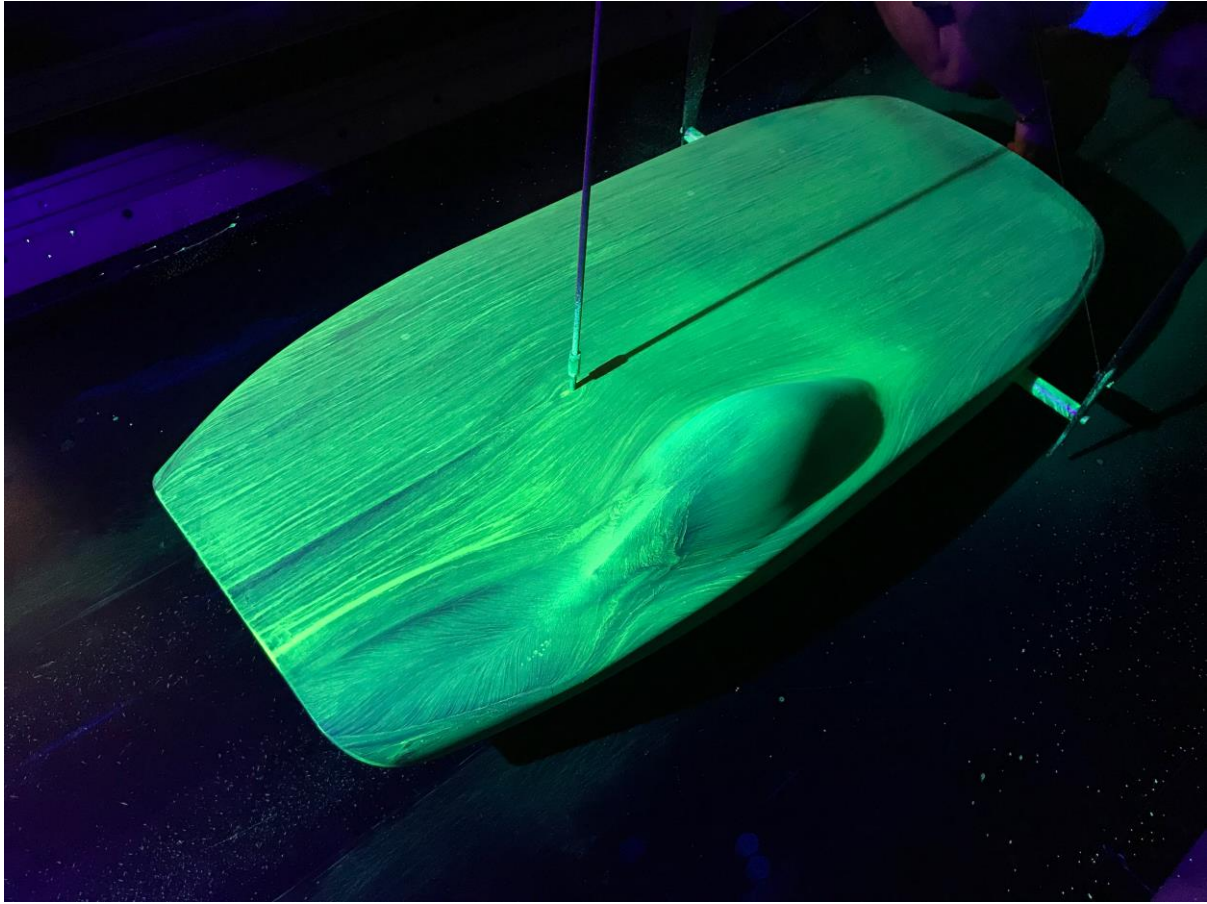


Figure 4: Coefficient of aerodynamic drag of SCIII (wind tunnel)

The results show that the  $C_d$  value reached a steady-state after 120 km/h wind tunnel speed (60 km/h for the actual size model) and settled at a value of approximately 0.163. Figure 5 is a photograph of one of the early versions of SCIII in the wind tunnel where the rolling road is visible. The mounting hardware (three vertical steel rods) can also be seen in this photo. The model was suspended as close as possible to the rolling road to increase the accuracy of the wind tunnel experiments. Figure 6 shows the same model coated with a special fluid which, when illuminated with a fluorescent lamp visually highlights the surface airflow patterns. Unwanted turbulent airflow can be seen at the trailing end of the occupant canopy and on the rear left and right corners of the car. These wind tunnel tests not only produce the coefficient of aerodynamic drag, but assist the iterative design process of the car body in order to obtain a neutral lift (near zero lift and downforce) and other desired body shape characteristics.



**Figure 5: SCIII prototype, wind tunnel test model – rear view**



**Figure 6: SCIII prototype, wind tunnel test model – fluorescent surface flow**

The wind tunnel results are normally used for calibrating a software simulation environment to do rapid simulation and evaluation when vehicle geometry is updated in the design or during the manufacturing process. Figure 7 shows the ANSYS® simulation results ( $C_d$  of 0.162) which support the wind tunnel results (at a 95 % confidence interval) and provides confidence to the user for future rapid simulations in the software environment. Crosswind and lift components were not considered in this work.

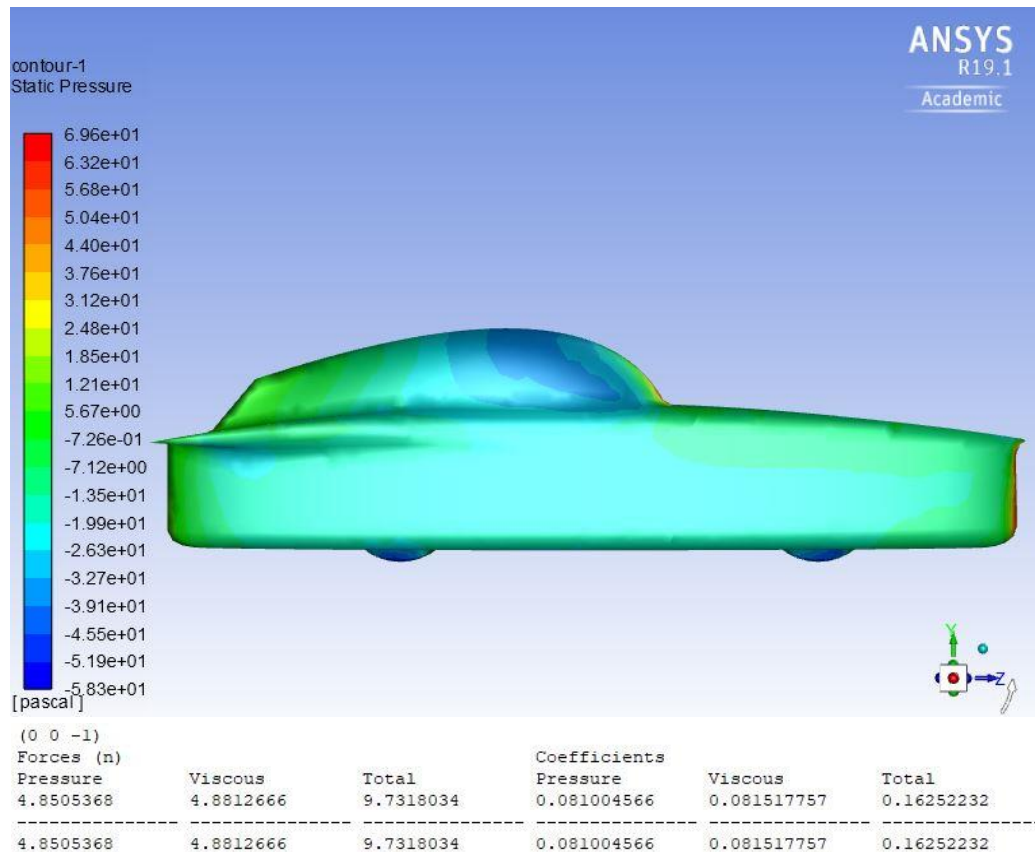


**Figure 7: Coefficient of aerodynamic drag of SCIII prototype (ANSYS®)**

Lastly, the coastdown method [14] was used to further experimentally validate the  $C_d$  value under real-world conditions. Coastdown testing is the process of accelerating a vehicle to a high speed on a flat, straight road and coasting in neutral down to a low speed. By recording the amount of time the vehicle takes to slow down, it is possible to obtain a model of the loss inducing forces affecting the vehicle. Obtaining valid coastdown results requires several steps, including experimental planning, data collection, and data processing. One of the secondary outcomes of using the coastdown method is that a very good approximation of the  $C_r$  value is also found.

### Electric motor efficiency

The motor and controller efficiency is a non-linear torque vs efficiency curve, usually described by a cubic function. Motor torque is calculated by making use of the r/min and the instantaneous mechanical power required. The SCIII team made use of a 2

kW PMSM with a manufacturer-specified efficiency plot, as illustrated in Figure 8. The red curve on the plot shows the data for the actual motor and controller efficiency tested under laboratory conditions. One reason for the lower overall efficiency of the test data compared to the manufacturer's data is that the PMSM has aged, the coil sensor circuitry needed re-calibration and bearings might need servicing or replacement to improve efficiency.

The motor efficiency plot only extends up to 16 N.m as the laboratory equipment restricted the experiment up to this point. The manufacturer's efficiency plot originally supplied a plot up to 30 N.m; however, there is less than 2 % variation in efficiency between 16 N.m and 30 N.m of the manufacturer plot as both these values are now in the steady-state phase of the response plot. The maximum efficiency, reached at 16 N.m by the manufacturer's plot is 93.8 % and 88.3 % by the measured plot. The motor torque constant was experimentally found (by measuring the current flow and torque produced) to be approximately 0.98 N.m/A.

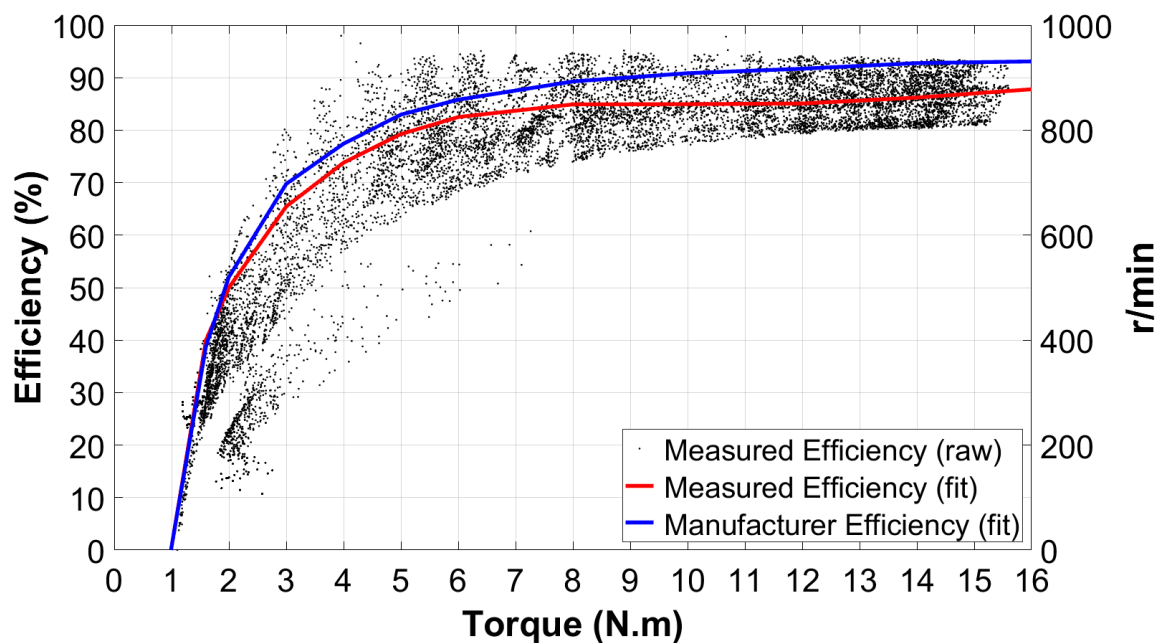


**Figure 8: PMSM efficiency plot**

Here it is clear to see that the torque demand, motor r/min and motor efficiency will play a role in the energy usage of the solar car.

## Solar irradiance

Equation (11) describes the useful solar power (watt) from the sun after the relative efficiencies, and solar collector area has been taken into consideration.

$$P_{sun(k)} = (GHI_k)(\eta_{elec})(A_{pv}) \quad (11)$$

here,  $\eta_{elec}$  is not a constant, but changes with the variation of the solar array temperature. The effect of the temperature variation of the MPPTs as well as the batteries have not been considered in this work. The temperature effect of the solar array on the  $\eta_{elec}$  parameter is shown in Figure 9. The loss percentage on the right-hand axis is a percentage of the loss in rated efficiency.

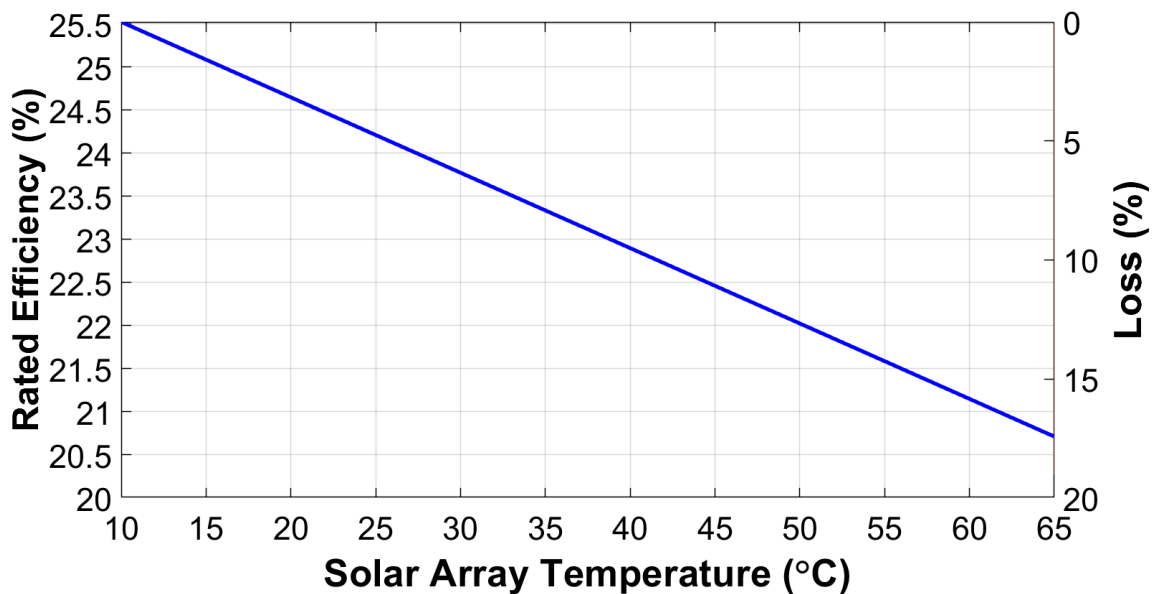


**Figure 9: Solar array - temperature vs efficiency**

The temperature of the solar array is typically a function of the ambient temperature, radiation heat and convection heat from the elevated temperatures inside the solar vehicle's carbon fibre chassis (quickly reaching temperatures 20 °C above ambient). The solar array is heated by the current flow through it, but the area surrounding the array may improve or impair its ability to cool down (by conduction) and is therefore of importance. The solar array is typically much cooler when driving at reasonable



speeds (as opposed to being stationary) as the rush of air on the solar surface can reduce the surface temperature somewhat. Turbulent airflow on the solar surface is desired for better cooling results [76], although solar vehicles are designed to have a low Reynolds number to decrease aerodynamic drag. The laminar airflow over the solar array will, however, still have some effect of cooling when compared to being stationary. The material on which the solar array is mounted, the shape and configuration of these materials as well as this material's heat transfer coefficient can also contribute to the rate of cooling of the solar array of a solar-powered vehicle.

The relationship was found to be approximately linear (at least in the estimated operational conditions region) and as a result, Equation (11) was re-written as (12) to compensate for the temperature increase of the solar array. The plot (Figure 9) shows that for approximately every 10 °C increase in temperature,  $\eta_{elec}$  will decrease by 0.58 %. When solar cells are exposed to the sun for prolonged periods without forced cooling, as is the case with the solar array on SCIII, their surface temperature can reach temperatures of up to 65 °C [77] which would result in reduced efficiency of over 17 %. The power available from the sun is then given by

$$P_{sun(k)} = (GHI_k)(\eta_{elec} - \frac{5.8T_{pv(k)}}{10000})(A_{pv}) \quad (12)$$

where  $T_{pv(k)}$  is the temperature of the solar array above or below room temperature (25 °C). Thus  $T_{pv(k)}$  is considered zero at room temperature and at that temperature the power is again given by  $P_{sun(k)} = (GHI_k)(\eta_{elec})(A_{pv})$ .

### Battery State of Charge

The next stage is quantifying the power flowing in and out of the battery, which can be described by:

$$P_{batt(k)} = P_{batt(k-1)} + P_{sun(k)} - P_{loss(k)} \quad (13)$$

where  $P_{batt(k)}$  is the power flowing in or out of the battery pack. The state of the energy stored (State of Charge,  $SoC$ ) in the battery pack is given by (14) where  $\alpha_{day(x)}$  is the required energy at the start of each day expressed as a percentage (details of this variable are described in Chapter V),  $x$  represents the current day and  $t_k$  is the physical driving time between two optimal speed states (measured at discrete intervals of  $k$ , which is in 1 km increments). Here, the energy is expressed as a percentage of the total energy storage capacity  $e_{cap}$ . Furthermore,  $k$  is the total number of intervals of the route, typically at 1 km resolution.

$$SoC_{day(x)} = \alpha_{day(x)} + \left( \frac{\sum_{k=1}^K [P_{batt(k)} t_k]}{e_{cap}} \right) 100 \quad (14)$$

### Acceleration forces

It has been shown [9] that the acceleration energy of the vehicle from a stationary starting point should not be neglected. However, this is often done to simplify an energy model. This study extended its energy model, which would now include the energy to accelerate the solar car, not just when considering accelerating from being stationary, but rather, from any point during the vehicle's movement. This acceleration energy cannot only be assumed to be the kinetic energy component,  $\frac{1}{2} m.v^2$ , as the initial speed is not necessarily zero. Equation (15) is a derived function that can describe the energy required to accelerate the vehicle from an initial speed to any final speed. The time ( $t_{acc}$ ) over which the acceleration takes place is always smaller than or equal to the driving time ( $t_k$ ) between two discrete intervals,  $k$ .

$$\begin{aligned} F_{acc(k)} &= m \left( \frac{v_{k+1} - v_k}{t_{acc}} \right) \\ P_{acc(k)} &= m \left( \frac{v_{k+1} - v_k}{t_{acc}} \right) \left( \frac{v_k + v_{k+1}}{2} \right) \\ E_{acc(k)} &= \frac{1}{2} m [(v_{k+1})^2 - (v_k)^2] \end{aligned} \quad (15)$$

It should be noted that  $E_{acc(k)}$  is independent of time and that the overall structure still resembles that of the classic kinetic energy equation,  $\frac{1}{2} m.v^2$ . Although the time



independency of  $E_{acc(k)}$  is true, the driver of the solar vehicle will always strive to gradually accelerate between two discrete intervals,  $k$ , such that  $t_{acc} = t_k$  (the physical driving time between two discrete intervals). This will ensure that no sudden acceleration or deceleration power, which might unnecessarily heat or overload the motor, is required. For instance, an immediate 2 000 W acceleration requirement will not be feasible while already maintaining a cruising speed which is consuming a continuous 3 500 W, assuming a 5 000 W maximum rated motor. This might, however, become feasible if the acceleration is performed gradually over the entire time  $t_k$  requiring less instantaneous power (which can potentially exceed the maximum power rating of the motor if applied to abruptly under harsh acceleration). Appropriate constraints were implemented to prevent the exceptional case where the sum of the continuous power requirement and the acceleration power requirement exceeds the maximum available power from the motor (these equations are discussed in the optimisation chapter). Equation (14) was now re-written as (16) to include the acceleration energy component.

$$SoC_{day(x)} = \alpha_{day(x)} + \left( \frac{\sum_{k=1}^K [P_{batt(k)} t_k] + \sum_{k=1}^K E_{acc(k)}}{e_{cap}} \right) 100 \quad (16)$$

### The expected value of $SoC$

Although Equations (7) to (16) describe the deterministic energy model of the solar car, the probabilistic nature of the weather variables is of particular importance. In this study, we considered just the solar irradiance ( $GHI$ ) component as probabilistic; the air density, total cloud cover and the wind components were considered to be deterministic. Therefore (11) was re-written as the expected value to become (17) as there is a probabilistic  $GHI$  component contained within  $P_{sun(k)}$ . The Probability Mass Function (PMF)  $p$ , has a certain number of intervals,  $L$ . The PMF is explained in greater detail in the next chapter of this work.

$$E\{P_{sun(k)}\} = \sum_{l=1}^L p(l) P_{sun(k,l)} \quad (17)$$

In the same manner, (13) and (16) have been re-written as (18) and (19) respectively.

$$E\{P_{batt(k)}\} = E\{P_{batt(k-1)}\} + (E\{P_{sun(k)}\} - P_{loss(k)}) \quad (18)$$

$$E\{SoC_{day(x)}\} = \alpha_{day(x)} + \left( \frac{\sum_{k=1}^K E\{P_{batt(k)} t_k\} + \sum_{k=1}^K E_{acc(k)}}{e_{cap}} \right) 100 \quad (19)$$

## MODEL VALIDATION

The following section will validate the mathematical model and evaluate the performance of the model by exposure to real-world environmental conditions. The experiments were performed during the SSC2016 event in September of 2016 where SCII traversed from Pretoria to Cape Town via national motorways over eight days. The same techniques were used to model both SCII as well as SCIII. Figure 10 illustrates SCII with its support vehicle on a local test track in South Africa.



Figure 10: Top: SSC2016, SCII and support vehicle

Bottom: SSC2016, SCII at the Graaff-Reinet Dutch Reformed Church on Day 5

### **Experimental equipment used**

All equipment was calibrated and operated according to supplier instructions. Data logging was done on a laptop computer (running LabVIEW® and MATLAB®) receiving data on all variables at a rate of 1 sample/second via a long-range wireless telemetry link from the solar car. Various sensors, including a Global Positioning Sensor (GPS) and solar irradiance sensor, were used in the solar electric vehicle to measure a variety of quantities of concern. The following is not an exhaustive list, but indicates some of the typical variables recorded during the SSC2016:

- vehicle speed
- motor power consumption/regeneration
- battery current (bi-directional)
- battery voltage
- *SoC* as reported by the battery management
- MPPT power in from solar array and MPPT power out to battery
- GPS coordinates
- elevation
- solar irradiance
- ambient temperature.

### **Experimental procedure**

During the SSC2016 the SCII solar electric vehicle covered a total of 1 478.8 km during Days 1, 2, 3, 4, 7 and 8. The logged data for Day 5 and Day 6 was corrupt and could not be recovered for analysis. Equations (7) to (16) were then used to calculate the estimated *SoC* profile for each day based on the recorded data. No wind component was used in Equation (7) as the equipment was not available to record frontal wind speed. Two consecutive GPS coordinates were used to calculate the slope (theta) required by Equation (8) and Equation (9). The recorded speed profile, motor efficiency and pre-defined auxiliary losses were used in Equation (10). The useful power in Equation (12) is described by the power recorded on the output side of the MPPT where all the applicable losses between the sun and the batteries have been accounted for. The energy used for accelerations was calculated by Equation (15), making use of two consecutive vehicle speed values recorded and the increase/decrease times between the said speeds. Finally, we were able to calculate

the energy loss/gain by integrating the battery current-flow recorded over time (the process of Coulomb Counting represented by Equation (18)) and adding this to the last known value of the  $SoC$  (Equation 19). This estimated  $SoC$  was then compared to the actual  $SoC$  received from the on-board Battery Management System of the solar car.

If the two curves matched well, then we could say that the mathematical model provides a reasonable estimation of the dynamic energy behaviour of the vehicle. To evaluate just how well the estimated  $SoC$  and the actual  $SoC$  correlate, some typical performance metrics have been used. These include the Bias ( $B$ ), the Mean Absolute Error ( $MAE$ ), the Root Mean Square Error ( $RMSE$ ) and the standard deviation ( $std$ ).

$$ERROR_k = SoC_{actual_k} - SoC_{estimate_k} \quad (20)$$

$$std = \sqrt{\frac{\sum_{i=1}^n (ERROR_k - \text{mean}(ERROR_k))^2}{n-1}} \quad (21)$$

$$B = \frac{1}{n} \sum_{i=1}^n (ERROR_k) \quad (22)$$

$$MAE = \frac{1}{n} \sum_{i=1}^n |ERROR_k| \quad (23)$$

$$RMSE = \sqrt{\frac{1}{n} \sum_{i=1}^n (ERROR_k)^2} \quad (24)$$

where  $n$  is the total number of recorded data points and  $ERROR_k$  is the  $SoC$  error percentage between the actual and the estimated (calculated). The bias metric alone is not enough to evaluate the model's precision and accuracy. However, a strongly biased result might serve as an early indicator that something in the model needs attention or adjustment. The actual amount of error is explained by the  $MAE$ , which is the average of all the absolute errors in the dataset. The  $RMSE$  provides a measure of the absolute fit between the calculated and actual data. It is important to note that this validation does not concern any future simulation, forecasts or predictions. Instead, it is a procedure to validate the mathematical model by making use of recorded data to verify the soundness and usefulness of the mathematical model. A lack of equipment meant that no wind data was recorded and was therefore not included in this experiment (wind was considered to be zero during calculation). However, the wind

will still affect the actual *SoC*, and it is anticipated that some of the error will be due to the wind.

### Experimental results and discussion

Figures 11 to 16 show the *SoC* comparison for the various days of the SSC2016. The solid black line represents the *SoC* estimated/calculated by the model, and the dashed black line represents the real world recorded *SoC* data.

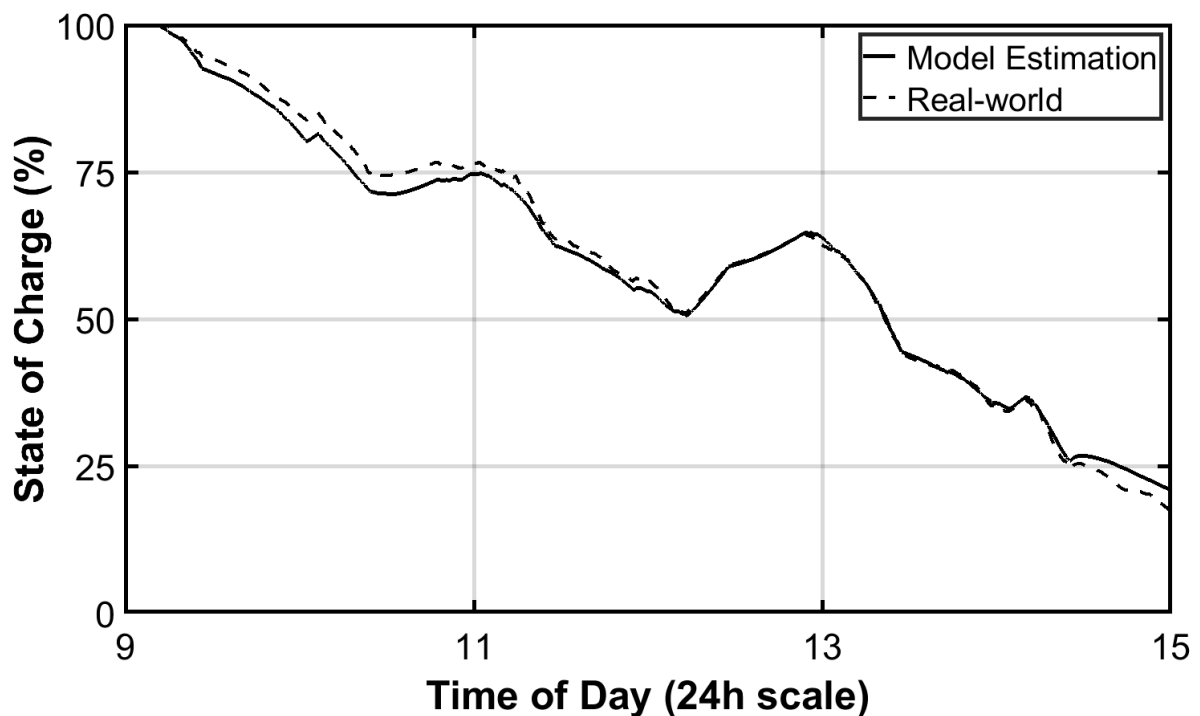


Figure 11: SSC2016 Day 1, *SoC* comparison

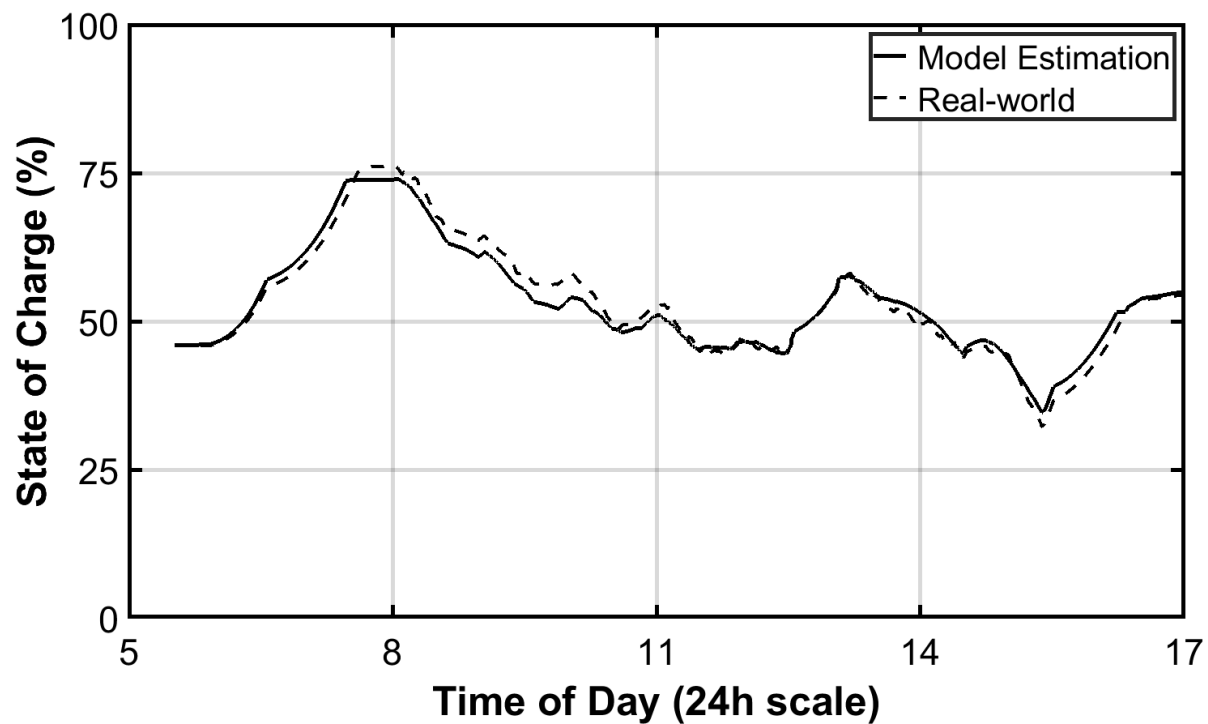


Figure 12: SSC2016 Day 2, SoC comparison

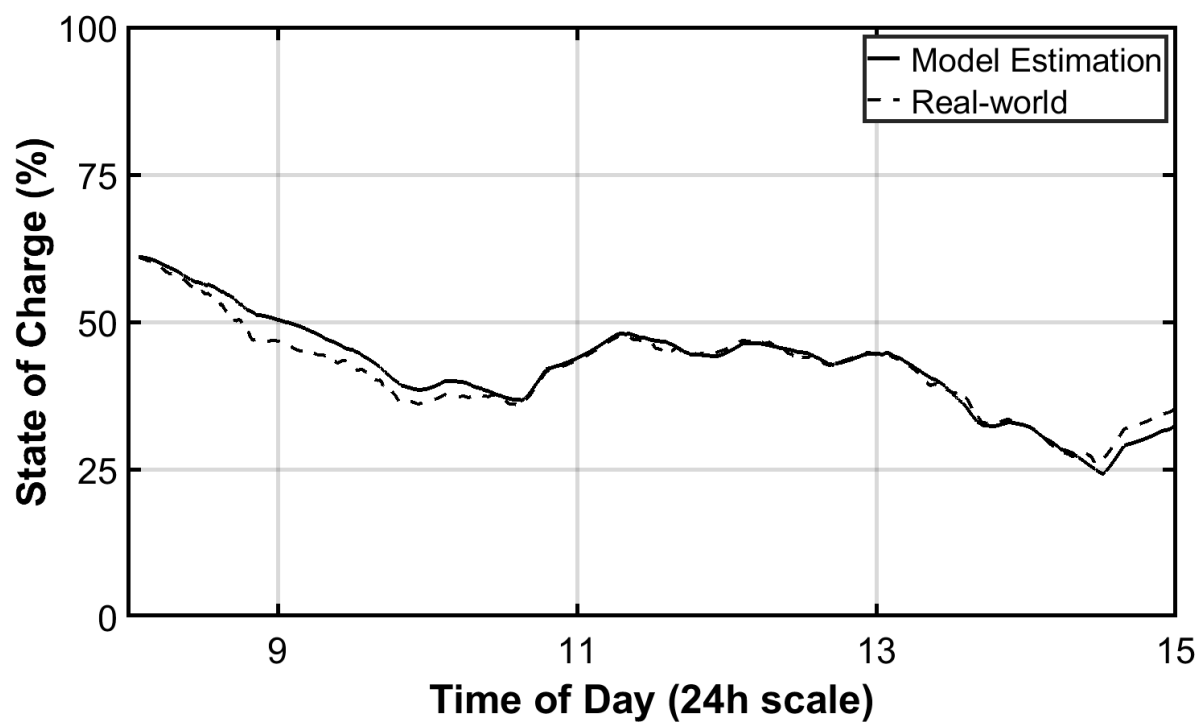


Figure 13: SSC2016 Day 3, SoC comparison

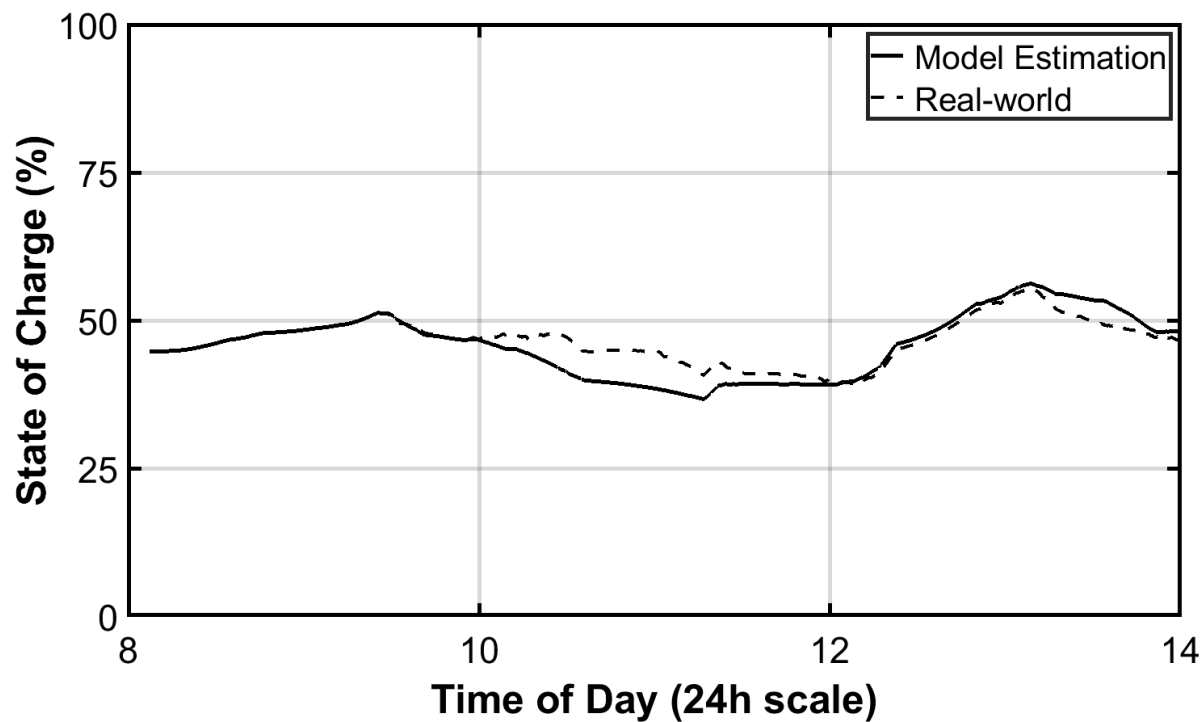


Figure 14: SSC2016 Day 4, SoC comparison

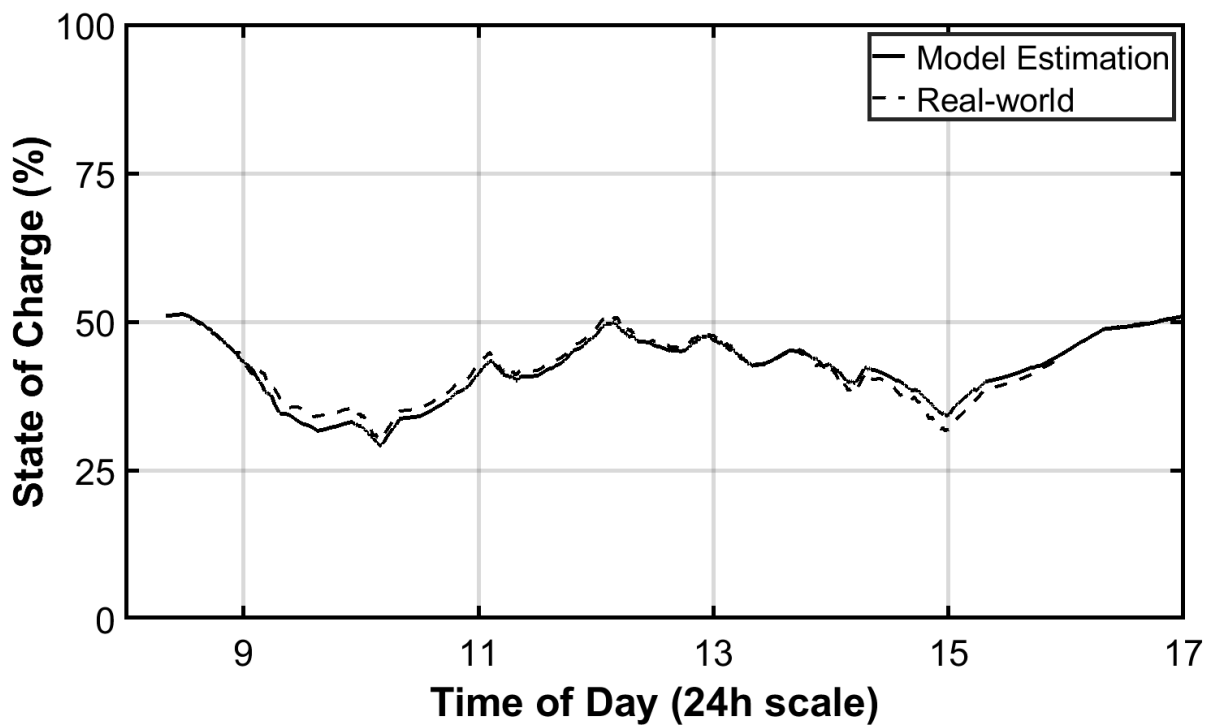


Figure 15: SSC2016 Day 7, SoC comparison



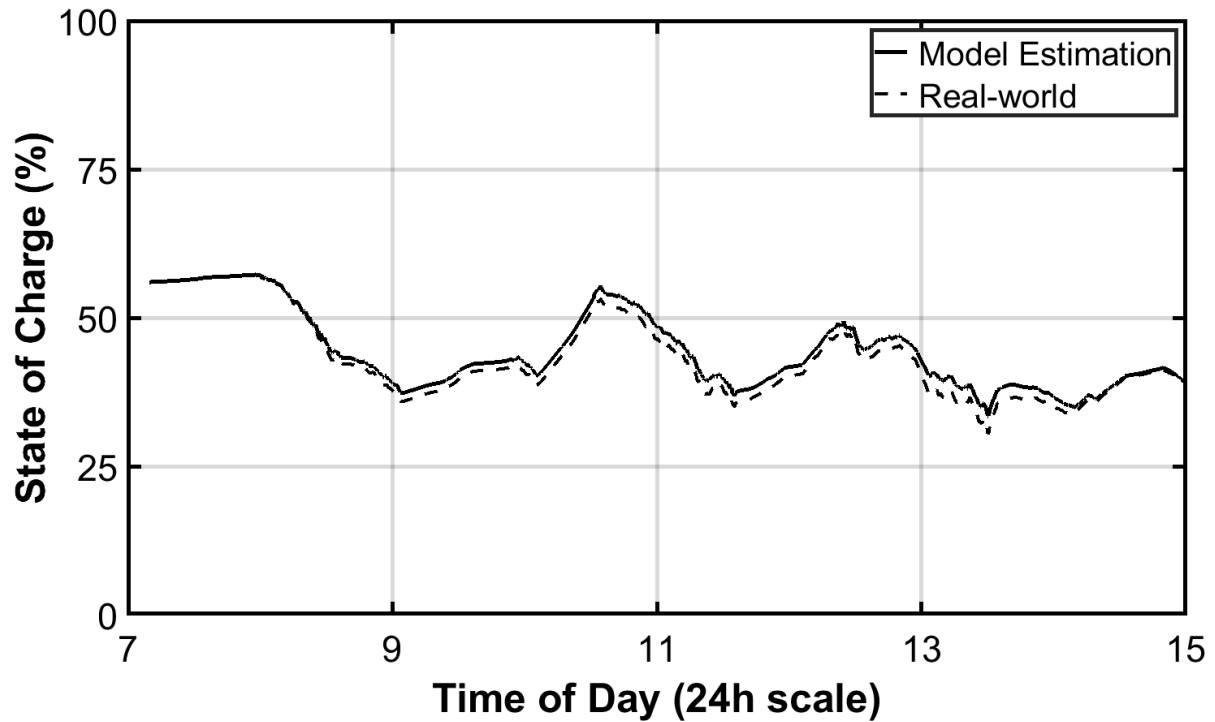


Figure 16: SSC2016 Day 8, *SoC* comparison

To complement the *SoC* comparison figures, Table 8 summarises additional information concerning the route, the environmental as well as physical conditions per day. The values shown for Global Horizontal Irradiance (*GHI*), cloud cover and wind speed were obtained from the Physical Analytics Integrated Data Repository (PAIRS) database maintained by International Business Machines (IBM). All averaged values given were considered from 06:00 to 18:00 daily, and the cloud cover values are unitless and range from zero to one, one being fully overcast.

Table 8: Experiment route summary (SSC2016)

	Day 1	Day 2	Day 3	Day 4	Day 7	Day 8
Distance travelled (km)	279.8	313.4	285	178.5	192.2	226.9
Average speed (km/h)	63.4	51.3	50.9	49.9	49.9	50.8
Total route ascent (m)	2220	1772	1136	2124	3262	3270

<b>Total route decent (m)</b>	2198	1745	1323	2640	3160	3373
<b>Average <i>GHI</i> (W.m<sup>-2</sup>)</b>	488.9	486.3	418.8	446.2	427.0	335.4
<b>Average cloud cover ( 0 to 1 )</b>	0	0	0.52	0.08	0.16	0.49
<b><sup>a</sup>Average NE wind speed ( km/h )</b>	11.2	4.0	23.0	21.6	9.4	8.6

<sup>a</sup>It has to be noted that the average wind speed is in a North-Easterly direction, as the predominant direction of travel for the solar car from Pretoria (Day 1) to Cape Town (Day 8) is South-West. These average daily conditions of the route elevations, sun, clouds, and wind will aid in the interpretation of the calculated and the actual *SoC* error results.

Finally, Table 9 reports the performance metrics evaluated for each day, expressed as percentages.

**Table 9: Model performance metrics**

	<b>Day 1</b>	<b>Day 2</b>	<b>Day 3</b>	<b>Day 4</b>	<b>Day 7</b>	<b>Day 8</b>	<b>Average</b>
<b><sup>a</sup><i>B</i></b>	-0.73	-0.11	0.46	0.49	-0.23	1.18	0.18
<b><i>RMSE</i></b>	1.95	1.73	1.88	2.62	1.19	1.49	1.81
<b><i>MAE</i></b>	1.56	1.40	1.41	1.82	0.95	1.28	1.40
<b><i>std</i></b>	1.81	1.73	1.82	2.57	1.17	0.90	1.67

<sup>a</sup>A negative bias percentage shows that the mathematical model under-predicts the *SoC* of the vehicle, which means that the model estimates is larger than actual energy usage.

No distinctive bias trend can be observed in the model as the bias is seen to be positive on some days and contrary on other days, while being reasonably close to zero (the desired state) with an average of 0.18 % except for Day 8. The average *RMSE* and standard deviation (*std*) for the six days is 1.81 % and 1.67 % with a minimum *RMSE* value at Day 7 of 1.19 % *SoC* and a maximum *RMSE* value seen at Day 4 with 2.62 % *SoC*. Although Day 4 is seen to have the largest *RMSE*, it has the second-largest wind speed, just less than Day 3. Logically, one would have thought that the day with the most significant observed errors would be the day with the most substantial wind observed as the wind was un-modelled during this experiment. The reason for this

phenomenon is that on Day 3 SCII had brake pads replaced during the late evening (after driving ceased for the day) but was only used for the first time late morning on Day 4 (the drivers are instructed to use regenerative braking and only use mechanical brakes in an emergency) increasing the rolling resistance ( $C_r$ ) as a result of the now increased temporary brake pad rub. In general, the cloud cover factor affected the Global Horizontal Irradiance ( $GHI$ ) value negatively as expected. The higher cloud cover values were seen on Day 3 and Day 8.

Another phenomenon, however, requires further evaluation. When comparing the average slope of Figure 11 with any of the other figures, one finds that Figure 11 has a unique negative-going slope. One noticeable difference between Day 1 (Figure 11) and all other days is that the average driving speed was over 20 % higher than on any other day. Furthermore, when comparing Days 1 and Day 2, it is seen that the driving conditions of these two days were very similar with near equal averages of  $GHI$ , cloud cover, and route profile characteristics. Some differences may be seen with regard to the wind speed where this is reflected by the higher  $RMSE$  found for Day 1. Ultimately, the only significant difference between Day 1 and Day 2 is the average driving speed, yet the graphs have completely different slope characteristics:

On Day 1, Sun Chaser II used over 80 % of its stored energy ( $SoC$  decreased) to cover a specific distance. On Day 2 however, Sun Chaser II gained over 10 % stored energy ( $SoC$  increases) and managed to do over 33 km more than on Day 1. Although the wind played some role in adding to the additional energy losses in Day 1, the major contributor was the aerodynamic losses that increased with an exponential function as the average speed of the vehicle on Day 1 was much higher when compared to all other race days.

### **Modelling conclusion**

Overall, the results are satisfactory and consistent when considering that the model does not contain any input from the wind speed. The small deviations seen between the measured  $SoC$  data and the model calculated  $SoC$  data are primarily the result of minor un-modelled components. These include Coriolis forces as well as a physical characteristic of the vehicle changing during the challenge (brakes temporarily binding

when new pads are inserted, tyre inflation, uneven wear of tyres influencing rolling resistance, as well as the mass differences between drivers of SCII used while recording data). Finally, when considering the phenomena of the large slope seen on Day 1, the experiment established the importance of having an optimal driving speed profile to conserve energy and maximise distance.

## IV. ENVIRONMENTAL CONDITIONS

From the literature it was found that the variable nature of major weather parameters are rarely incorporated into energy models. Instead, weather constants or weather assumptions are widely adopted as a result of the difficulty of acquiring real-time weather data, the processing requirement thereof as well as the usability due to the stochastic nature of these forecasts. Furthermore, it has been recognised that weather parameters are commonly treated as deterministic, which disregards the importance of the inherently variable nature of the weather. Some research has shown to improve local forecasting, but no such previous work has applied the forecast improvement to a solar electric vehicle application in the South African region.

In order to create a comprehensive and realistic mathematic model of a solar car, it is essential to incorporate weather forecasts into the model as the amount of expected *GHI* forecast is fundamental to such a model. For the purpose of this work, only the *GHI* forecast component will be treated as stochastic and refined for accuracy and forecast confidence inclusion while the other weather forecast components will be used as they are received in their raw format from the forecaster.

The objective of this chapter is to show how the variability of the *GHI* forecasts can be made useful without adding unnecessary computational complexity and significant modifications to existing energy system algorithms. This is achieved through characterising the statistical behaviour of the *GHI* forecasts from Meteomatics AG and by extrapolating the most relevant performance metrics from the forecast data. These *GHI* performance metrics are then made useful by incorporating them into the energy simulations in the form of forecast confidence intervals. Furthermore, the outcomes of this chapter will lead to:

- better understanding the *GHI* forecast performance as a function of the forecast horizon of nine days
- better understanding the *GHI* forecast performance as a function of the amount of cloud cover
- better understanding the *GHI* forecast performance as a function of the hour of the day
- an improved energy forecast system for solar electric vehicles

We characterised the variability of the *GHI* weather forecast from the Meteomatics AG API for the South African region, only.

## EXPERIMENTAL EQUIPMENT AND PROCEDURE

The weather forecast for up to nine days in advance was acquired via an API available from Meteomatics AG (similar to PAIRS which was previously used in the chapter on modelling), which typically uses the ECMWF database as a raw data source. The variables that were requested from the Meteomatics AG API to use in the optimisation problem are presented in Table 10. In addition to the weather variables recorded in this table, the air density is calculated by using  $T_{dew}$ ,  $T_{air}$ , and  $P_{air}$  with a polynomial method proposed by [78]. The minimum mandatory route (typically around 2000 km over the entire eight-day SSC event) for each day was divided into approximately 1-kilometre intervals. At each of these intervals, the GPS coordinates were saved in an array, and all the variables in Table 10 were requested for the entire range of GPS coordinates. In addition to this, the weather variables were also requested at a 1-kilometre resolution along the route for the additional loop road sections stipulated for each day. The distance and elevation between each GPS coordinate pair were then used to calculate the slope between each GPS pair. The number of optimal speed states,  $k$ , for a route was set at a 1-kilometre resolution. However, the energy calculations (lost or gained) would happen at a higher resolution to ensure that the road profile (gradient) is accurately characterised.

**Table 10: Forecasted weather variables from Meteomatics AG**

Symbol	<sup>a</sup> Variable	Units
<i>GHI</i>	Global Horizontal Irradiance	W.m <sup>-2</sup>
<i>TCC</i>	Total Cloud Cover	%
<i>V<sub>wind_dir</sub></i>	Wind direction	0 ° - 360 °
<i>V<sub>wind_spd</sub></i>	Wind speed	m/s
<i>T<sub>dew</sub></i>	Dew point temperature (air)	K
<i>T<sub>air</sub></i>	Temperature (air)	K
<i>P<sub>air</sub></i>	Pressure (air)	hPa

<sup>a</sup>All weather variables are available in one-hour resolution as standard, but are increased by using a higher-order function to fit the data to an appropriate function. The final datasets have a 15-minute resolution with a range between 06:00 to 18:00.

The variability of the *GHI* forecast can be characterised using a PMF which is a probability measure that shows probabilities of the possible values for the discrete random variable *GHI* with a range  $R_{GHI} = \{ghi_1, ghi_2, \dots, ghi_L\}$ . Equation (25) is the PMF of the discrete random variable *GHI*.

$$P_{GHI}(ghi_l) = P(GHI = ghi_l), \text{ for } l = 1, 2, \dots, L \quad (25)$$

The expected values of the usable solar power (a combination of the *GHI* component and efficiencies) and their dependency on the *TCC* was investigated. For this work, the *GHI* alone has been considered to be probabilistic, and only the expected values (most probable value occurrence for the *GHI* sample set) were extracted from the PMF functions subject to various cloud conditions and forecast horizon for use in the model. For this reason, it was appropriate to use the PMF (Probability Mass Function, discrete) and not the PDF (Probability Density Function, continuous).

The ground station data was obtained from a public data source provided by the Southern African Universities Radiometric Network (SAURAN) [79] and data for 2018 to the end of 2019 was requested from this public source. This data source provides hourly averaged measured values for a variety of meteorological variables; however, just the *GHI* and *TCC* components were of concern for this work.

The measured *GHI* data was recorded by a SAURAN Weather Station mounted on the roof of an Engineering building at Stellenbosch University in Stellenbosch, South Africa. The *GHI* forecast data was retrieved via an API made available by Meteomatics AG, who are experts in meteorological data processing. These *GHI* forecasts were requested and saved daily for a full nine-day time horizon. Both datasets were processed in one-hour intervals for 24 months to ensure characteristics from all four seasons are included in the datasets. The only data considered was that which was gathered precisely between 06:00 to 18:00 each day, as the night-time data could have skewed the outcome of the analysis towards seemingly more accurate results. Generally, the *GHI* forecast for night-time is zero and the measurement at night will

also be near zero. A pre-analysis of the raw 24-month forecast and recorded *GHI* data, revealed that there are specific patterns in the accuracy of the prediction when considering the amount of *TCC* for a specific day as well as the forecast horizon. The daily mean *TCC* was used when the dataset was divided into the following four categories to group the most likely patterns observed: clear sky (when  $TCC \leq 2\%$  daily mean cloud cover),  $2\% < TCC \leq 33\%$ ,  $33\% < TCC \leq 66\%$  and  $66\% < TCC \leq 100\%$ .

Performance metrics similar to those used in the modelling chapter were used to evaluate the *GHI* forecast here. After the *GHI* error data had been pre-processed, an appropriate distribution function was needed to represent the *GHI* forecast error variation, which is shown later in Figure 18. While it is commonly found that *GHI* forecasts can be described by a normal distribution, this cannot however always be assumed. We made a visual inspection of the standard normal distribution plot superimposed onto the data distribution, inspected the QQ plot, found the kurtosis values and finally, made use of well-known normality hypothesis tests such as the Anderson-Darling test as well as the Kolmogorov-Smirnov test.

## EXPERIMENTAL RESULTS AND DISCUSSION

The performance metrics for the *GHI* forecast can be seen in Tables 11 to 14. The data has been grouped into four *TCC* categories: clear sky, and three categories where the *TCC* ranges between values just larger than zero up to 100 %. Through simple inspection of the rows of Table 12 to Table 14 (except for the *FB*) ranging from clear-sky (leftmost column) to 100 % *TCC* (rightmost column), a noticeable and almost unvarying ascending error trend is visible. This shows that the *MAE*, *RMSE* and *std* error values, between the *GHI* forecast and the actual values, generally increase with a rise in *TCC*, no matter if it is the next day or a nine-day- ahead forecast. A similar trend, although not as prominent and with less slope, can be observed upon inspection of the last two columns of Tables 12 and 14 (again except for the *FB*) when looking from the top of each column downwards (one day ahead at the top, to 9 days ahead at the bottom). The first two columns (clear sky and 1/3 *TCC*) exhibit much less of a trend and the variation seem more random. The *FB* table reveals that very little Forecast Bias is present, irrespective of the forecast horizon and the state of the *TCC*. No real trends can be identified in the *FB* results (Table 11).



**Table 11: Forecast Bias error**

<i>FB (percentage)</i>				
	Clear sky	$0 < TCC \leq 1/3$	$1/3 < TCC \leq 2/3$	$2/3 < TCC \leq 3/3$
1 day ahead	-0.1	0.7	-0.3	1.5
2 days ahead	0.3	0.3	-0.1	1.8
3 days ahead	0.2	1.0	0.4	1.0
4 days ahead	0.1	0.6	1.2	0.5
5 days ahead	0.1	1.0	0.5	-0.7
6 days ahead	0.8	1.0	0.5	-0.5
7 days ahead	0.1	0.7	1.0	-1.0
8 days ahead	0.2	1.7	-0.1	-0.7
9 days ahead	0.4	1.2	0.7	-2.6

**Table 12: Mean Absolute Error**

<i>MAE (percentage)</i>				
	Clear sky	$0 < TCC \leq 1/3$	$1/3 < TCC \leq 2/3$	$2/3 < TCC \leq 3/3$
1 day ahead	17.7	21.4	23.7	27.4
2 days ahead	17.0	21.0	23.1	28.9
3 days ahead	15.4	21.6	25.3	28.5
4 days ahead	16.8	20.7	25.6	28.1
5 days ahead	16.3	22.0	26.9	29.0
6 days ahead	20.3	22.3	25.7	30.7
7 days ahead	24.1	19.1	25.2	28.9
8 days ahead	21.3	21.3	26.9	28.8
9 days ahead	18.8	22.6	25.8	31.1

**Table 13: Root Mean Squared Error**

<i>RMSE (percentage)</i>				
	Clear sky	$0 < TCC \leq 1/3$	$1/3 < TCC \leq 2/3$	$2/3 < TCC \leq 3/3$
1 day ahead	25.5	30.2	31.5	36.1
2 days ahead	24.4	30.2	31.2	37.8
3 days ahead	22.6	30.2	34.4	37.6
4 days ahead	24.1	30.7	34.7	36.6
5 days ahead	23.3	31.3	35.7	36.6
6 days ahead	29.4	31.6	35.0	39.0
7 days ahead	34.0	27.5	34.1	38.1
8 days ahead	26.1	30.4	35.5	37.4

**Table 14: Standard deviation assuming a normal distribution**

<i>std (percentage)</i>				
	<b>Clear sky</b>	<b><math>0 &lt; TCC \leq 1/3</math></b>	<b><math>1/3 &lt; TCC \leq 2/3</math></b>	<b><math>2/3 &lt; TCC \leq 3/3</math></b>
<b>1 day ahead</b>	25.5	30.0	31.5	35.9
<b>2 days ahead</b>	24.4	30.2	31.2	37.4
<b>3 days ahead</b>	22.6	29.8	34.4	37.5
<b>4 days ahead</b>	24.1	30.5	34.3	36.6
<b>5 days ahead</b>	23.3	30.8	35.7	36.5
<b>6 days ahead</b>	29.1	31.3	35.0	39.0
<b>7 days ahead</b>	34.1	27.3	33.8	37.9
<b>8 days ahead</b>	34.2	29.4	35.6	37.4
<b>9 days ahead</b>	26.2	30.5	34.7	37.9

The *GHI* forecast error data distribution of the combined dataset exhibit a seemingly similar shape to that of the bell-shaped normal distribution (Figure 18) but fail both the Anderson-Darling test as well as the Kolmogorov-Smirnov tests with the standard 5 % confidence interval rejecting the null hypothesis that the data is normally distributed [80]. Furthermore, the Quantile-Quantile (QQ) plot of the combined datasets (Figure 17) reveals that the data is somewhat over-dispersed which means that the data has an increased number of outliers resulting in slightly heavier tails of the distribution function. A Kurtosis of 5.8 for the combined dataset corroborates the heavier tails as a positive Kurtosis [81] more significant than 3 indicates more peakedness of the data distribution around the mean in addition to more outliers at the tails.

By considering the different normality test results, it was concluded that the t-distribution function would describe the data better than a normal distribution function would. The t-distribution is popularly applied to data distributions with marginally heavier tails and more peakedness around the mean than the normal distribution. With a normal distribution, one standard deviation shows the confidence interval at a 68 % probability of the sample set, which is not necessarily the case with the t-distribution. The t-distribution requires the use of a t-score table or the Inverse Cumulative Distribution Function (ICDF) to calculate the confidence interval for a specified percentage probability of, for instance, 68 %.

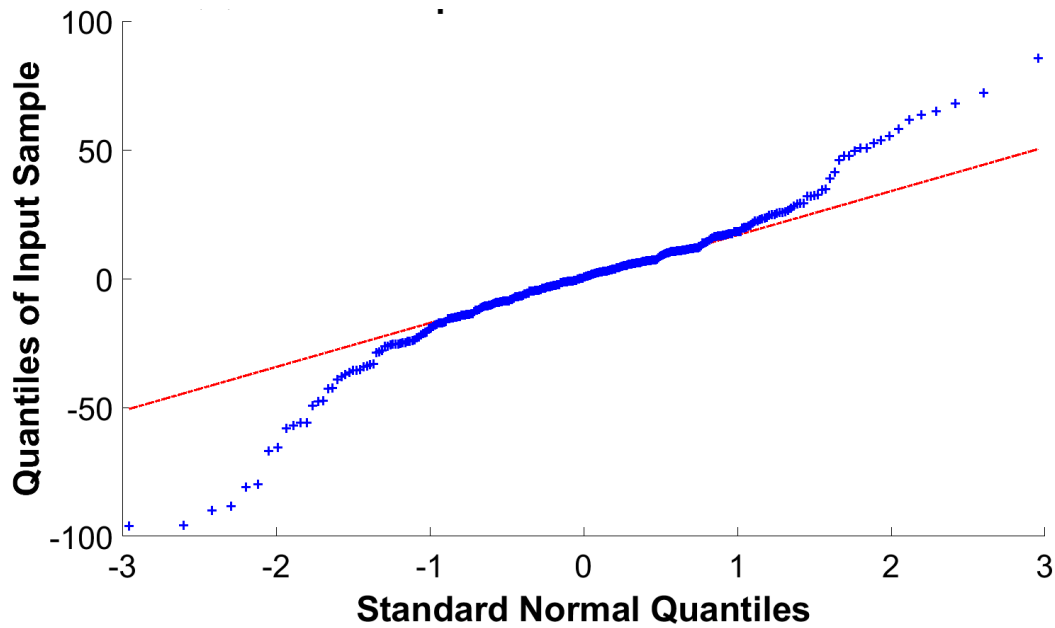


Figure 17: QQ plot of *GHI* forecast data

The red line in Figure 17 represent the line which the data would follow if both the control data set (typically normally distributed data) as well as the data set in question (*GHI* forecast error) was of the same distribution type, such as a normal distribution. The blue markers deviate from the straight red line which tells us that the dataset in question is not similar to the control dataset and therefore not normally distributed.

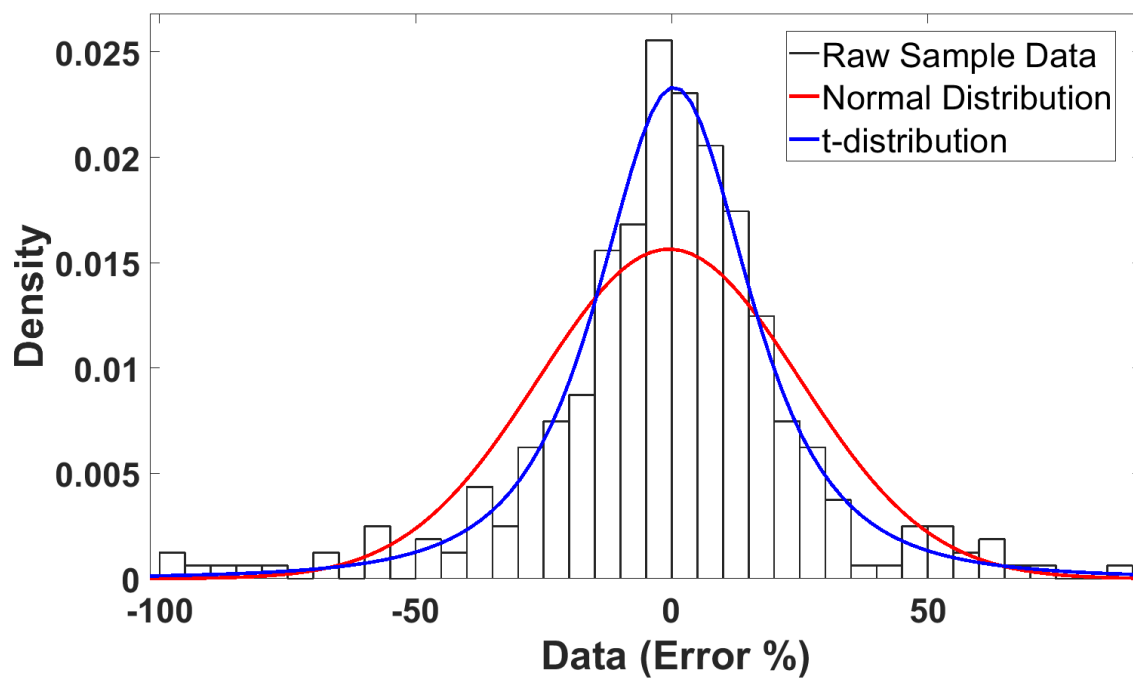


Figure 18: Normal vs t-distribution

Table 15 and 16 record the t-distribution function confidence intervals for 68 % (this percentage was used to easily compare with one standard deviation of a normal distribution; however, it can be found for any percentage interval desired) calculated as non-absolute percentage values to be used as upper and lower bounds. These upper and lower bounds are appropriate as they include the effects of the *FB* values (positive and negative forecast bias), which made them more useful for the solar car team. The upper and lower bounds meant that statistically, there was a 68 % chance that the *GHI* forecast would take on a value with a percentage error of equal or less than the upper bound and equal or greater than the lower bound. It was essential to recognise the differences between the upper and lower bounds of the t-distribution (Tables 15 and 16) and the values of one standard deviation of the standard normal distribution (Table 14). This is why it was critical to select the distribution function that best described the data (before constructing the confidence intervals). In this case, it was not a normal distribution.

**Table 15: T-distribution upper bounds (forecast confidence)**

Upper bounds				
	Clear sky	$0 < TCC \leq 1/3$	$1/3 < TCC \leq 2/3$	$2/3 < TCC \leq 3/3$
<b>1 day ahead</b>	19.5	25.5	24.3	38.7
<b>2 days ahead</b>	19.3	22.8	25.2	42.9
<b>3 days ahead</b>	16.9	28.0	30.0	38.7
<b>4 days ahead</b>	18.8	21.3	34.0	37.5
<b>5 days ahead</b>	18.1	27.8	35.4	31.3
<b>6 days ahead</b>	24.6	28.0	31.2	36.7
<b>7 days ahead</b>	26.0	22.7	34.2	32.3
<b>8 days ahead</b>	25.0	28.0	31.4	31.9
<b>9 days ahead</b>	23.6	32.0	32.5	25.6

**Table 16: T-distribution lower bounds (forecast confidence)**

Lower bounds				
	Clear sky	$0 < TCC \leq 1/3$	$1/3 < TCC \leq 2/3$	$2/3 < TCC \leq 3/3$
1 day ahead	-18.6	-22.3	-31.6	-30.9
2 days ahead	-17.9	-21.7	-28.8	-31.5
3 days ahead	-15.7	-20.1	-28.9	-33.4
4 days ahead	-17.3	-20.8	-26.1	-34.3
5 days ahead	-17.4	-20.4	-31.2	-38.7
6 days ahead	-18.1	-20.4	-29.8	-40.8
7 days ahead	-27.5	-17.0	-25.0	-40.3
8 days ahead	-22.4	-16.1	-33.5	-39.0
9 days ahead	-17.9	-20.4	-27.8	-46.8

If a normal distribution had been used for the upper and lower bounds (as in Table 14), then the analysis would have been a poor representation of the data and forecast error, possibly even misleading the energy manager. For this reason, it was important to choose the t-distribution to represent a specific dataset. The energy manager had the freedom to select the upper and lower bounds for a chosen confidence interval. Desired values of more than 68 % would have resulted in a wider confidence interval, meaning that statistically, the data was more likely to fall within the interval. However, the wide interval made it difficult for the energy manager to accurately estimate the amount of risk involved in the predicted *SoC* profile.

Similarly, desired values of less than 68 % would have resulted in a narrower confidence interval; meaning that statistically, the data would have been less likely to fall within the interval. The narrow interval however, made it easier for the energy manager to accurately estimate the *SoC* profile. This trade-off between the amount of risk taken and the accuracy required was left up to the energy manager to decide, based on their experience and intuition.

The upper and lower bounds were now able to be used (and added to a typical *SoC* simulation output from the Tshwane University of Technology energy management strategy) to provide some confidence intervals for the energy manager to be able to assess the risk involved when analysing the simulation results. Although other factors within the model could also cause the *SoC* to vary, we considered the model a good representation of the actual vehicle dynamics [15] which meant that a variation of the

*GHI* component would have a large effect on the *SoC*. Figure 19 represents the *SoC* simulation (one-day forecast) compared to actual results for the first day of the Sasol Solar Challenge 2018 for the Sun Chaser III vehicle's model with the developed *GHI* confidence intervals. The team covered a total of 493 km over eight hours that day. The simulation that produced this figure is discussed in detail in the following chapters. The clouds on this day were initially low at about 20 % *TCC* in the morning, descending until around midday, after which the cloud cover increased steadily to about 70 % at 16:00.

The confidence intervals in Figure 19 demonstrate room for improvement and sharpening of the intervals as the actual and estimated *SoC* results are quite far from the interval borders.

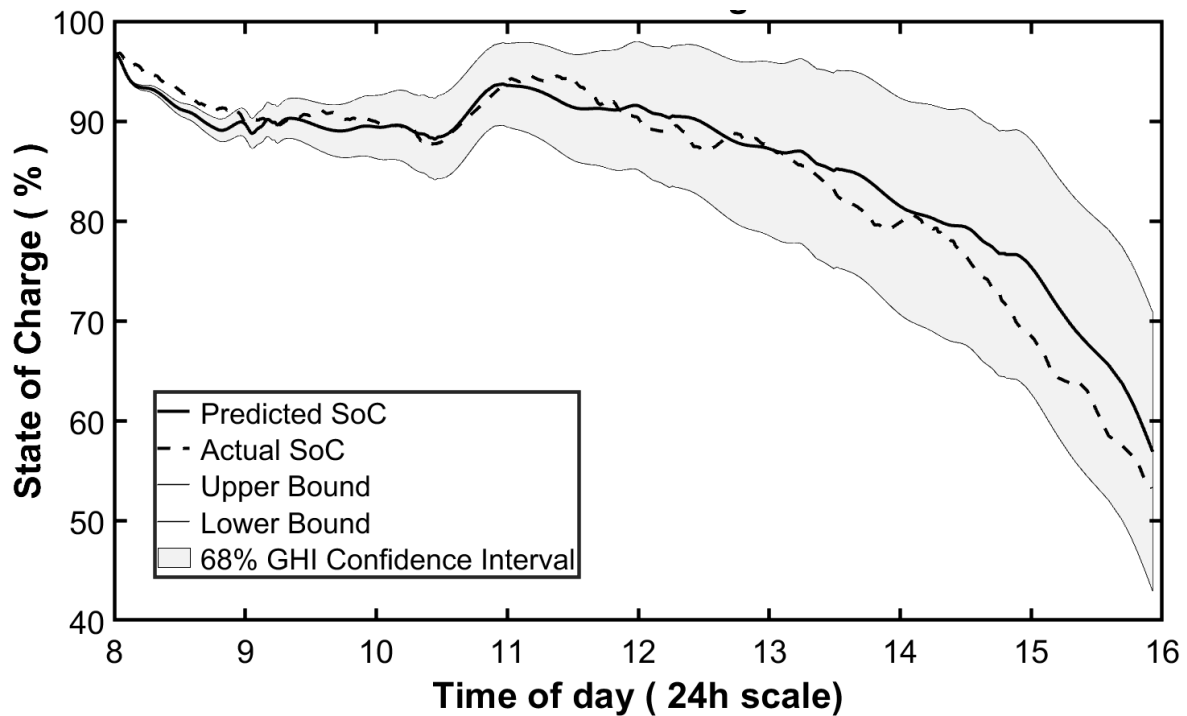


Figure 19: *GHI* confidence intervals

## EXPERIMENTAL CONCLUSIONS

This section presented the methodology of evaluating the forecast performance of the *GHI* component for the South African region. This was done by making use of 24 months of weather station-based measured data as well as forecasted data for a specific location in South Africa. Some performance metrics were used to describe the

relationship between the predicted and the actual data. The *GHI* forecast performance is shown for various cloud conditions as well as for a forecast horizon of nine days. In general, an increasing error trend can be seen with an increase in clouds as well as some trend with the increase in the forecast horizon. The t-distribution was used to create probability mass functions as the data was seen to be non-normally distributed. Upper and lower bounds were found for the 68 % confidence interval of the t-distributions. The upper and lower limits of this confidence interval were graphically used to assist the energy manager in assessing the forecast and simulation risk involved and its effect on the vehicle energy (i.e. its' *SoC*).

## **FORECAST BIAS CORRECTION**

To increase the *GHI* forecast performance (that is to say, to tighten the upper and lower confidence bounds without losing robustness of the intervals), a forecast bias correction can be applied. Although Table 11 shows minimal bias present, these are daily averaged values evaluated for the forecasts of a whole day on average. To reveal a higher resolution forecast bias, it is necessary to analyse for every hour of the day (07:00 to 17:00).

This was done by taking twelve random months' data (from the sample set collected as explained in the previous sections) as training data and the remaining twelve months' data for validation purposes. The forecast and actual data was compared on an hourly basis to find the average forecast bias error percentage per hour. Figure 20 shows the *GHI* forecast bias error percentage results on an hourly basis for the twelve months of random sample data.

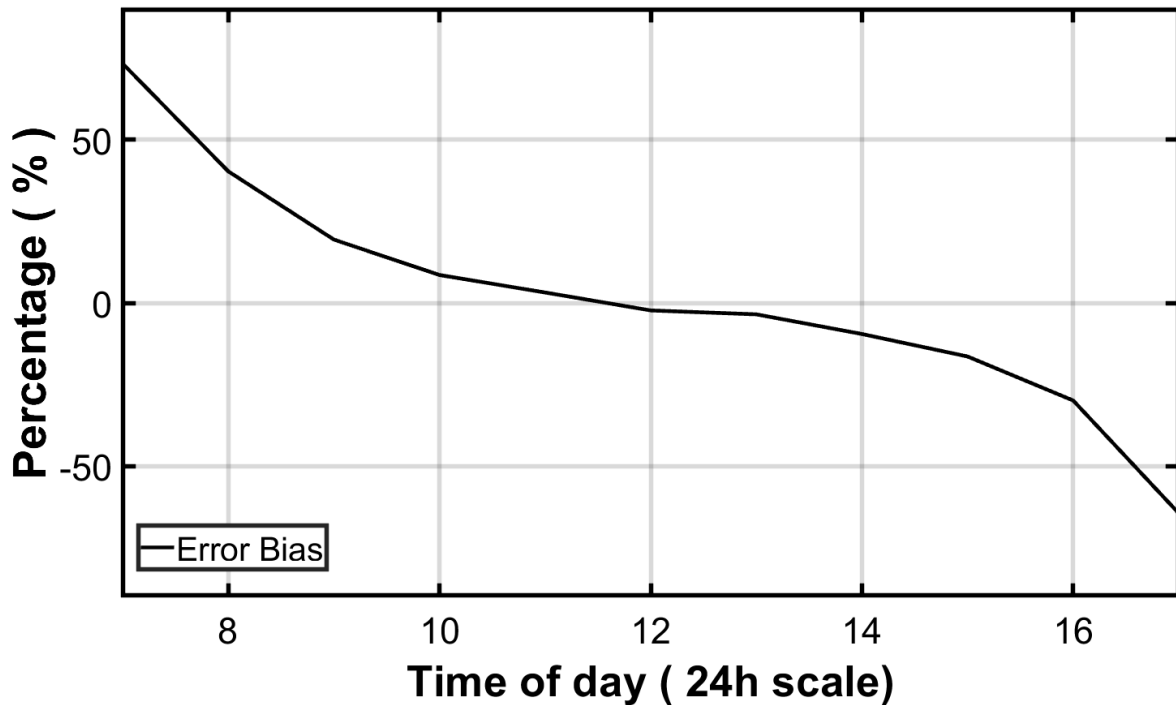


**Figure 20: Forecast bias**

The evaluation indicated that the forecast generally over-predicts in the morning, under-predicts in the evening and displays relatively low mean errors between 10:00 and 14:00. It is important to note that a 50 % forecast bias in the early morning or late afternoon does not necessarily constitute large solar irradiance error values and might be as small as  $10 \text{ W.m}^{-2}$ . The *GHI* magnitude in the morning and afternoon are much lower than the *GHI* magnitude in the middle of the day. This hourly forecast bias function represents the combined *TCC* conditions, and the average of the combined hourly function is 0.39 % *FB* which is approximately equal to the average of all the *FB* values of Table 11 (which is 0.37 %). This validates the results as it was expected to see approximately similar *FB* (however, not exactly the same, because Table 11 used 24-month data and the hourly forecast bias function used only half of this data). We now possess a *FB* function, the inverse of which can be applied to all *GHI* forecasts at each hour to reduce the bias in the forecast and improve (narrow down) the confidence interval of the prediction.

After applying the hourly mean forecast bias correction to the resulting 12 months' validation forecast data and comparing to the actual data, an average improvement of approximately 23 % (based on the old upper and lower bounds) is noticeable when comparing Table 17 and 18 (forecast bias compensated) with Table 15 and 16 (raw



performance of Meteomatics AG forecast). This improvement means that for the same 68 % confidence interval, the *GHI* forecast error is now on average 23 % more likely to fall closer to zero (the desired improvement) after making use of the hourly forecast bias correction method. The improved distributions and confidence intervals are still described by a t-distribution similar to the raw Meteomatics AG forecast data.

**Table 17: Upper bounds (Forecast Bias compensated)**

Upper bounds (percentage)				
	Clear sky	$0 < TCC \leq 1/3$	$1/3 < TCC \leq 2/3$	$2/3 < TCC \leq 3/3$
1 day ahead	14.4	19.9	19.1	29.0
2 days ahead	14.7	17.4	19.2	32.5
3 days ahead	12.8	21.8	23.4	29.0
4 days ahead	14.2	16.9	26.9	28.5
5 days ahead	13.2	21.7	28.0	23.9
6 days ahead	18.6	21.2	24.8	27.9
7 days ahead	19.4	17.7	27.0	24.2
8 days ahead	18.3	21.2	24.2	23.1
9 days ahead	17.7	25.0	25.7	19.8

**Table 18: Lower bounds (Forecast Bias compensated)**

Lower bounds (percentage)				
	Clear sky	$0 < TCC \leq 1/3$	$1/3 < TCC \leq 2/3$	$2/3 < TCC \leq 3/3$
1 day ahead	-14.0	-17.9	-25.0	-23.0
2 days ahead	-13.0	-16.1	-22.0	-23.1
3 days ahead	-11.2	-15.3	-22.1	-25.7
4 days ahead	-13.8	-16.3	-20.1	-25.3
5 days ahead	-13.6	-15.2	-24.6	-29.5
6 days ahead	-13.9	-15.1	-23.8	-30.6
7 days ahead	-20.0	-13.3	-19.9	-30.1
8 days ahead	-16.0	-12.6	-26.5	-29.3
9 days ahead	-13.0	-15.1	-22.7	-35.9

It is important to note that this hourly *FB* correction only applies to a particular region; in this case, Stellenbosch, South Africa. The results could be less accurate, although still acceptable, when applied to forecasts significantly further away from this location.

Figure 21 illustrates the narrower confidence intervals as a result of the *FB* compensation. Here it may be quite distinctly seen that even though a reasonably trivial hourly *GHI* forecast bias compensation has been applied, the intervals are narrower and provide more confidence to the energy user. It is interesting to note that on both Figures 19 and 21 at the very start of the *SoC* curves, the actual *SoC* lies outside the confidence interval. This may well not have anything to do with the accuracy of *GHI* forecast, but rather other influences such as: driving slower than the optimal speed profile yielding higher actual *SoC* than expected.

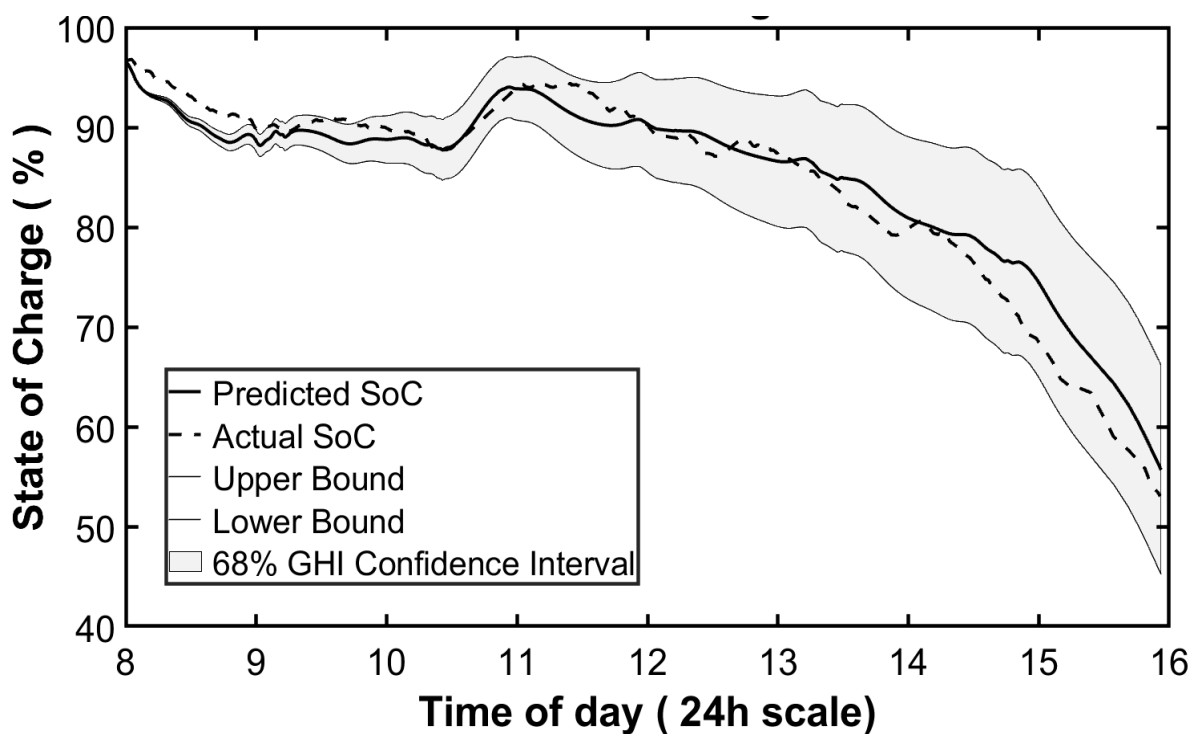


**Figure 21: *GHI* Confidence intervals (Forecast bias compensated)**

It should also be noted that the upper and lower bound values (Tables 17 and 18) are very similar in magnitude (but differ in sign) and can, therefore, be combined as an absolute value confidence interval for ease of use. When applied as upper and lower bounds, the inclusion of the appropriate sign (positive or negative) has to be made.

In the literature review chapter of this work, a baseline forecast performance for the *GHI* component, as seen from the ECMWF model, was given in Table 5. This baseline performance figure refers to one-day-ahead clear-sky-only forecast. In Table 19, the

first section of the table shows the forecast performance of the raw data as received from the Meteomatics AG API compared to the actual measured data. The forecast performance (*RMSE*) saw a significant improvement after being processed by the Meteomatics AG server and outperformed the baseline up to a five-day-ahead clear sky *GHI* forecast. The second section of Table 19 contains the compensated forecast performance in terms of *RMSE*. Here, a further improvement is evident for all cloud conditions. This forecast performance improvement validates and complements the improved results of the forecast correction method seen in Tables 17 and 18 and Figure 21.

**Table 19: *RMSE* comparison**

<b><i>RMSE</i>, before compensation (<math>\text{W.m}^{-2}</math>)</b>				
	<b>CS</b>	<b><math>0 &lt; TCC \leq 1/3</math></b>	<b><math>1/3 &lt; TCC \leq 2/3</math></b>	<b><math>2/3 &lt; TCC \leq 3/3</math></b>
<b>1 day ahead</b>	79.7	134.1	130.8	128.5
<b>2 days ahead</b>	85.0	130.4	126.1	144.4
<b>3 days ahead</b>	76.2	138.6	140.0	149.7
<b>4 days ahead</b>	87.9	124.6	155.5	147.7
<b>5 days ahead</b>	87.4	164.2	156.5	155.2
<b>6 days ahead</b>	144.8	163.0	179.9	151.5
<b>7 days ahead</b>	148.1	161.8	185.5	146.0
<b>8 days ahead</b>	147.0	174.4	178.3	153.9
<b>9 days ahead</b>	207.3	177.6	165.1	171.6
<b><i>RMSE</i>, after compensation (<math>\text{W.m}^{-2}</math>)</b>				
	<b>CS</b>	<b><math>0 &lt; TCC \leq 1/3</math></b>	<b><math>1/3 &lt; TCC \leq 2/3</math></b>	<b><math>2/3 &lt; TCC \leq 3/3</math></b>
<b>1 day ahead</b>	58.6	114.7	113.2	124.0
<b>2 days ahead</b>	71.6	113.7	108.4	138.9
<b>3 days ahead</b>	68.9	123.4	127.9	144.3
<b>4 days ahead</b>	78.2	111.2	136.6	142.2
<b>5 days ahead</b>	85.7	148.3	134.3	153.5
<b>6 days ahead</b>	132.9	140.6	169.1	146.2
<b>7 days ahead</b>	136.5	137.5	170.4	136.7
<b>8 days ahead</b>	133.7	147.3	165.9	147.8
<b>9 days ahead</b>	198.0	155.9	144.9	167.7

## MODEL OUTPUT STATISTICS

Further deeper analysis and characterisation in regard to the probabilistic nature of the *GHI* component can also result in an improvement in forecast accuracy as well as more reliable confidence intervals. The aim is to use conditional probabilities (with multiple variables) based on the expected value of the *GHI* in certain situations of clouds, time of day, forecast horizon and geographical location to achieve this goal.

### Experimental equipment and procedure

Ground station measured data has been taken from strategic locations along the typical SSC route in South Africa. The chosen locations were Pretoria (University of Pretoria), Bloemfontein (Central University of Technology), Port Elizabeth (Nelson Mandela University) and the Cape Town area (Stellenbosch University).

SAURAN has a total of 23 ground measurement stations across South Africa. However, the limitation of a maximum allowed daily data point requests imposed by the forecast provider (Meteomatics AG), limited the Application Program Interface (API) requests to four locations in South Africa per day only. All four cities are major stopover locations for the SSC event and span the entire route from start to finish. Forecast data for all four locations were made available by Meteomatics AG. An API script was developed and used over 24 months to request the *GHI* and *TCC* daily forecast for each of the four locations over a nine-day horizon. This data was then stored in a multi-dimensional matrix format (MATLAB®) with an appropriate date and location information stamp for identification. At the end of the API script, an email is daily automatically generated and sent to the researcher to verify that the data has been received as expected. In this study, after all the forecast data had been captured for the two years, the SAURAN ground station based data was imported into the MATLAB® environment with some initial pre-processing of the data. Night-time data of each day was then appropriately removed. This reduced the risk of having bias results; as previously mentioned, night time *GHI* data is not statistically meaningful (near zero values). The forecast and the measured data for each of the four locations were then analysed and compared.

To increase the local *GHI* forecast performance (compared to the raw Meteomatics AG forecast as well as forecast bias correction), a Model Output Statistics (MOS)

correction function was developed and applied to the data in the form of a simple multiplication scaling function. As the *GHI* forecast is available in a one-hour resolution, it is appropriate to create a MOS correction function for every hour between 06:00 and 18:00. Twelve of the months' data was used to develop the MOS correction function. In contrast, the remaining twelve-month data was used for validation and to test the performance of the improved MOS based *GHI* local forecast model. With the initial analysis in the previous section of the raw Meteomatics AG data and the forecast bias correction, an initial four categories of *TCC* was sufficient for grouping forecast error trends. While this section aimed to improve the accuracy further, a higher resolution forecast error trend grouping was appropriate and therefore increased the *TCC* categories to five.

The MOS correction function is deterministic and was found by using the expected value of the conditional probability based on the *TCC* (with clear sky and four 25 % increasing intervals, which yields five *TCC* categories), the forecast horizon (*day*) as well as the hour of the day (*h*) as shown in Equation (26).

$$f_{MOS} = E\{GHI|TCC, day, h\} \quad (26)$$

To expand this MOS correction function to a GMOS (Gridded Model Output Statistics) function, we can rewrite Equation (26) to include an interpolated value of the forecast characteristics of the two nearest of the four sites based on the current location (*gps*) of the car as a further conditionality:

$$f_{GMOS} = E\{GHI|TCC, day, h, gps\} \quad (27)$$

Equation (27) now contains the statistically improved expected value of the *GHI* forecast based on the cloud conditions, the forecast horizon with the time of day as well as the location of the car on the route. The improved GMOS *GHI* model is based on statistical knowledge of the mean conditional hourly error. This does however not wholly ratify all error variation, and thus some of the error will still be present in the output results. For this reason, the energy simulation user needs to comprehend this remaining error variation in a simple yet useful manner. This was achieved by determining the improved probability or confidence interval of the expected GMOS

*GHI* forecast by creating a probability mass function of the remaining error variation. The desired confidence interval of 68 % was chosen (which is one standard deviation, but any range between 0 % and 100 % may be selected) and upper and lower forecast confidence bounds were developed. These bounds further assist the user in assessing the risk involved with the expected value output of Equation (27). The GMOS error probability mass function is given by Equation (28).

$$ePMF_{GMOS} = P(GHI|TCC, day, h, gps) \quad (28)$$

By applying the GMOS *GHI* correction function in Equation (27) and the forecast confidence function in Equation (28) to the *SoC* energy simulation of the solar car, the user is equipped with more accurate *SoC* results in addition to robust confidence intervals which reveals the risk involved in the simulation. The *SoC* error is not solely dependent on the accuracy of the *GHI* forecast but it has been shown [15] that with an accurate electromechanical mathematical model describing the energy behaviour of the vehicle, the *SoC* error is not solely dependent on the accuracy of the *GHI* forecast but about 94 % of the *SoC* error is due to weather forecast error, in which *GHI* error predominates.

## Experimental results and discussion

Tables 20 through 23 contain the results of the t-distribution standard deviation of the raw Meteomatics AG *GHI* prediction error (as seen in the t-distribution values of Tables 15 and 16) as well as the improved localised GMOS t-distribution standard deviation prediction error values. All the values are shown as relative error percentages. Figure 22 contains a summary of the cloud cover days of the sample set for each of the four locations based on the five newly identified categories.

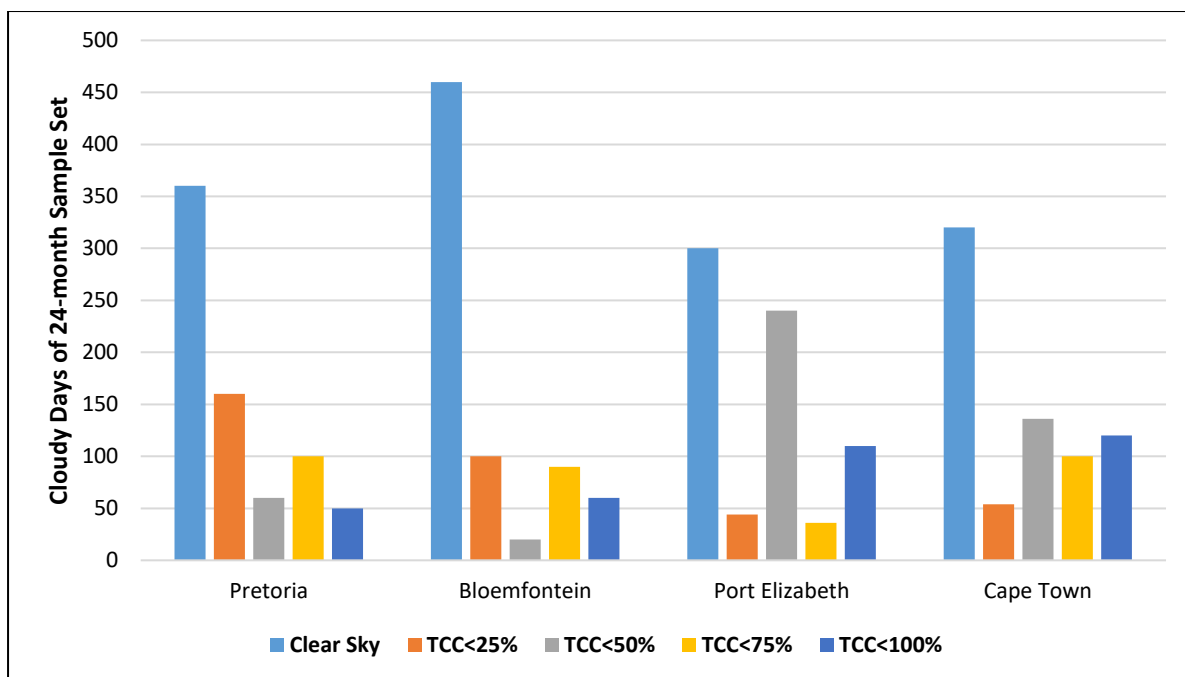


Figure 22: Cloudy days summary (GMOS)

Table 20: Standard deviation comparison, Pretoria

Forecast horizon (days)	Clear Sky		0%<TCC ≤25%		25%<TCC ≤50%		50%<TCC ≤75%		75%<TCC ≤100%	
	raw	GMOS	raw	GMOS	raw	GMOS	raw	GMOS	raw	GMOS
One	20.3	8.1	23.2	16	25.8	17.5	29.6	21.9	31.5	26.8
Two	20.6	8.3	24.8	19.1	26.3	25	32	26.8	33.6	26.9
Three	18.2	11.5	21.7	14.4	24.3	18.1	30.5	21.4	32.3	28.8
Four	20.5	10.9	26.4	17.8	28.2	19.3	32.2	22.6	34.2	28.9
Five	19	10.8	24.7	15.2	23.7	14.5	33	24.9	34.3	22.8
Six	23.3	12.8	25.8	17.9	29.3	19.8	32.1	23.9	34.9	26.2
Seven	27.8	10.5	21	12.9	19.6	13.5	30.8	20.5	32.5	22.7
Eight	30.8	12.8	23.7	15.7	25.4	17.2	31.5	24.6	33.7	25
Nine	21.5	13	22.5	14.6	26.1	15	28.5	23.8	33.4	29.1

**Table 21: Standard deviation comparison, Bloemfontein**

Forecast horizon (days)	Clear Sky		0%<TCC ≤25%		25%<TCC ≤50%		50%<TCC ≤75%		75%<TCC ≤100%	
	raw	GMOS	raw	GMOS	raw	GMOS	raw	GMOS	raw	GMOS
One	20.5	9.3	22.7	15.6	25.9	17.4	27.4	21.6	30.4	23.7
Two	23.1	8.7	24.5	20.3	28.1	18.2	32.3	25.8	35.7	25.4
Three	16	10.2	22.9	12.3	24.8	16.9	28.7	21.8	30.2	27.1
Four	20.3	10.9	25	14.5	26.5	18.8	30.7	22.6	32.8	30
Five	18.7	11.5	24.8	15	24.8	19.4	30.5	24.9	33.7	26.3
Six	25.4	11.2	25.5	17.6	27.8	20.9	32.7	24.1	34.3	28.9
Seven	27.9	13	19.9	12.9	22	14	30.4	23.3	29.6	28.1
Eight	26.5	11.5	23.4	15.8	29.7	16.6	31.6	23.6	34.8	29.6
Nine	22.2	14.5	23.8	14.2	25.4	16.3	30.9	23.8	31.4	32.9

**Table 22: Standard deviation comparison, Port Elizabeth**

Forecast horizon (days)	Clear Sky		0%<TCC ≤25%		25%<TCC ≤50%		50%<TCC ≤75%		75%<TCC ≤100%	
	raw	GMOS	raw	GMOS	raw	GMOS	raw	GMOS	raw	GMOS
One	14.8	7	16.9	12.8	24.9	15	26.8	19.2	30.7	20.2
Two	15.4	7.3	20.9	12.7	27	12.6	32.1	20.5	33.9	22.8
Three	13.2	8.9	13.8	11.5	24.8	18.9	27.4	18.3	29.9	20
Four	13.7	7.9	25.5	16.7	27.4	20.8	33.5	21.3	34.4	25.7
Five	15.9	10.1	18.9	14.8	25	17.2	30	19.6	31.4	19.1
Six	17.5	9.5	26.2	15.1	27.3	21.4	30.5	22.2	29.3	28
Seven	19	12.8	20.1	16.8	20.6	20	25.1	19.2	29.4	30
Eight	17.4	15	22.4	15.9	26.9	18	30.5	22	32.2	27
Nine	18.6	15.7	17	15.4	25.1	20.1	29.3	22.7	31	31.1



Table 23: Standard deviation comparison, Stellenbosch

Forecast horizon (days)	Clear Sky		0%< $TCC$ ≤25%		25%< $TCC$ ≤50%		50%< $TCC$ ≤75%		75%< $TCC$ ≤100%	
	raw	GMOS	raw	GMOS	raw	GMOS	raw	GMOS	raw	GMOS
One	19.5	10.8	21.6	14.7	20.3	15.1	27.6	21.4	38.7	27.3
Two	19.3	11.6	23.4	12.9	25.8	15.4	31.5	26.1	42.9	33.0
Three	16.9	12.1	21	13.2	23.1	17.5	27.1	22.4	38.7	24.2
Four	18.8	9.2	22.5	17.5	26	22.2	29.3	23.0	37.5	30.5
Five	18.1	13.1	14.8	17.5	19.9	10.5	30.5	18.7	31.3	23.7
Six	24.6	14.5	24.6	15.9	29.4	18.4	29.9	26.9	36.7	34.2
Seven	26.0	15.8	19.8	18.3	14.7	20.8	28.5	21.4	32.3	22.3
Eight	25.0	15.9	23	16.8	23.9	22.7	34.1	30.1	31.9	24.0
Nine	23.6	15.3	21.2	18.4	19.4	23.3	28.2	23.2	25.6	28.6

The average forecast error improvement across all sites is given in Figure 23. The figure contains values based on the average difference between the raw  $GHI$  and the GMOS forecast for the full forecast horizon, including the condition of the sky (the value of  $TCC$ ).

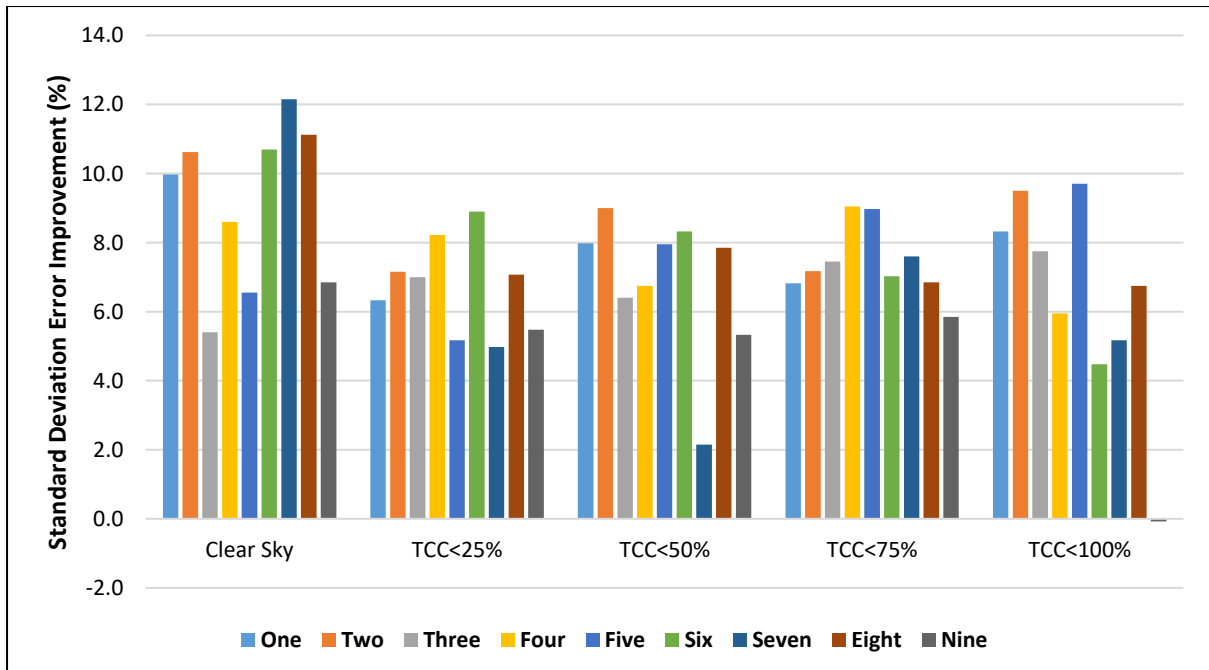


Figure 23: Standard deviation improvement (GMOS)

Significant forecast improvements were achieved with clear sky conditions, but decreasing in performance as the sky is covered with more clouds. It is however interesting to note the somewhat-out-of-trend error improvement of the  $50\% < TCC \leq 75\%$ , which may require further investigation in future work. Table 24 contains the average forecast performance of the four locations combined.

**Table 24: Standard deviation comparison, an average of all sites**

Forecast horizon (days)	Clear Sky		$0\% < TCC \leq 25\%$		$25\% < TCC \leq 50\%$		$50\% < TCC \leq 75\%$		$75\% < TCC \leq 100\%$	
	raw	GMOS	raw	GMOS	raw	GMOS	raw	GMOS	raw	GMOS
One	18.8	8.8	21.1	14.8	24.2	16.3	27.9	21.0	32.8	24.5
Two	19.6	9.0	23.4	16.3	26.8	17.8	32.0	24.8	36.5	27.0
Three	16.1	10.7	19.9	12.9	24.3	17.9	28.4	21.0	32.8	25.0
Four	18.3	9.7	24.9	16.6	27.0	20.3	31.4	22.4	34.7	28.8
Five	17.9	11.4	20.8	15.6	23.4	15.4	31.0	22.0	32.7	23.0
Six	22.7	12.0	25.5	16.6	28.5	20.1	31.3	24.3	33.8	29.3
Seven	25.2	13.0	20.2	15.2	19.2	17.1	28.7	21.1	31.0	25.8
Eight	24.9	13.8	23.1	16.1	26.5	18.6	31.9	25.1	33.2	26.4
Nine	21.5	14.6	21.1	15.7	24.0	18.7	29.2	23.4	30.4	30.4

Throughout Tables 20 to 23 it is evident that the *GHI* forecast accuracy deteriorates gradually with an increase in *TCC*. This is probably due to the increasing difficulty of forecasting *GHI* accurately due to the accumulation of clouds [82]. No significant error increment trend when observing the forecast horizon was found in this study. On average, the coastal location of Port Elizabeth (Table 22) is seen to have the best clear sky raw *GHI* as well as GMOS forecast performance. As the same method of analysis and compensation was applied to all four locations, the higher forecast errors at the remaining three locations can only be explained by some deficiency or characteristic behaviour of the ECMWF source model forecast used by Meteomatics AG.

The mean forecast performance standard deviation error of the raw *GHI*, forecast bias corrected *GHI* and GMOS *GHI* model for the combination of the four sites across the whole forecast horizon is as follows:

• Clear sky:	20.6 %,	15.9 %,	11.4 %
• $0\% < TCC \leq 25\%$ :	22.2 %,	18.1 %,	15.5 %
• $25\% < TCC \leq 50\%$ :	24.9 %,	22.3 %,	18.0 %
• $50\% < TCC \leq 75\%$ :	30.2 %,	25.3 %,	22.8 %
• $75\% < TCC \leq 100\%$ :	33.1 %,	27.5 %,	26.7 %

Values were interpolated from sections which had just four *TCC* categories to create five comparable values between the raw forecast and each of the two methods of improvement detailed in this chapter, namely the Forecast Bias correction as well as the GMOS model implementation.

These mean forecast performance standard deviation error values subsequently confirm the expected increasing error trend with the increase in cloud cover [82]. An overall (all cloud conditions and all forecast horizon over all four locations) mean forecast performance standard deviation error improvement of 4.4 % is observed after the forecast bias correction function was applied to the raw Meteomatics AG t-distribution data and a 7.3 % standard deviation error improvement with the application of the GMOS model to the raw Meteomatics AG t-distribution data.

The solar car team from Tshwane University of Technology (TUT) participated in the SSC2018 with a car by the name of Sun Chaser III. The team had developed an energy simulation platform to assist the energy manager in making informed decisions in regard to the speed and distance they could travel each day. This was based on the dynamics of the car, the route to be driven, the weather conditions and other characteristics such as remaining stored battery energy. In 2018, these *SoC* simulations did not yet make use of the GMOS model described here. The authors [83] showed simulated *SoC* results compared to recorded data during the SSC2018 for Sun Chaser III. Figures 24 to 26 show how the GMOS model could have improved the *GHI* forecast accuracy for the same data and how this relates to an improvement in the predicted *SoC* for this solar car. The authors referred to three specific days (Day one, six and eight) in the SSC2018 where factors of weather parameters and driving

speed negatively influencing the *SoC* were minimal, leaving the *GHI* prediction accuracy to be one of the significant contributors to the remaining *SoC* errors observed on these days. Table 25 provides a summary of the three days mentioned.

**Table 25: SSC2018, SCIII results (Day 1,6,8)**

SSC2018 Day	Date	Origin and destination	Distance travelled (km)	Nearest ground stations
One	22/09/2018	Pretoria to Kroonstad via Sasolburg	493	Pretoria and Bloemfontein
Six	27/09/2018	Port Elizabeth to Sedgefield via Kareedouw	371	Port Elizabeth and Stellenbosch
Eight	29/09/2018	Swellendam to Stellenbosch via Bredasdorp	403	Port Elizabeth and Stellenbosch

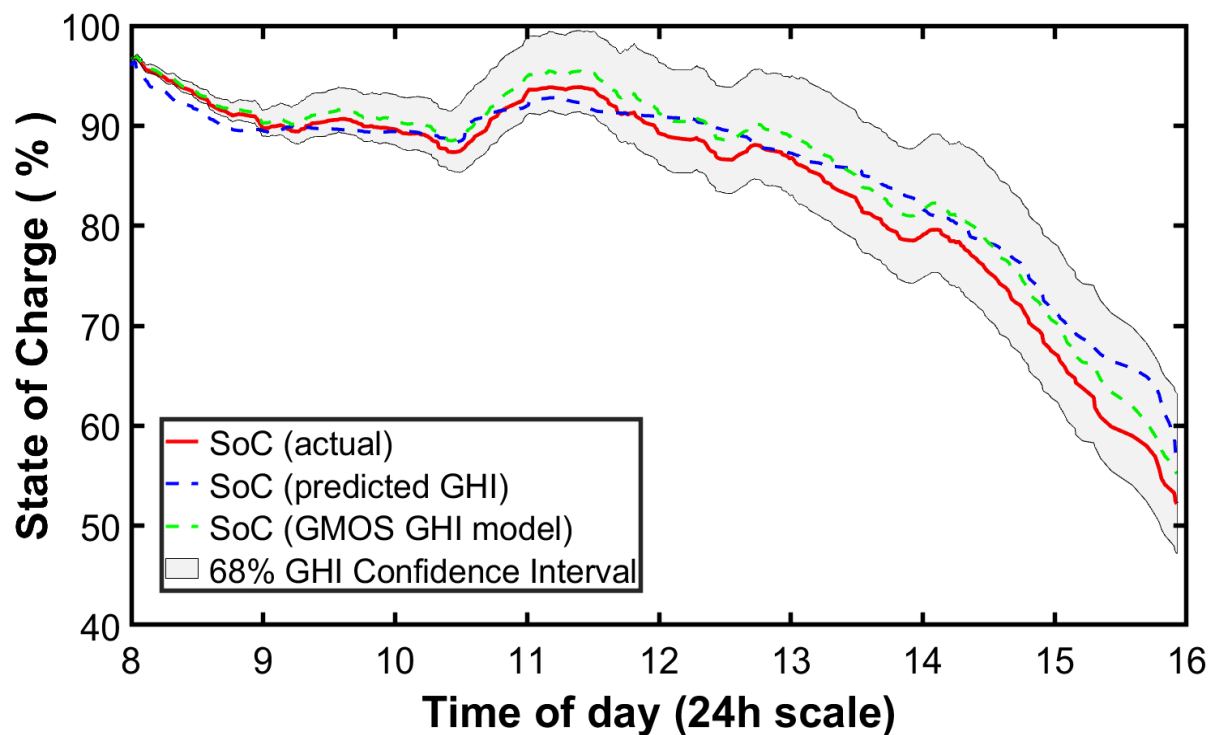


**Figure 24: SSC2018 Day 1, *SoC* comparison (GMOS)**

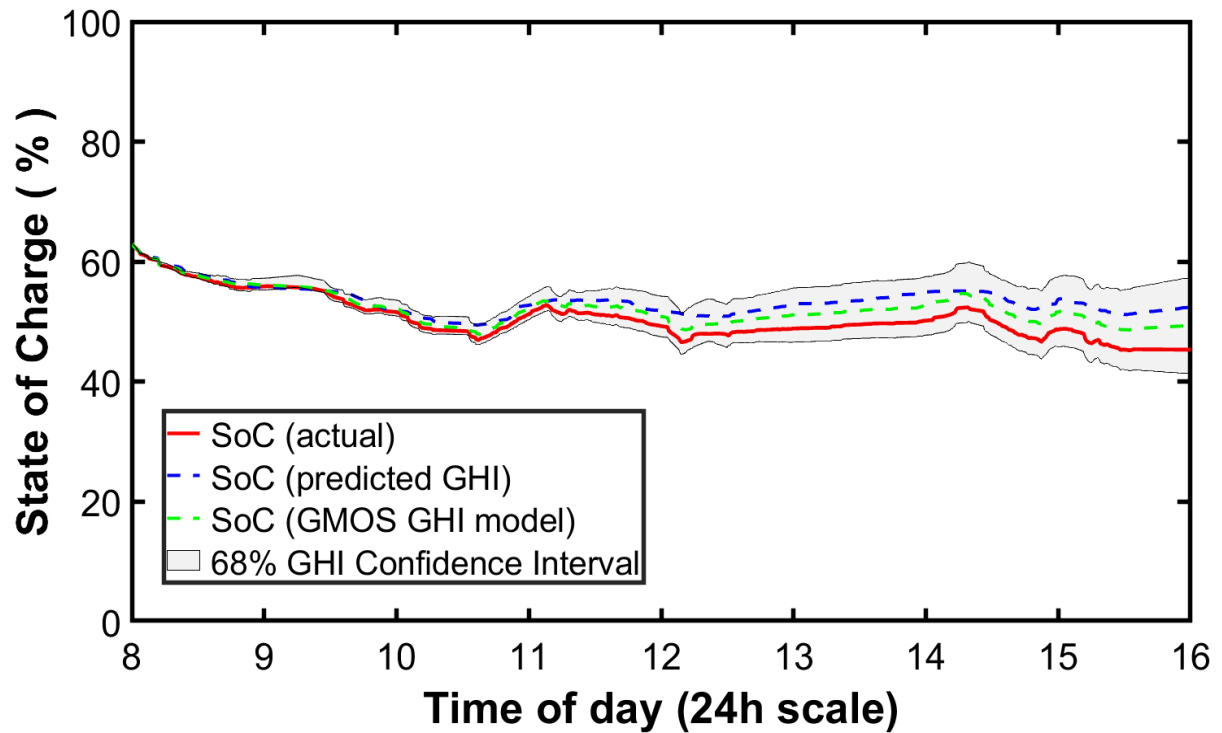


Figure 25: SSC2018 Day 6, *SoC* comparison (GMOS)

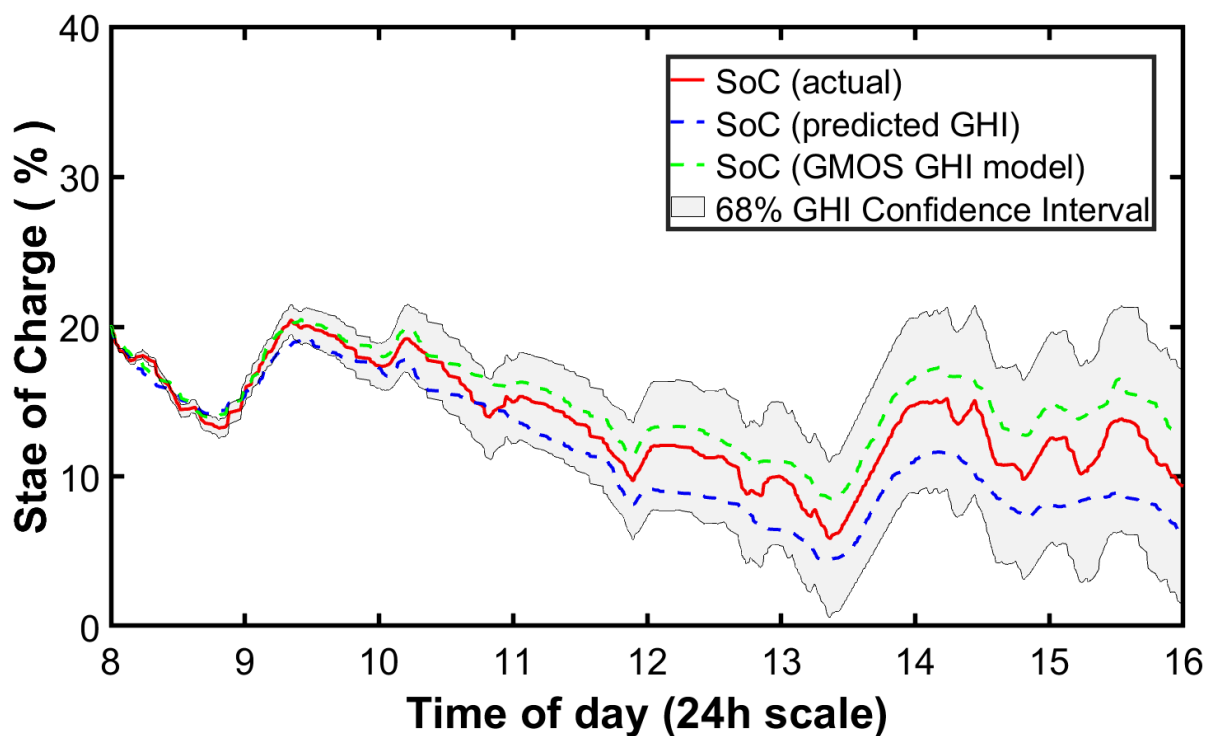


Figure 26: SSC2018 Day 8, *SoC* comparison (GMOS)

These figures, Figures 24 to 26, also contain the GMOS *GHI* one standard deviation (one-sigma) upper and lower bounds (confidence intervals). These confidence

intervals are based on compounding forecast errors of the maximum expected GMOS *GHI* standard deviation errors. *SoC* forecast improvements are observed on all days; the first two days the GMOS *GHI* model followed suit and yet still over predicted; however, with fewer errors than the original prediction. On the last day (Day 8, Figure 26), the original model under-predicted where the GMOS model yet again over-predicted, however, with less absolute error. Table 26 records the GMOS performance results for the three days of the Sasol Solar Challenge 2018. It contains the actual, raw *GHI* predicted as well as GMOS based *SoC* final values. In addition, the *RMSE* for the *SoC* is recorded here, too.

**Table 26: GMOS performance results**

<b>SSC2018 Day</b>	<b><i>SoC RMSE:</i> raw <i>GHI</i></b>	<b><i>SoC RMSE:</i> GMOS <i>GHI</i></b>	<b>Final <i>SoC</i>: Actual</b>	<b>Final <i>SoC</i>: raw <i>GHI</i></b>	<b>Final <i>SoC</i>: GMOS <i>GHI</i></b>
<b>One</b>	1.62	1.40	51.04	58.06	56.51
<b>Six</b>	1.02	0.75	45.22	53.85	49.21
<b>Eight</b>	2.01	1.16	10.10	6.18	13.31

The mean *SoC RMSE* of the initially predicted *GHI* forecast is 1.55 %, in contrast with the improved GMOS *SoC RMSE* at a reduced 1.10 %. Considering the final *SoC* of each day, the GMOS *GHI* model had the most significant impact on Day 6 (4 % *SoC* closer to the actual *SoC*) and the smallest impact (1 % *SoC* closer to the actual *SoC*) on Day 8. The reason for this is that Day 6 had the lowest wind and other weather variable errors [83] on the day leaving the *GHI* accuracy to have a significant impact on the *SoC*. Day 8, however, had significant wind forecast errors (nearly double those of Day 6) which resulted in the effectiveness of the improved *GHI* accuracy to be less prominent on the *SoC* for that day. In addition to the *SoC* improvements, the energy simulation user is now also able to visualise the amount of statistical risk involved in a simulation, aiding in critical decision making regarding the energy of the vehicle.

## **Experimental conclusion**

It is essential to mention the effectiveness of the interpolation between the MOS models (Equation (26), for all four locations), which gave birth to the GMOS model

(Equation (27)). Each of the three days evaluated in the previous section was re-simulated with a MOS model of the nearest ground measurement location to the vehicle's rear, as well as with a MOS model of the nearest ground measurement location to the front of the car. This was done in order to quantify the performance effect it would have on the *SoC* in comparison (Table 27) to the interpolated GMOS model's performance.

**Table 27: GMOS vs MOS performance results**

SSC2018 Day	<i>SoC</i> <i>RMSE</i> : MOS <i>GHI</i> (rear location)	<i>SoC</i> <i>RMSE</i> : MOS <i>GHI</i> (front location)	<i>SoC</i> <i>RMSE</i> : GMOS <i>GHI</i>	Final <i>SoC</i> : Actual	Final <i>SoC</i> : MOS <i>GHI</i> (rear location)	Final <i>SoC</i> : MOS <i>GHI</i> (front location)	Final <i>SoC</i> : GMOS <i>GHI</i>
One	1.49	1.52	1.40	51.04	57.11	57.68	56.51
Six	0.88	0.87	0.75	45.22	51.01	49.82	49.21
Eight	1.32	1.06	1.16	10.10	13.93	12.89	13.31

The GMOS model is a function of linear interpolation between the locations of two ground measurements (two MOS models) based on the current GPS location. The corresponding two MOS models are, however, conditional statistical models based on the cloud conditions as well as the forecast horizon and most importantly the time of day. Therefore, it is not trivial to expect a visible linear relationship in the performance results of the rear and front MOS models compared to their GMOS model. It is evident throughout Table 27 that the GMOS does produce improved outcomes; however small the improvement might be. There is one exception, on Day 8, where the front location MOS model outperformed the GMOS model by 0.42 % *SoC* error. Furthermore, on every account, the individual MOS models still outperformed the raw *GHI* predicted *SoC* error.

The GMOS method to improve the *GHI* component was only realised after the Sasol Solar Challenge 2018, which meant that it had not yet been implemented in the simulation results following in the optimisation chapter. However, the forecast bias compensated *GHI* model was used in the optimisation implementation.

## V. OPTIMISATION

The earlier chapters explained how a comprehensive mathematical model of a solar car can be created which includes locally refined and useful weather forecasts of the most essential weather components. This chapter shows how the model developed in previous chapters (part analytical and part numerical) is used by optimisation structures to minimise energy usage while maximising distance travelled by a solar car. These optimisation methods are specifically focussed and used in the context of a Sasol Solar Challenge event in South Africa.

Optimisation is a subfield of mathematics; the first known optimisation technique was formalised by Guass in the eighteen-hundreds. This gradient-based method was known as the Steepest Descent method. For centuries, significant optimisation problems were mainly treated using heuristic approaches as a result of computational limitations and a lack of other suitable methods. Today optimisation techniques are integrated into our daily lives. Optimisation is regularly applied to areas such as finance, economics, risk assessment, prediction of natural disasters, weather forecasting, avionics, communication networks and medical applications. With the refinement of optimisation methods and the advancement of computing power, we can solve many complex and unimaginably large optimisation problems with a fair amount of ease. Optimisation or mathematical programming is widely studied, researched and applied by scientists, engineers and a variety of other professionals in our modern technological society.

A particular case of mathematical optimisation is known as multi-level optimisation. This refers to the situation where optimisation functions are nested within another, operating in parallel or chronological succession. Multi-level optimisation strategies are not limited in their number of levels; however, it is common to find two levels producing satisfactory results in a variety of application cases. This strategy is called bi-level optimisation. Typically, these problems can be divided into two sets, the upper level (or leader) and the lower level (or follower). Both of these levels have their objective functions, constraints and variables.

These problems follow a hierarchical structure. The upper level contains the value of the shared variable optimising the argument of the lower-level function. The upper level includes variables from both levels while the lower level contains just the



variables from the lower level and treats all other variables as known constants. In other words, the lower-level problem is a parametric optimisation problem that is solved for the lower-level decision vectors. In contrast, the decision vectors in the upper-level set act as parameters. The lower-level problem set is a constraint on the upper-level problem set in the following way: only the lower-level optimal solutions that satisfy the upper-level constraints are considered feasible.

The general nested form of the bi-level optimisation problem is given by Equation (29).

$$\begin{aligned}
 \text{Minimise:} & & f_1(y, z^*) & & (29) \\
 \text{subject to:} & & b_1(y, z^*) = 0 \\
 & & b_i(y, z^*) \leq 0 \\
 & & z^* \in \operatorname{argmin}\{f_2(y, z)\} \\
 \text{subject to:} & & c_1(y, z) = 0 \\
 & & c_j(y, z) \leq 0 \}
 \end{aligned}$$

where  $i \in \{1, 2, 3, \dots, I\}$  and  $j \in \{1, 2, 3, \dots, J\}$  and  $b_i$  represents the upper-level (leader) constraints and  $c_j$  represents the lower-level (follower) constraints. Furthermore,  $y \in \mathbb{R}^{n_y}$  for the upper-level variables and  $z \in \mathbb{R}^{n_z}$  for the lower-level variables.

It is evident that a hierarchical structure is followed as the optimal value of the lower-level problem is included in the constraints of the upper-level problem. The lower level treats the variables of the upper level as fixed. It is also important to define the general constraint region for a bi-level problem for the points, which would satisfy both levels' constraints:

$$\Omega = \{(y, z) \in \mathbb{R}^{n_y \cdot n_z} : b_1(y, z) = 0, \dots, b_i(y, z) \leq 0, c_1(y, z) = 0, \dots, c_j(y, z) \leq 0\} \quad (30)$$

More practically, we would like to define the feasible upper-level region by projecting the constraint region just on  $\mathbb{R}^{n_y}$ . This is the set of upper-variables which renders the lower-level problem feasible:

$$\Omega(Y) = \{y \in \mathbb{R}^{n_y} : \exists z : (y, z) \in \Omega\} \quad (31)$$

The lower-level feasible region for  $y$  is fixed by considering the upper-level variable as a parameter:

$$\Omega(y) = \{y \in \mathbb{R}^{n_z} : c_1(y, z) = 0, c_j(y, z) \leq 0\} \quad (32)$$

A set of optimal solutions exist for fixed feasible values of  $y$ , and this set is called the rational reaction set:

$$\Pi(y) = \{z^* \in \mathbb{R}^{n_z} : z^* \in \operatorname{argmin}(f_2(y, z) : z^* \in \Omega(y))\} \quad (33)$$

Lastly, the induced region or feasible region of the bi-level problem is defined as the set of feasible upper-level variables of  $y$  which corresponds to the lower-level optimal solutions as given by the set of  $\Pi(y)$ :

$$I = \{(y, z) \in \mathbb{R}^{n_y \cdot n_z} : y \in \Omega(Y), z \in \Pi(y)\} \quad (34)$$

Furthermore, as multiple solutions to the lower-level problem might exist, the bi-level problem in Equation (29) is under-defined. There are generally two approaches to remedy this: the pessimistic and optimistic solutions, with the optimistic solution being most commonly implemented. In the presence of multiple lower-level optimal solutions, the leader expects the follower to choose that solution from the optimal set  $\Pi(y)$ , which leads to the best objective function value at the upper-level. On the other hand, in a pessimistic approach (in the presence of multiple lower-level optimal solutions), the leader optimises for the worst case where it assumes that the follower may choose that solution from the optimal set which leads to the worst objective function value at the upper level for  $z^* \in \Pi(y)$ . As the optimistic approach is more tractable as compared to the pessimistic approach and information can be shared between the two levels (some cooperation is possible); this study will focus on the optimistic solution.

This chapter explains the use of various optimisation methods through a multi-level approach to effectively find the optimal driving speed profile (minimise energy usage) of the vehicle as well as the optimal (maximise distance) number of loop road sections to be driven daily during a Sasol Solar Challenge event. The problem formulation makes specific reference to the characteristics and constraints typically found/seen

during such an event. However, with some modifications, the method can easily be used in a broader application area.

Essentially, two fundamental quantities have to be optimised. The first quantity is the optimal speed profile (integer or fraction values) for each of the days of the SSC, which minimises energy usage while adhering to typical constraints:

- Maximum and minimum  $SoC$
- Maximum and minimum speed
- Maximum and minimum driving time per day
- Maximum and minimum instantaneous motor power demand

The second quantity is the optimal number of loop road sections (integer values only) to be driven daily during a SSC event to maximise the distance travelled while adhering to typical constraints:

- A full loop road section must be travelled, no fractions allowed
- Maximum loop road section quantities will be enforced for each day based on historical information
- Maximum and minimum  $SoC$  values per day

The process by which these two quantities may be optimised can be described by a bi-level problem function and solved with appropriate solvers. Solvers are root-finding algorithms or mathematical software which aid in the computation of numerical mathematical problems.

## **UPPER-LEVEL: PROBLEM FORMULATION**

The allowed driving time ( $ADT_{day}$ ) that the vehicle is allowed to drive for a specific day (which may be regulated by an event rule or, by the user's needs) is found by subtracting the trip start time from the trip end time for any particular day. Despite the teams not being obliged to have a minimum driving time during an event such as the SSC, in this work, we assumed that the car would always be in motion except for the

control stops. The real driving time ( $RDT_{day}$ ) is the sum of each actual distance travelled for each interval divided by the optimal speed for each interval, on any specific day. The basic structure of the speed profile optimisation problem (the upper-level problem) is given by the objective function in Equation (35) followed by its succeeding constraints. The first five rows of Table 28 report the acceptable range for each of the constraint variables governing the objective function of Equation (35).

$$\begin{aligned}
 &\text{Maximise:} && f_u(v_k, x, \Psi^*, \beta^*) && (35) \\
 &\text{subject to:} && \beta^{*(min)} \leq \beta^* \leq \beta^{*(max)} \\
 & && \gamma^{min} \leq \gamma \leq \gamma^{max} \\
 & && \sigma^{min} \leq \sigma \leq \sigma^{max} \\
 & && \tau^{min} \leq \tau \leq \tau^{max}
 \end{aligned}$$

Consider in Chapter II that:  $\alpha_{day(x+1)}$  is the minimum expected *SoC* at the start of each day, which is the final State of Charge ( $SoC_{day(x)}$ ) at the end of the previous day.

The control or decision variable is  $v_k$ , which is the speed of the vehicle at each discrete period  $k$ . The objective function ( $E\{SoC_{day(x)}\}$ ) is described by  $f_u$ , and the nature of this objective function is a single variable (maximising only the expected *SoC* of the battery). However, the output or controlled variable is a vector which contains a single optimal speed for each 1 km route section.  $\Psi^*$  is the optimal loop section for each day and is considered a variable for the lower-level optimisation until the optimal value of the lower-level objective function has been found. Once it has been found, the upper-level optimisation problem can now regard the value of  $\Psi^*$  as a constant which forms part of the upper-level objective function. The energy remaining in the battery pack at the end of each day ( $SoC_{day(x)}$ ), described by constraint  $\beta^*$ , will ensure that the vehicle has the required amount of energy available at the start of each day (that is,  $\alpha_{day(x+1)}$ ) to finish the entire route without depleting the battery pack during any single day while maximising distance travelled. This constraint will also ensure that the battery pack cannot be charged to exceed its maximum rating (of not more than 100 %), nor discharged to below 5 %, as this is a critical safety risk. These variables are found as

a by-product of the lower-level optimisation computation and become part of the constraints of the upper-level problem.

The real driving time ( $RDT_{day}$ ) described by constraint  $\gamma$ , introduces a short grace period that has been added to the time constraint to convert what would have been an equality constraint, to an inequality constraint. It was observed that with this specific optimisation problem, the computation time decreased by using just the inequality constraints.  $\sigma$  Is the constraint for the nominal motor power required ( $P_{loss}$ ), and, in most cases, these motors can operate at well over double their rating, provided that they are kept below a specific temperature. To ensure that the motor is sufficiently air-cooled as well as maintaining a minimum safe driving speed ( $v_k$ ), a driving speed constraint is described by  $\tau$ .

**Table 28: Acceptable range for constraint variables**

Symbol	Minimum	Maximum	Units
<b>Upper-level</b>			
$\beta^*$	$\alpha_{day(x+1)}^{NB}$	100	%
$\Psi^*$	0	$\varphi^{max\ NB}$	-
$\gamma$	$ADT_{day} - 300$	$ADT_{day} + 300$	s
$\sigma$	-5000	5000	W
$\tau$	11.11	33.33	m/s
<b>Lower-level</b>			
$\beta$	$\alpha_{day(x+1)}$	100	%
$\Psi$	0	$\varphi^{max}$	-
$\Omega$	5	100	%

<sup>NB</sup>These values are determined by the lower-level optimisation routine

## LOWER-LEVEL: PROBLEM FORMULATION

The primary function of the lower-level optimisation is to estimate informed starting points for the number of extra loop roads to be covered every day. As part of the computation needed to find the optimal number of loops, the values for  $\alpha_{day(2)}$  to  $\alpha_{day(8)}$  (denoted by  $\beta$ ) are also found, knowing that  $\alpha_{day(1)} = 100\%$  as the teams are allowed to start the Sasol Solar Challenge on Day 1 with a fully charged battery.  $Arr_0$

denotes the predicted unique amount of energy used to cover each day without performing any loops. The predicted unique amount of energy used to cover each day with one loop included, is denoted by  $Arr_1$ . By subtracting  $Arr_0$  from  $Arr_1$  it is possible to find the energy loss components ( $\varepsilon_{day(x)}$ ), which provide useful information on the amount of energy consumed by one loop for each day. We make use of  $x$  ( $x = 1, 2, \dots, N$ ) where  $N$  is the total number of days of the Sasol Solar Challenge.

$$\Delta_{day(x)} = \left( \frac{\sum_{x=1}^8 (\delta_{day(x)})}{\delta_{day(x)}} \right) \quad (36)$$

$$e_{day(x)} = \left( \frac{\varepsilon_{day(x)}}{\sum_{x=1}^8 (\varepsilon_{day(x)})} \right) \quad (37)$$

Equations (36) and (37) provide the ratio or weight of each loop distance ( $\Delta_{day(x)}$ ) when compared to the sum of all the loop distances and the ratio or weight of energy loss for each loop ( $e_{day(x)}$ ) compared to the amount of the energy required for all the loops respectively.  $e_{day(x)}$  can be considered an expected value as it depends on the random variable of  $GHI$ . Consider Equation (38) as a function that would describe the favourability of performing a certain number of loops on a particular day.

$$f_l = \frac{e_{day(x)} \Delta_{day(x)}}{\varphi_{day(x)}} \quad (38)$$

A considerable loop distance value ( $\delta_{day(x)}$ ) and a large number of loops per day ( $\varphi_{day(x)}$ ), as well as a low loop energy loss value ( $\varepsilon_{day(x)}$ ) tends to decrease the value of  $f_l$ . Therefore, the lower the value of  $f_l$ , the more favourable the loop of that specific day is considered to be, in terms of distance and the loop's energy consumption. If we consider the number of loops for each day to be  $\varphi_{day(x)}$ , then the general structure of the lower-level optimisation problem can be given by Equation (39).

$$\text{Minimise:} \quad f_l(v_k, x, \Psi, \beta) \quad (39)$$

$$\text{subject to:} \quad \Psi^{min} \leq \Psi \leq \Psi^{max}$$

$$\beta^{min} \leq \beta \leq \beta^{max}$$

The nature of the objective function ( $f_l$ ) is a single variable (minimising the function  $f_l$ ) although the output or controlled variable is a vector, which contains the optimal number of additional loop sections ( $\varphi_{day(x)}$ ) for each of the eight days in which the driving should maximise the distance travelled. This vector, in turn, affects the objective function ( $f_u$ ) of the upper-level problem. The optimal number of loops for each day ( $\varphi_{day(x)}$ ) is represented by a constraint variable  $\Psi$ . The minimum energy values required at the start of each day ( $\alpha_{day(x+1)}$ ) is governed by  $\beta$ . The last rows of Table 28 disclose the acceptable range for each of the constraint variables governing the objective function of Equation (39). It is important to note that this method for loop quantity optimisation was not necessarily intended to achieve the highest accuracy, but rather for computational efficiency and to arrive at an informed starting point of loop quantities for the upper level to consider.

This implies that the larger the number of loops chosen for one specific day, the less realistic the loop energy loss might be as the input data relies on the weather conditions when performing just one loop per day. If more loops were performed, then the weather might be different later during the day when the sun is positioned at a different angle. This would result in a small variation of the actual energy that would be used for the second, third, fourth and any more loops. The objective function of Equation (39) makes explicit provision for such a constraint to be imposed by the user through  $\Psi$ , the value of which would be chosen based on prior experience and historical statistics. In regard to the Sasol Solar Challenge, poorly-performing cars tend to do zero to one loop per day, while cars with mediocre performance may do anything up to three loops per day, whereas highly competitive cars (normally from international teams) can do anything up to nine loops per day.

## **BI-LEVEL OPTIMISATION: PROBLEM FORMULATION**

Regarding the general form of the bi-level optimisation problem (Equation (29)) as well as the upper-level (Equation (35)) and lower-level (Equation (39)) structures listed, the following represents the nested bi-level optimisation problem, according to [84].

$$\begin{aligned}
&\text{Maximise:} && f_u(v_k, x, \Psi^*, \beta^*) && (40) \\
&\text{subject to:} && \beta^{*(min)} \leq \beta^* \leq \beta^{*(max)} \\
&&& \gamma^{min} \leq \gamma \leq \gamma^{max} \\
&&& \sigma^{min} \leq \sigma \leq \sigma^{max} \\
&&& \tau^{min} \leq \tau \leq \tau^{max} \\
&&& (\Psi^*, \beta^*) \in \operatorname{argmin}\{f_l(v_k, x, \Psi, \beta) \\
&\text{subject to:} && \Psi^{min} \leq \Psi \leq \Psi^{max} \\
&&& \beta^{min} \leq \beta \leq \beta^{max}\}
\end{aligned}$$

## SOLUTION METHODS

The aim of this work was not to develop novel ways of computation, but instead, it sought reliable solvers capable of solving the proposed bi-level problem efficiently.

The issue of convexity or non-convexity, one local minimum or many local minima of the proposed problem function [85] was not of great concern in our case. The constraints identified in Equation (35) and Equation (39) simplified the problem sufficiently to allow for a narrow optimisation space wherein the solver could confidently find a single optimal solution. This implies that the global optimum and the local optimum would essentially be the same point. Global optimisation techniques, such as the Differential Evolution, were not needed to solve this problem. They would possibly have resulted in an increase in computational time, which was unwanted in our case, where near real-time updates could be periodically required.

The optimisation solver used for the upper-level problem was a gradient-based Sequential Quadratic Programming (SQP) method, which is well known and considered to be an industry preferred gradient-based method for solving non-linear constrained optimisation problems. At each iteration, all the constraints as well as the objective function are handled by successive quadratic approximations where the Hessian matrix provides the necessary second-order differential information. The Broyden-Fletcher-Goldfarb-Shanno (BFGS) method is employed to approximate the Hessian matrix. In turn, finite forward differences are used to approximate the objective function's gradient, which supplements the BFGS method. Finally, line searches are used to find the solution to the approximate sub-problem. It was shown that solving bi-



level optimisation problems are NP-hard problems [86] and that the coding of such problems normally involves extensive ad-hoc programming to existing solvers such as CPLEX from the IBM Corp as well as some built-in MATLAB® optimisation functions.

MATLAB® employs such an SQP method for easy software integration. For this reason, the equation set for the SQP method is not presented in detail as it has been thoroughly documented by [87]. Now, regarding the lower-level optimisation, if we consider eight days and limit the number of loops per day to three (based on event statistics of the mid-range competitors of the SSC), then the number of loop and day combinations or permutations to find the optimal energy usage and maximum distance becomes very low. By constructing a matrix of paths and costs, this data can easily be represented as a classical shortest path problem. For this reason, a Dynamic Programming (DP) approach was chosen. Because of the somewhat arbitrary nature of the DP method, MATLAB® does not necessarily implement DP as a standard function for ease of use. Therefore, the technique needs more explanation from first principles. Let us consider the generic structure of the finite-horizon DP method to aid in the interpretation of the solution algorithm. Assume a discrete-time system that is described by:

$$z_{x+1} = f_x(z_x, u_x, w_x), \quad \text{for } x = 1, 2, \dots, N - 1 \quad (41)$$

The horizon or, the number of times that control is applied, is denoted by  $N$ , while  $x$  is the discrete-time interval between the applied control stages.  $z_x$  is the current value of the state being optimised and  $u_x$  is the decision or control variable.  $w_x$  is the random parameter (or stochastic variable), which is commonly averaged to indicate the expected value of this variable. The DP method makes use of so-called optimisation policies. These policies can also be named feedback control laws or rules/functions. These feedback rules provide information on what the decision/control variable ( $u_x$ ) should be, given the current value of the state ( $z_x$ ). These policies ( $u_x$ ) or functions are described by Equation (42) and map states  $z_x$  into controls  $u_x = u_x(z_x)$ .

$$u_x = \mu_x(z_x), \quad \text{for } x = 1, \dots, N - 1 \quad (42)$$

In this manner, the decision variables are chosen and adapted based on what has happened in the past (this is an example of feedback laws in operation) by optimising

these sequences of policies or functions:  $\pi = \{\mu_0, \mu_1, \dots, \mu_{N-1}\}$ . A generic cost function of these policies is shown by:

$$J_\pi(z_0) = E\{g_N(z_N) + \sum_{x=0}^{N-1} g_x(z_x, u_x, w_x)\} \quad (43)$$

Here,  $g_x$  is the cost incurred,  $g_N$  is the cost at the terminal state, and  $z_N$  is the value of the final (terminal) state. In some cases, the cost at the terminal state is not unique and may be made zero. The terminal cost will then be calculated as part of the summation term (second term) in Equation (43). The DP now aims to compute the optimal cost function at state zero by minimising all the policies as shown by:

$$J^*(z_0) = \min_{\pi} J_\pi(z_0) \quad (44)$$

$$J_{\pi^*}(z_0) = J^*(z_0) \quad (45)$$

Furthermore, because we are dealing with functions, typically, an optimal policy  $\pi^*$  exists, which satisfies Equation (45) for all the values of the zero state  $z_0$  while still being independent of this initial state. This phenomenon of the existence of optimal policy is a consequence of the DP algorithm. In 1957, Richard Bellman [88] explained the principle of optimality, which states that an optimal policy has the property that whatever the initial state and initial decision is, the remaining decisions must constitute an optimal policy concerning the state resulting from the first decision. In other words, the tail policy is optimal for the sub-problems of the entire tail. The DP, in turn, solves all the tail sub-problems in a given time length, using the solution of the tail sub-problem of a shorter time length. This results in solving the problem from the tail side to the front and is called 'backward induction'. Initially, we start one step from the end ( $N - 1$ ) and solve that specific tail sub-problem, and, as a result, the third last step ( $N - 2$ ) is now simplified based on the knowledge of the second final step, and soon this too can easily be solved. This process is repeated until the initial state is reached.

To use the DP method in MATLAB®, we would need to re-write the generic structure of the lower-level problem previously defined by Equation (39) to arrive at a suitable DP algorithm, which we would be able to implement pragmatically in code:

Let  $J_x(z_x)$  be the optimal cost of the tail problem starting at  $z_x$  with initial condition  $J_N(z_N) = G_N(z_N)$  beginning at the last state tail sub-problem.

From here we move backwards, starting at the end, such that  $x = N - 1, \dots, 0$  by making use of:

$$J_x(z_x) = \min_{u_x \in U_x(z_x)} \mathbb{E}_{w_x} \{g_x(z_x, u_x, w_x) + J_{x+1}(f_x(z_x, u_x, w_x))\} \quad (46)$$

where  $U_x$  is the set of constraints as stipulated in Equation (39) and  $w_x$  is the random variable ( $e_{day(x)}$ ) of the discrete-time system in Equation (39).  $g_x$  is the cost of the terminal state and  $f_x$  is some cost function.

Solve all the tail sub-problems (all the values of  $J_x$ ) at time  $x$  by minimising the sum of the  $x^{th}$  stage cost and the cost of the next tail problem starting from the next state at time  $x + 1$ .

When the last step is generated,  $J_0(z_0)$ , this will be equal to the optimal cost  $J^*(z_0)$  as well as the optimal policy  $\pi^* = \{\mu_0^*, \mu_1^*, \dots, \mu_{N-1}^*\}$  where  $\mu_k^*(z_x)$  minimises the right-hand side of the  $J_x(z_x)$  at each  $z_x$  and  $x$ .

Now we are ready to apply the lower-level optimisation problem formulation in this thesis to the DP algorithm as described above. The discrete-time system will be given by Equation (47) with  $N$  representing the number of days ( $N = 8$  in the context of the SSC2018):

$$z_{x+1} = z_x + u_x \delta_{day(x)}, \text{ for } x = 1, 2, \dots, N \quad (47)$$

In Equation (47),  $z_N$  is the total number of kilometres travelled as a result of the sum of loop sections of each day. It is important to note that this distance does not include the mandatory driving distances for each day.  $u_x$  is the decision or control variable, which is the optimal number of loops to travel each day while adhering to the constraint set ( $U_x$ ), as seen in Equation (39). Furthermore,  $u_x$  is also a function of the random variable (expected value) of  $e_{day(x)}$ , resulting in Equation (47) being rewritten as  $z_{x+1} = \mathbb{E}\{z_x + u_x \delta_{day(x)} | e_{day(x)}\}$ . The cost function is simplified as the terminal state does not have any unique cost requirements, but rather, it is treated in a similar manner to the rest of the series of states. This means that the first term in  $J_x(z_x)$  falls away. The cost function can now be given by:

$$J_x(z_x) = \min_{u_x \in U_x(z_x)} \mathbb{E}_{e_{day(x)}} \left\{ J_{x+1} \left( f_x(z_x, \phi_{day(x)}, e_{day(x)}) \right) \right\} \quad (48)$$

Here,  $f_x$  refers to Equation (39) and  $J_{x+1}$  is the cost of the next state based on the current state.  $\varphi_{day(x)}$  is the decision or control variable (number of loops per day) and  $e_{day(x)}$  is the expected value of the random variable. By minimising  $J_x(z_x)$  over the horizon of  $N$ , we can find the optimal number of loops for each day ( $\varphi_{day(x)}$ , represented by the constraint  $\Psi_{(x)}$  in Equation (39)) based on the expected energy to be consumed during each loop on each day and the importance of the loop distance (favourability of loop) of each day. Another secondary result of the minimisation will be the minimum amount of energy needed at the start of each day ( $\alpha_{day(x)}$ , represented by the constraint  $\beta_{(x)}$  in Equation (39)); this information is essential to the upper-level and energy manager and serves as validation of the results of the daily number of loops. Finally, the outcome of the DP optimisation is to select the optimal number and combination of loops that use the least energy and yield the most significant distance. In this manner, we can maximise the distance travelled indirectly. This optimal information then provides information to the objective function of the upper-level's optimisation objective function as well as its constraint set.

By providing the necessary input data from the various sensors, solar car telemetry, and API based weather forecast, these algorithms in combination are able to predict the optimal speed profile for any day of the SSC for any solar vehicle in high resolution. Furthermore, the target loop quantities found (from the lower-level optimisation results) will be used to re-construct the route input data used by the upper-level optimisation structure for all eight days to verify the validity and feasibility of the loop quantities proposed. The progress of each day can now be calculated and re-calculated in high resolution.

## IMPLEMENTATION

The implementation was approached with IoT and 4IR in mind. The implemented system is connected to various external sensors, inputs and Cloud-Based data sources and was developed to be flexible to make future improvements/modifications possible.

This bi-level optimisation is applied to a mobile context (on-the-road use) where just limited hardware and internet connectivity is available. The interface used by the energy manager is in the form of a User Interface (UI). This UI makes it possible for the user to effortlessly interact with the complex mathematical functions and data matrices, which through bi-level optimisation are able to generate the required optimised profiles required.

This section explains the code workflow, which makes the mathematical energy model and bi-level optimisation useful for the solar car team.

Annexure A contains a summary of the main variables/parameters used by the UI. The lengthy pages of physical code are not included. Instead, sequential bullet form coding workflow are supported by flow diagrams for ease of interpretation. All the code was developed in a MATLAB® environment.

The UI consists of one primary interface and three function scripts. The code workflow, as well as flow charts of each section, are presented in this section.

### Primary script

#### 1. Main UI

##### 1.1 Part I (Pre-processing and preparing for upper-level optimisation)

- Calls lower-level optimisation function

##### 1.2 Part II (Pre-processing operations)

- Calls weather API function
- Calls upper-level optimisation function

##### 1.3 Part III (Post-optimisation operations)

### Function scripts

#### 2. Upper-level optimisation script (contains an objective function, calculations and constraint information)

#### 3. Lower-level optimisation script (contains an objective function, calculations and constraint information)

#### 4. Weather forecast API (requests weather forecasts from Meteomatics AG)

Methods of skilled programming have been employed throughout the coding process to ensure efficient execution of code, which included vectorisation, size and dimension pre-allocation of all variables, using of vectors and matrices where possible, making use of functions and minimising the use of global variables.

### **Main UI**

#### 1.1 Part I (Pre-processing and preparing for upper-level optimisation)

The first part of the pre-processing operations is responsible for gathering the required information from the lower level which the upper level might need, and *vice versa*. This part of the programme is run just once per day. Before the bi-level optimisation can be solved, the lower level requires some information from the upper level to be able to optimise its own objective function (maximise distance). This, in turn, allows the upper level to finally optimise its objective function (minimise energy usage). Here a modified version of the upper-level optimisation is called, after which the lower-level optimisation function is called and executed.

#### 1.2 Part II (Pre-processing operations)

The second part of the pre-processing operations is to gather the data required for the mathematical model, get additional energy manager inputs, read stored variables, request and import weather forecasts, construct route data matrices and finally, call the optimisation solver. This part is run every time the user requests an update. This might be several times per hour or as required. The program flow is given in bullet point form below:

- The user chooses to do a calculation for the full-time horizon (all remaining days of the challenge) or only for a specific day/s
- All the mathematical model parameters are shown, and the user can modify if desired (Annexure A). Additional variables that can be modified here:
  - Optimisation resolution (default 1 km)

- Start and finish times for a specific day (default 8:00 to 17:00)
- Mandatory control stops (default 30 minutes)
- Amount of loops for each day (default as recommended by the lower-level optimiser)
- Minimum and maximum speed (default national motorway limits)
- Import live GPS and date/time information
  - This is requested from a mobile weather station
- Import live *SoC* as reported by the solar car wireless telemetry system (only used when doing on-route calculations for increased accuracy, not applicable when doing initial calculations before departure)
- Load pre-saved route data of planned route such as distance, elevation, GPS locations, and bearing, all according to the resolution specified (Annexure A).
- Request weather forecast API for all GPS locations of the desired route
- Use the number of loops for each day to construct matrices of the complete route
  - All matrices have to be the same dimensions for computational consistency
- Calculate air density with the coefficients method [46] by making use of the forecasted air temperature, dew point temperature and air pressure.
  - Also, consider the loops of each day and construct the air density matrix with the same dimensions as before
- Calculate the current location on the route
  - This data is used for knowing what sections of the route have already been passed
  - Trim (delete) all route data matrices to have the first value in all matrices correspond to the current location and time, and the last values in the matrix correspond to the terminus location and estimated time on the route. If the current location is found to be zero (not yet departed), no modifications are made to route data matrices

- Apply efficiency constant and forecast bias correction functions to *GHI* data matrix for improved accuracy; the GMOS function (as explained in the last part of Chapter IV) can be applied here in future versions of the code
- Based on the current GPS location and real-world time, the distance and time remaining to get to the mandatory 30-minute control stop are calculated as the speed needs to be zero during the control stop. This is added as an additional constraint to the upper-level optimisation problem to ensure that this zero speed is taken into consideration while creating an optimal speed profile
- Finally, the upper-level optimisation function is called and executed by sending all the pre-processed matrices and data to this function.

### 1.3 Part III (Post-optimisation operations)

When all the required information has been returned from the bi-level optimisation problem, the final section of the main script is data validation, user feedback reporting and construction of meaningful plots and graphical data.

- The following plots are generated from the data received back from the bi-level optimisation. These are typically the plots that are used in the results section of this work (Chapter VI). All outputs are based on time of day and distance at that time as calculated by the solvers.
  - Optimal speed profile vs time
  - *SoC* vs time profile
  - Route elevation profile vs time
  - *TCC* profile vs time
  - Air density profile vs time and rain probability profile vs time
  - Frontal wind profile vs time and Useful solar power vs time
- In addition to the graphical plots, the following information and validations are presented to the user for inspection to ensure that the solver adhered to the constraints and to verify the integrity of the results
  - Total calculated driving time and total calculated driving distance



- Minimum, mean and maximum information about the optimal speed, the motor power, motor efficiency, *GHI* component and air density
- The losses due to aerodynamics, road graded as well as rolling resistance
- Distance validation for each of the optimal speed intervals
- Time validation for each of the optimal speed intervals
- Motor power validation for each of the optimal speed intervals
- *SoC* validation to ensure the values never exceed the critical parameters

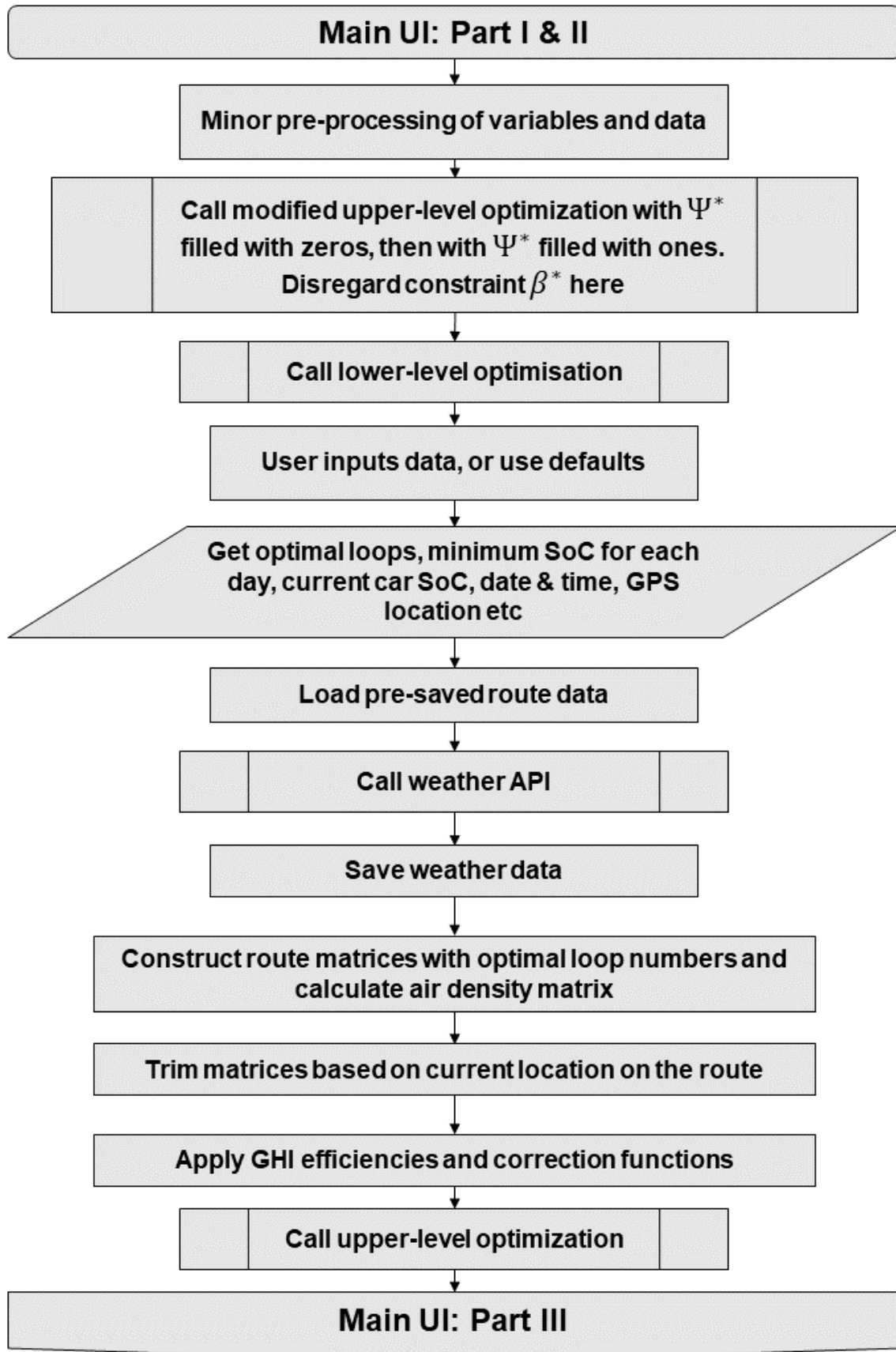


Figure 27: Implementation: Main UI Part I & II - flow diagram

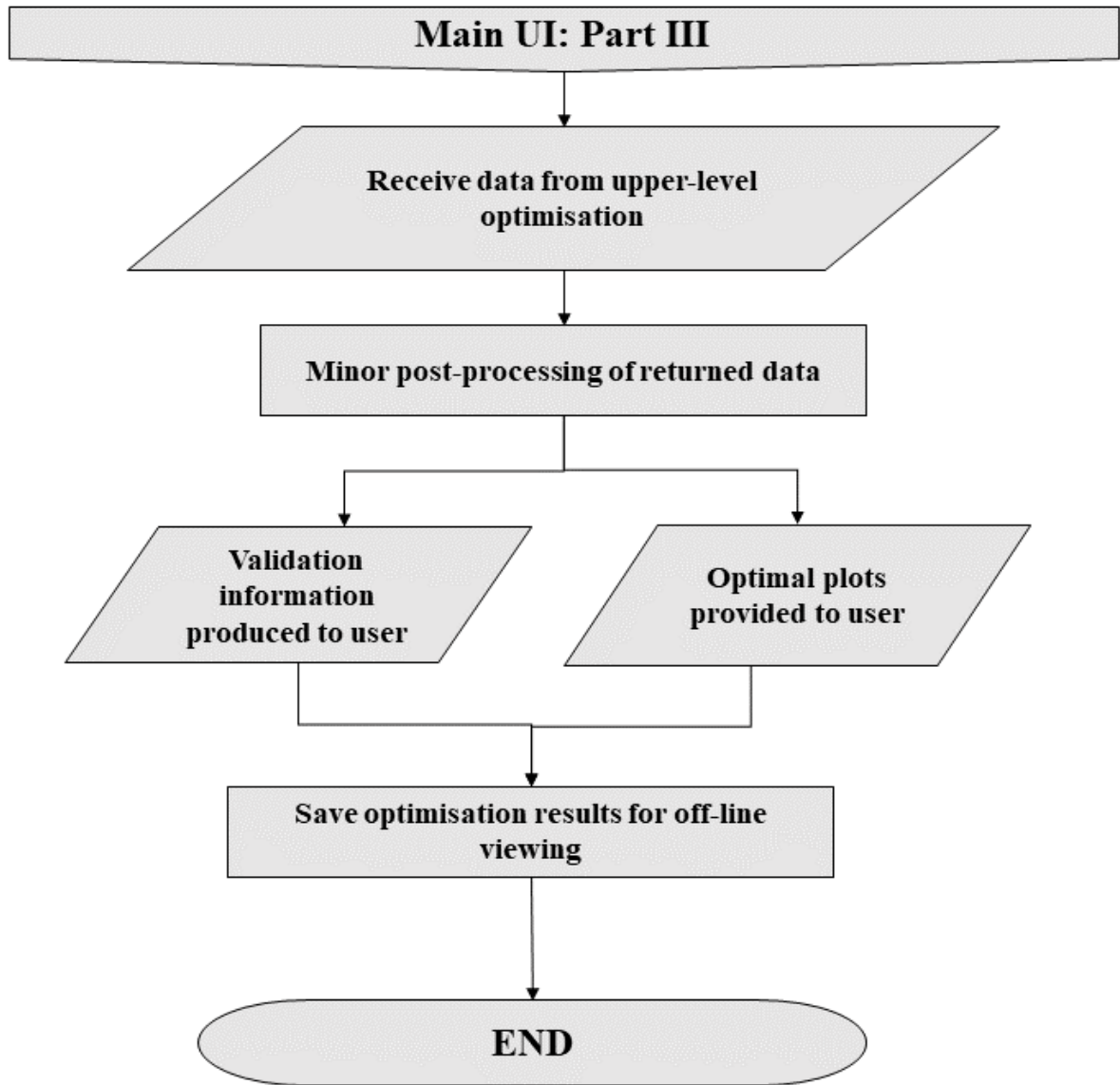


Figure 28: Implementation: Main UI Part III - flow diagram

### Lower-level optimisation function workflow

Variables such as  $Arr_0$ ,  $Arr_1$  and  $\varepsilon_{day(x)}$  are required before the lower-level optimisation can commence.

- $Arr_0$  is found by calling a modified version of the upper-level optimisation (executed before this lower-level optimisation) for all eight days with zero loop sections. Next,  $Arr_1$  is found by duplicating the process with one loop section for each day. These two vector variables are then subtracted and  $\varepsilon_{day(x)}$  is found. For these two

operations taking place in the modified upper-level function,  $\Psi^*$  is a vector containing zeros when finding  $Arr_0$  and ones when finding  $Arr_1$ . The variable  $\beta^*$  is disregarded during these two operations. Values are sent back to the lower-level function for processing

- The function now has the required information to assemble  $f_l$  (the lower-level objective function) as shown in Equation (39)
- The solver is implemented to solve Equation (39) as was described by the Dynamic Programming implementation section and Equation (47) to (48)
- The following outcomes result from the successful lower-level problem optimisation (the outcomes can be matrices or vectors depending on whether a single day or full-time horizon (all remaining days of the challenge) was requested for calculation)
  - Optimal loop road sections for each day ( $\varphi_{day(x)}$ , a function of  $\Psi$ )
  - Required minimum *SoC* at the start of each day ( $\alpha_{day(x+1)}$ , as a function of  $\beta$ )

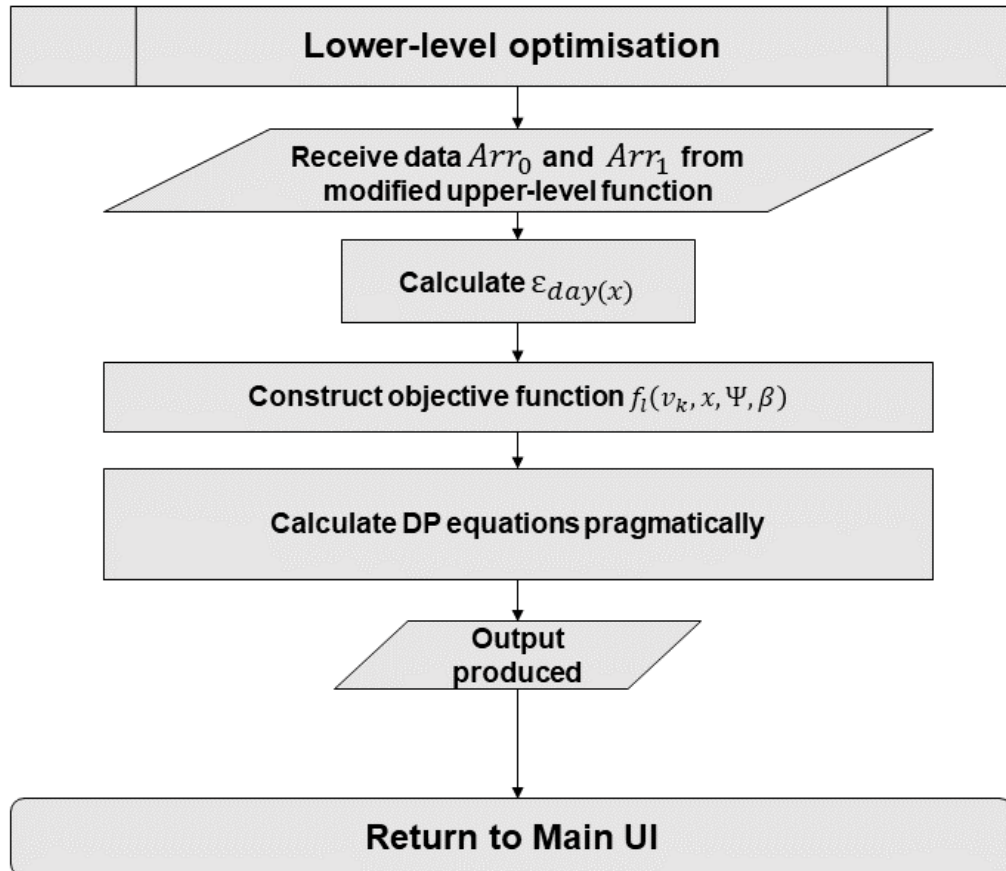


Figure 29: Implementation: lower-level optimisation - flow diagram

### Upper-level optimisation function workflow

Throughout this function the optimal speed  $v_k$  is treated as the decision variable and is not given a definite value by the user; instead, the solver uses this decision variable throughout the objective function and constraints to arrive at a suitable optimal solution.

- Receive all prepared data from the main function as well as initialise some local variables
- Compute wind component ( $v_w$ ) affecting car front from the front or from the rear by making use of trigonometry, the bearing matrix as well as the wind northbound and wind eastbound forecast matrix. This is used in Equation (7) of the energy model
- Air density variation ( $p$ ) in Equation (7) is applied by making use of the calculated air density matrix
- The power loss equation (Equation (10))  $P_{loss(k)}$  is constructed and extended
- The efficiency of the motor has to be applied to Equation (10) and requires the wheel rpm and torque, which are both a function of the decision variable  $v_k$ . This efficiency is then used as shown in Equation (10)
- The route matrix is evaluated for areas where the force due to gravity ( $F_{3(k)}$  in Equation (9)) is larger than the sum of the other forces. If these forces become so large that  $v_k$  surpasses its constraints, it is expected that regenerative braking will be used to brake and recover some energy to the extent of keeping  $v_k$  at the maximum speed set out in the constraints
- Construct objective function ( $E\{SoC_{day(x)}\}$ ) by making use of model Equation (7) to (19) of Chapter III
- Each of the energy calculations in this function is done in sections of the required resolution as specified by the user (default 1 km intervals)
- All the constraints in Equation (35) are defined and the SQP solver within MATLAB® is initialised
- The following outcomes result from the successful upper-level problem optimisation (can be matrices or vectors depending on whether a single day or full-time horizon

was requested for the calculation). All outputs are based on time of day and distance at that time as calculated by the solver

- Optimal speed profile
- Corresponding *SoC* profile
- Corresponding solar irradiation profile
- Corresponding *TCC* profile
- Corresponding wind profile
- Corresponding motor torque profile
- Return all optimised results to main function.

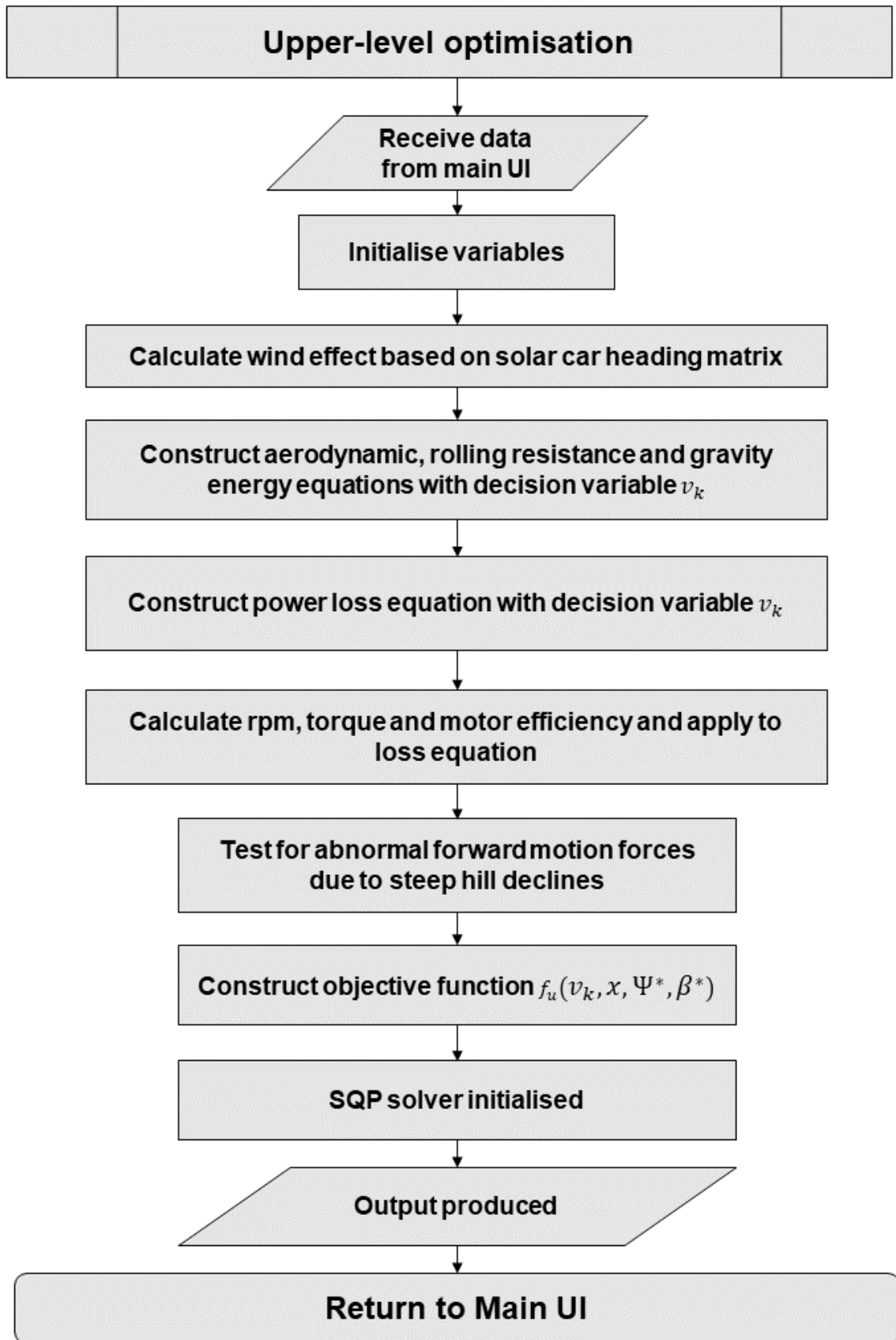


Figure 30: Implementation: upper-level optimisation - flow diagram

### Weather API function

- The time and date stamp is received from the main function
- The API data supplier subscription account username and password are made available to the Representational State Transfer (REST) web-based communication protocol structure in MATLAB®
  - Data is requested from 06:00 to 18:00 and received in a raw format in 1-hour intervals. A cubic interpolation function is used to estimate a continuous function in order to increase the resolution and re-construct into a vector format of 15-minute intervals (by default)
- Weather data is saved in individual files for use when internet service is not available

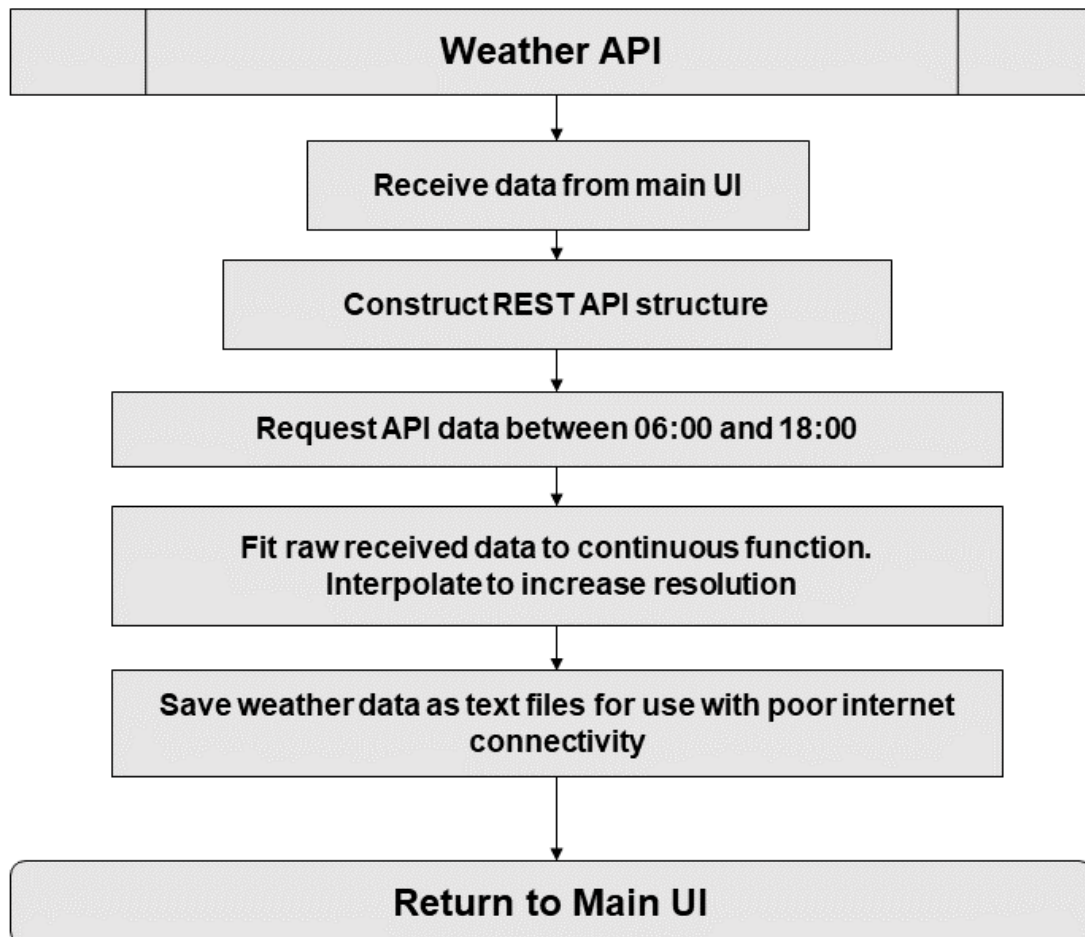


Figure 31: Implementation: weather API - flow diagram



Annexure B contains additional information on the UI in terms of computation time, length of code, number of memory locations used and other supplementary information on the development of the optimisation and other code.

## **FIELD TEST SETUP**

The bi-level optimisation strategy was implemented during the eight days of the SSC2018, and all the data from the solar vehicle was transferred via long-range Wi-Fi to the support vehicle where it was recorded in a LabVIEW® and MATLAB® software environment at a rate of 1 sample/second. Weather data was collected and recorded (1 sample/second) with a calibrated Gill MaxiMet® GMX501. This sensor was mounted high above the roof of the support vehicle to eliminate any aerodynamic interference that the support vehicle itself might have on the wind speed and direction recordings, as illustrated in Figure 32.

The support vehicle was equipped with two portable laptop computers: one for monitoring the solar car systems and recording data and the other to execute the bi-level optimisation routines. This setup served as a mobile command centre. It ensured IoT connectivity with the solar car as well as a stable internet link for weather forecast retrieval and other real-time web or Cloud-Based requirements. The mobile command centre was able to display as well as record all data from the solar car and sensors. Additional data, such as battery cell temperatures, tyre pressures, electrical sub-system voltages, MPPT feedback and any other data registers available on the solar car CAN bus system were also able to be retrieved. The solar car CAN bus enables component-level communication between all parts of the solar car and is the primary communications backbone of the solar car. Typically, the energy manager of the team (also the author of this thesis) was in charge of the mobile command centre equipment. The bottom part of Figure 32 shows the TUT team energy manager in the command centre seat.

The results section summarises all eight days, followed by an in-depth look at the first, seventh and last day of the SSC2018.

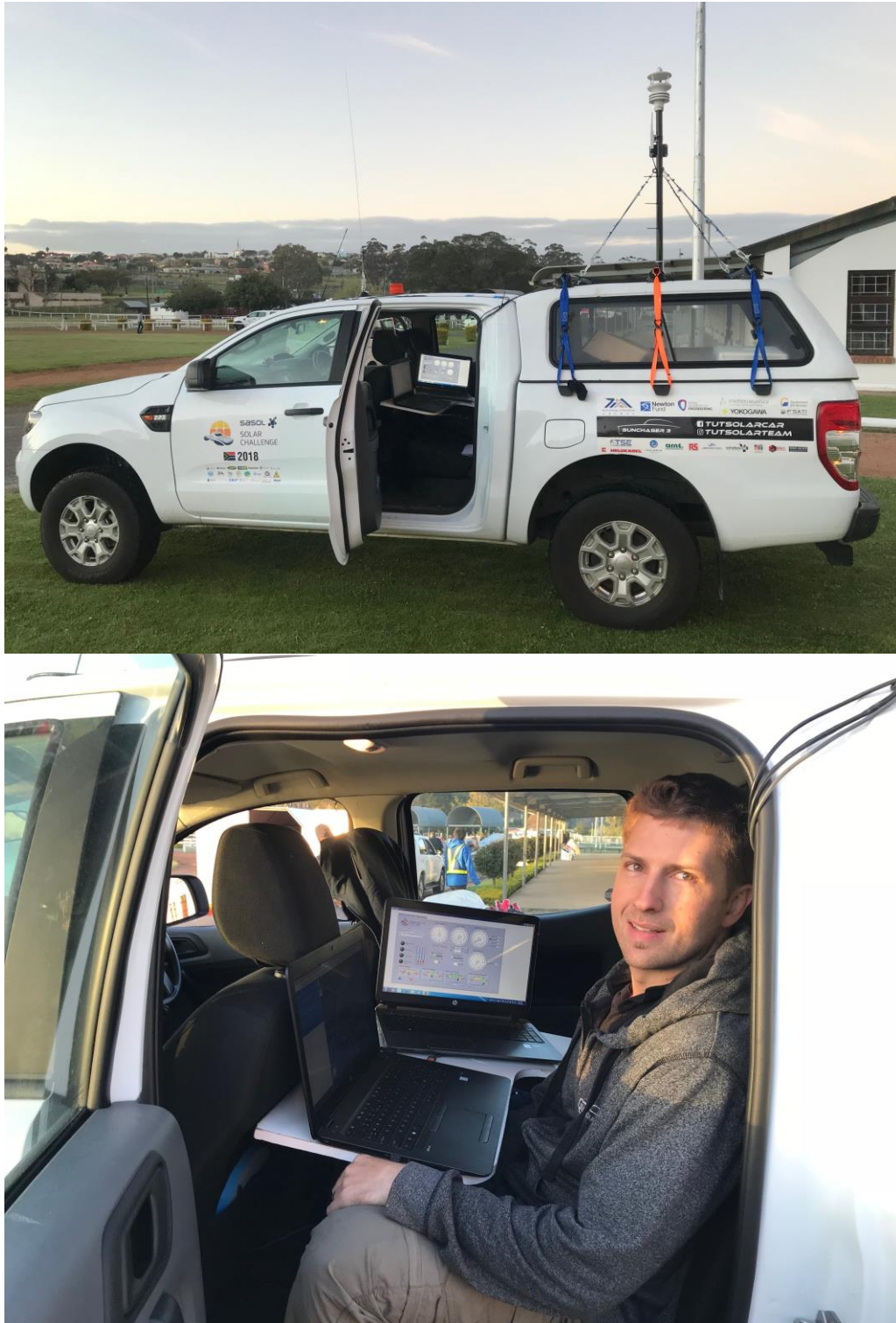


Figure 32: Top: Support vehicle with IoT, radio and weather sensors.

Bottom: Mobile data acquisition and command centre

## VI. CASE STUDY RESULTS

The Tshwane University of Technology (TUT) entered their third-generation solar-powered vehicle (Sun Chaser III) into the Challenger category of the SSC2018, which took place in South Africa during September 2018. The car is shown in Figure 33.



**Figure 33: SSC2018, Sun Chaser III solar vehicle**

The team placed 4<sup>th</sup> overall and 1<sup>st</sup> among the local participants. The Sun Chaser III team managed to cover approximately 2400 km over eight days, and much of its success was attributed to the implemented optimisation technique and the advantage it provided to the team from TUT. The physical characteristics of the Sun Chaser III are presented in Table 7. The official event results of Sun Chaser III during the SSC2018 challenge are recorded in Table 29.

**Table 29: SSC2018, SCIII results (all days)**

Date during 2018	Locations in South Africa	Distance covered (km)	Loop quantity and distance (amount, km)
22 September (Day 1)	Pretoria to Sasolburg via Kroonstad	493	3, 74
23 September (Day 2) <sup>b</sup>	Kroonstad to Bloemfontein via Winburg	117	0 <sup>a</sup> , 73
24 September (Day 3) <sup>b</sup>	Bloemfontein to Gariep Dam via Edenburg	164	1 <sup>a</sup> , 82
25 September (Day 4)	Gariep Dam to Graaff Reinet via Middelburg	291	1, 36
26 September (Day 5) <sup>b</sup>	Graaff Reinet to Port Elizabeth via Jansenville	249	0 <sup>a</sup> , 65
27 September (Day 6)	Port Elizabeth to Sedgefield via Kareedouw	371	1, 59
28 September (Day 7)	Sedgefield to Swellendam via Mosselbay	308	2, 29
29 September (Day 8)	Swellendam to Stellenbosch via Bredasdorp	403	2, 75

<sup>a</sup> These loop quantities are not the optimal loop quantities as the vehicle's performance was compromised due to technical issues, which made it impossible to adhere to the speed as well as loop recommendations. After each of these days, a re-calculation for the coming days was done to update the optimal speed profiles and optimal loop quantities.

<sup>b</sup> On these days the car suffered mechanical or telemetry difficulties, which compromised the recorded data for these days, rendering it unusable for most of the formal analysis.

## PERFORMANCE METRICS

To measure the performance of the optimisation technique, similar performance metrics to those used in the earlier chapters were employed here, and the summary of results is provided in Table 30. In addition to these performance metrics, the total useful solar irradiation energy from the sun (including solar panel area and all transfer efficiencies to the battery), as well as the total energy consumed from the battery during each day (given in Table 31), ensures a comprehensive description of the performance of the optimisation technique's simulation predictions and weather forecast performance for each day. All values expressed in Table 30 are given as relative error percentages.

Table 30: SSC2018, optimisation performance metrics

Day 1					
	<i>RMSE</i>	<i>MAE</i>	<i>FB</i>	<i>std</i>	<sup>a</sup> CoD
<i>SoC</i> error	1.62	1.17	0.47	0.05	-
Speed error	16.46	10.11	6.04	4.99	0.38
Wind error	78.80	72.12	-32.32	22.52	0.18
rho <sup>b</sup> error	2.92	2.82	-0.78	0.48	0.05
<i>GHI</i> error	34.25	19.41	-14.85	6.43	0.35
DAY 4					
	<i>RMSE</i>	<i>MAE</i>	<i>FB</i>	<i>std</i>	<sup>a</sup> CoD
<i>SoC</i> error	5.53	4.54	-2.79	0.19	-
Speed error	41.67	29.38	27.55	16.14	0.3
Wind error	65.74	53.76	48.52	25.91	0.23
rho <sup>b</sup> error	1.67	1.35	-1.23	1.12	0.07
<i>GHI</i> error	193.22	132.65	-74.52	40.47	0.34
DAY 6					
	<i>RMSE</i>	<i>MAE</i>	<i>FB</i>	<i>std</i>	<sup>a</sup> CoD
<i>SoC</i> error	1.02	1.17	0.29	0.16	-
Speed error	14.46	9.33	4.12	3.89	0.33
Wind error	42.83	40.12	19.36	12.56	0.23
rho <sup>b</sup> error	1.23	2.52	1.63	1.44	0.03
<i>GHI</i> error	29.11	20.18	-12.34	6.43	0.40
DAY 7					
	<i>RMSE</i>	<i>MAE</i>	<i>FB</i>	<i>std</i>	<sup>a</sup> CoD
<i>SoC</i> error	5.33	3.5 1	1.91	0.89	-
Speed error	62.32	38.11	37.45	19.11	0.39
Wind error	32.51	31.44	15.34	7.31	0.30
rho <sup>b</sup> error	5.22	3.35	1.83	2.62	0.02
<i>GHI</i> error	24.11	21.41	14.66	13.01	0.24
DAY 8					
	<i>RMSE</i>	<i>MAE</i>	<i>FB</i>	<i>std</i>	<sup>a</sup> CoD
<i>SoC</i> error	2.01	1.97	1.19	1.13	-
Speed error	16.56	11.43	6.22	5.25	0.25
Wind error	71.34	66.12	50.33	14.52	0.37
rho <sup>b</sup> error	3.27	3.01	1.01	0.95	0.03
<i>GHI</i> error	29.11	20.18	12.34	4.43	0.27

<sup>a</sup> CoD is the Coefficient of Determination between the *SoC* error and the corresponding error parameter.

All values except CoD are expressed as relative error percentages. <sup>b</sup> rho refers to the air density

**Table 31: SSC2018, energy prediction summary**

Day <sup>a</sup>	Predicted <i>GHI</i> (kWh)	Actual <i>GHI</i> (kWh)	Predicted battery usage (%)	Actual battery usage (%)	Initial and final <i>SoC</i> (%)
Day 1	2.95	2.8	45	52	100 – 48
Day 2	-	-	-	-30 <sup>b</sup>	48 – 78
Day 3	-	-	-	-22 <sup>b</sup>	78 – 100
Day 4	2.17	1.9	5	20	100 - 80
Day 5	-	-	-	17	80 - 63
Day 6	2.1	2	24	18	63 – 45
Day 7	1.65	1.7	5	25	45 – 20
Day 8	2.19	2.3	14	10	20 - 10

<sup>a</sup> These days refer to the days during the SSC2018, similarly to Table 30

<sup>b</sup> Negative values refer to the energy gained

The data sets collected on Days 2 and 3 was not usable as the Sun Chaser III team had a major mechanical failure due to a strong gust of wind leading to damage to the car at the end of the first day. The repairs took place during the first part of Day 2. Nevertheless, the car managed to increase the battery charge by 30 % whilst repairs were undertaken and subsequently, it covered 117 km without following any optimised speed profile. Likewise, on Day 3, the data was not usable as the team only completed the first stage of the day with one loop, after which the solar car had to be put on a trailer for the rest of the day. This was due to continuing technical issues arising from the damage sustained on the first day. The team still managed to cover 164 km and fully charge the battery while on the trailer, gaining about 22 %, which meant starting with a full battery on Day 4. On Day 5, the telemetry recording system on the support vehicle failed and no data was recorded for this day. Day 5 used 17 % of the battery pack. Usable data was recorded for Day 1, Day 4 and Day 6, Day 7 and Day 8. Optimisation re-calculations were done daily to compensate for the various inconsistencies arising from the technical equipment failures and other factors.

## CASE STUDY SUMMARY

Day 1 and 6 (Figures 34 and 35 respectively) display similar performance metrics with their speed errors comparably small on both days.

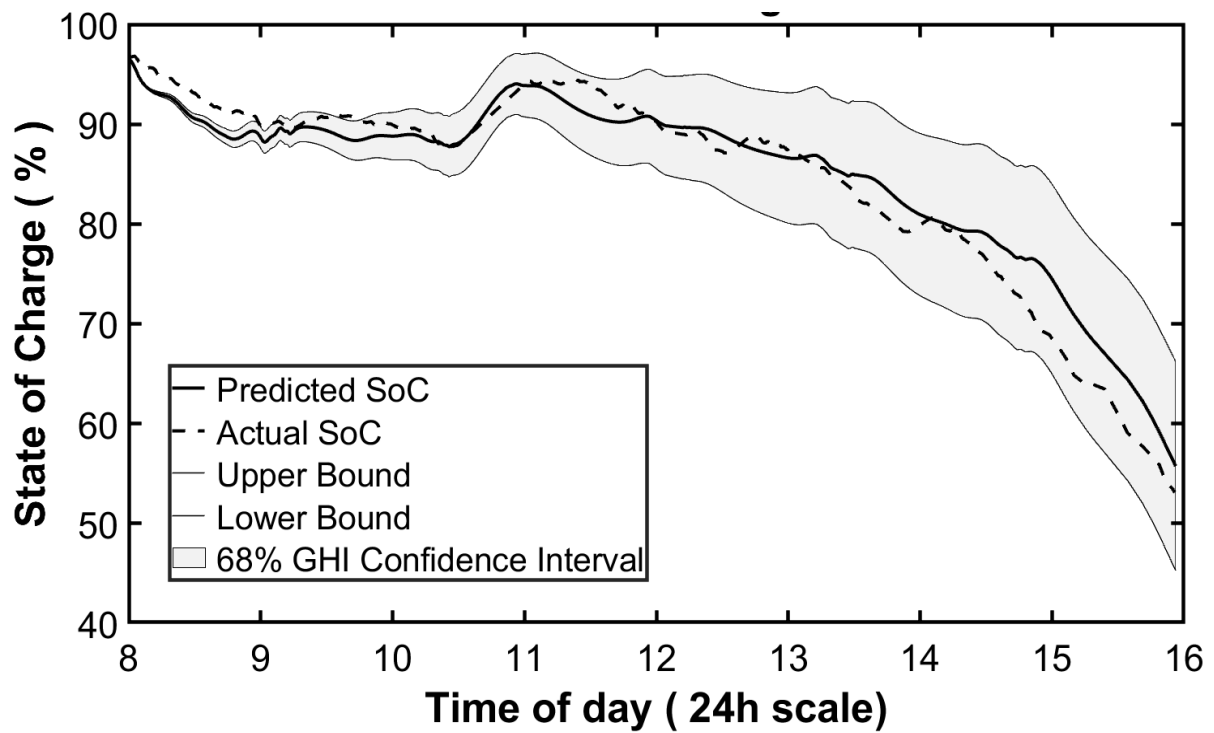


Figure 34: SSC2018 Day 1, SoC comparison

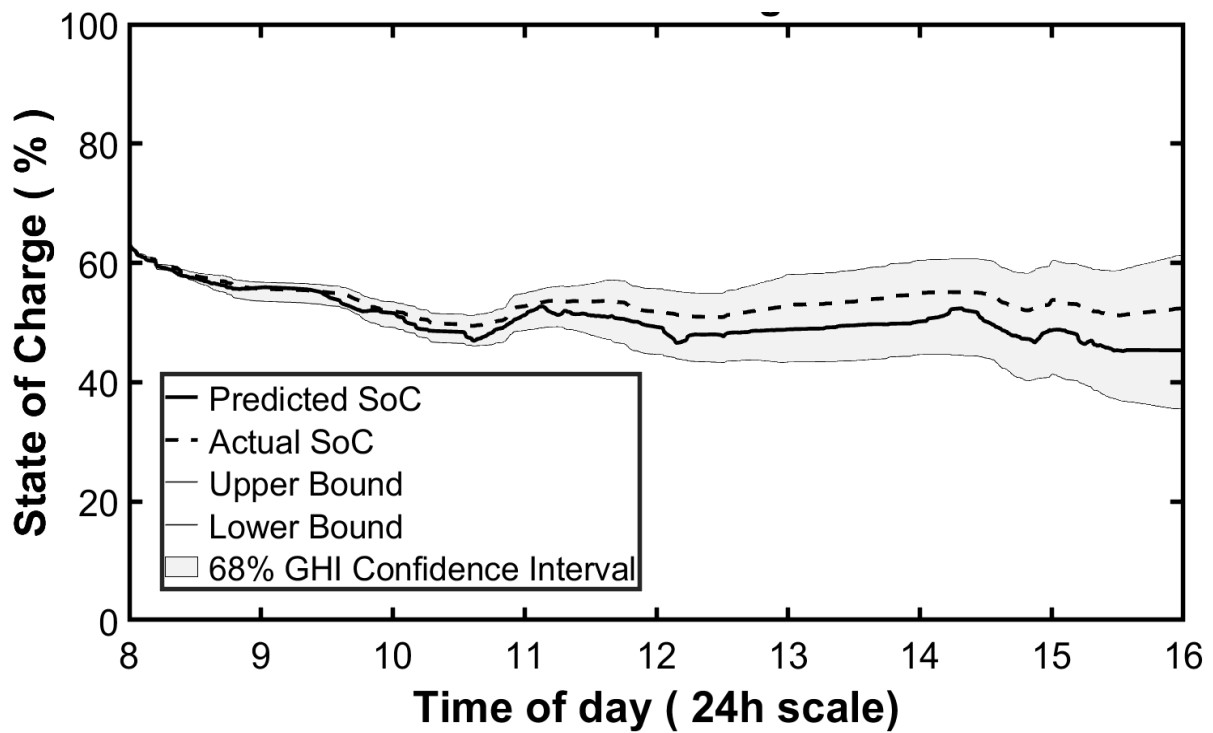


Figure 35: SSC2018 Day 6, SoC comparison

The only noticeable difference in the performance metrics between Day 1 and Day 6, is that on Day 1, on average, the car, experienced more wind from the front (Figure 36) than predicted and on Day 6, on average, the car experienced more wind from the rear (Figure 37) than predicted. Here, the wind was the primary contributor, which yielded 7 % higher and 6 % lower energy usage respectively, despite roughly a 5 % over-prediction of the *GHI* component on both these days, as seen in (Table 31).

On both of these days, a strong coefficient of determination (CoD) between the *SoC* error and both the speed and *GHI* errors, may be seen. This was expected, as the remaining energy-consuming variables for these two days have relatively low prediction errors, allowing most of the *SoC* error variance to be described by the *GHI* and speed error components. Day 4 and Day 7 (Figure 38 and Figure 39, respectively) compared well as both had much larger speed errors (Figure 40) than Day 1 and Day 6. As a result of driving at a higher speed than predicted on Day 4, an apparent phase shift can be seen in the *SoC* plot (Figure 38) as the predicted plot lags the actual plot by over an hour. The team stopped driving at around 14:00 on Day 4 and used the remaining hours for charging their batteries by the sun, which can be seen by a steady *SoC* increase from 14:00 to 16:00 in Figure 38.

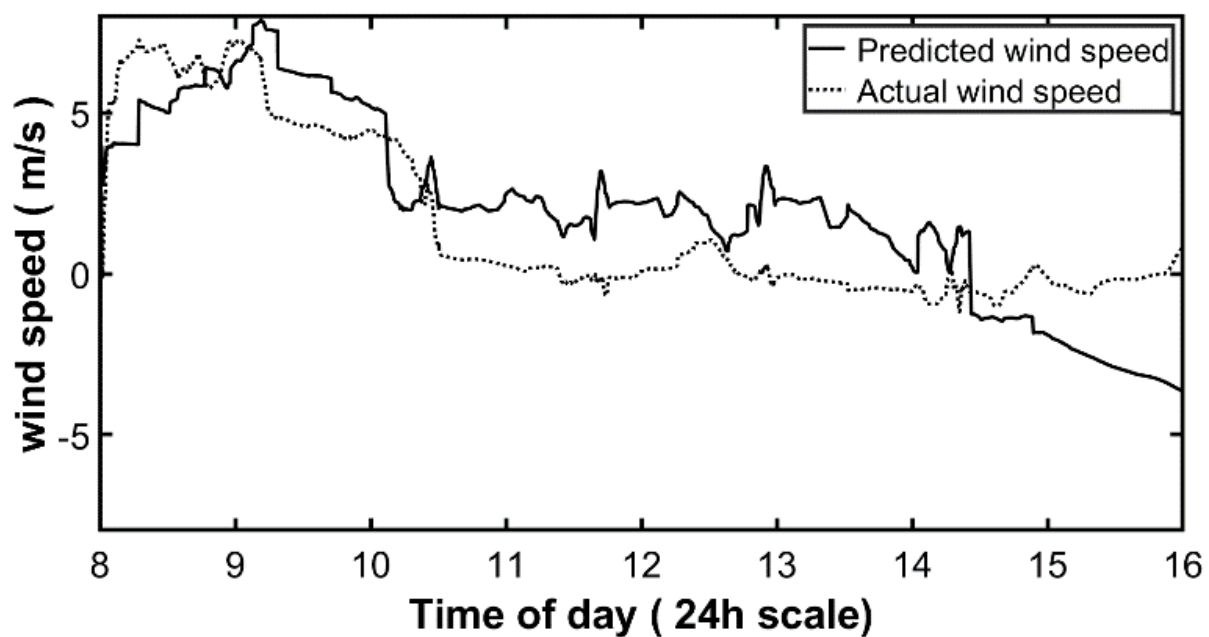


Figure 36: SSC2018 Day 1, wind comparison



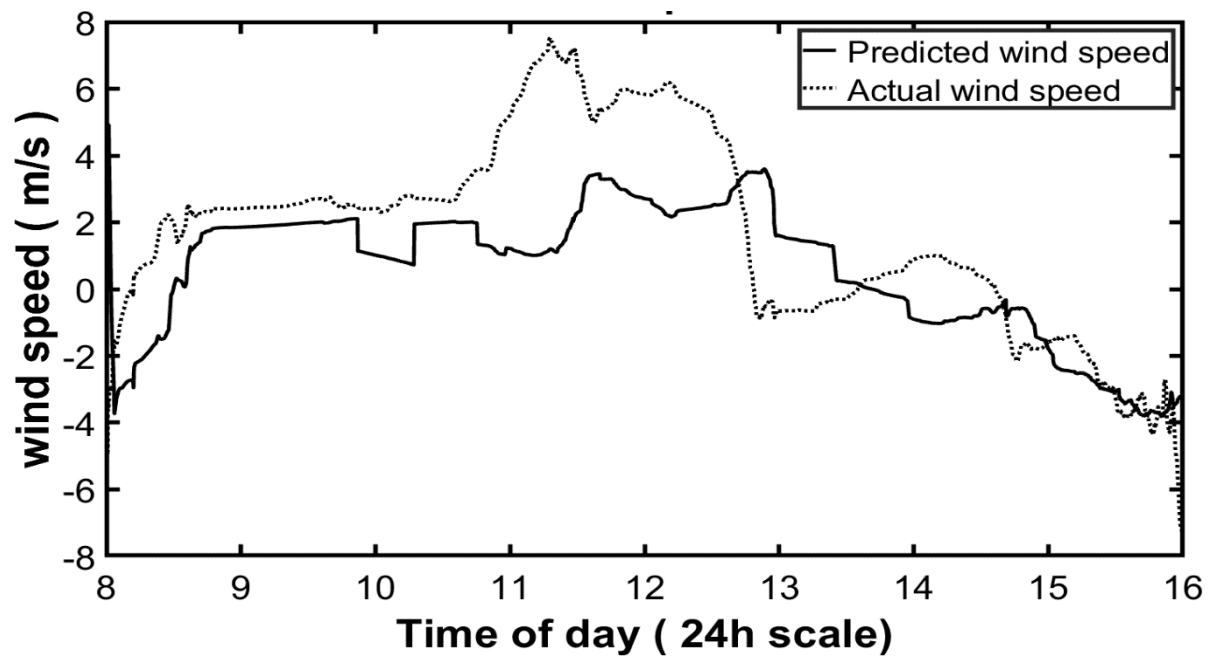


Figure 37: SSC2018 Day 6, wind comparison

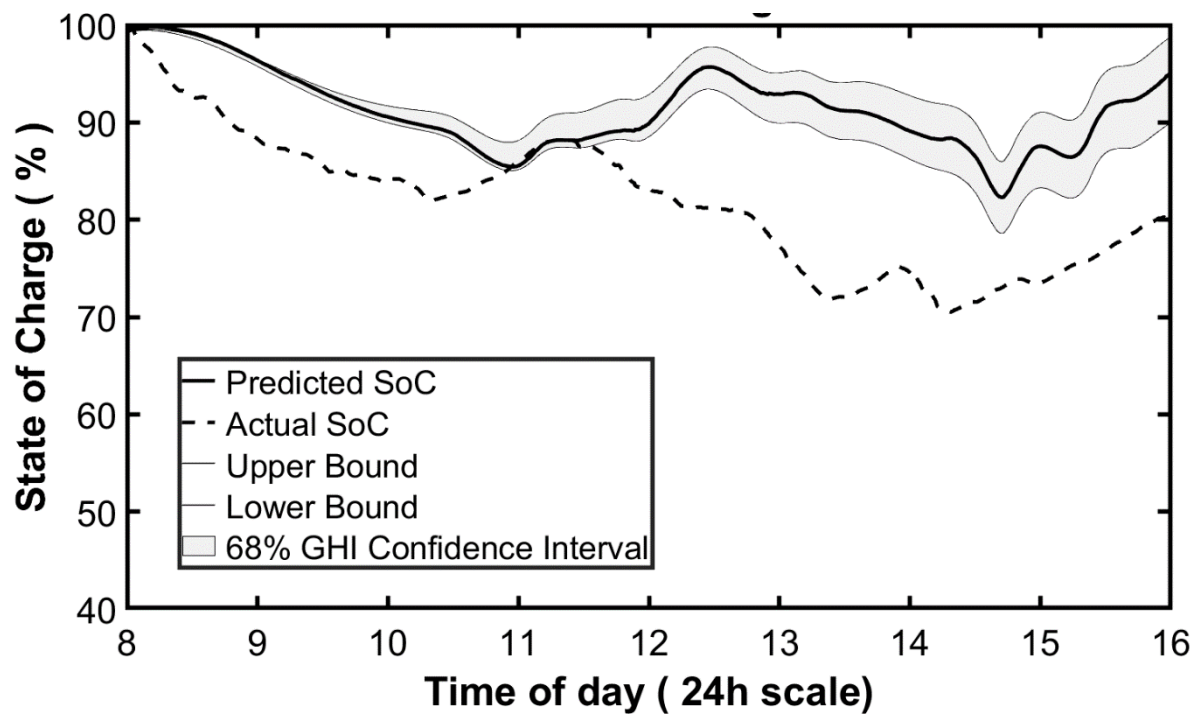


Figure 38: SSC2018 Day 4, SoC comparison

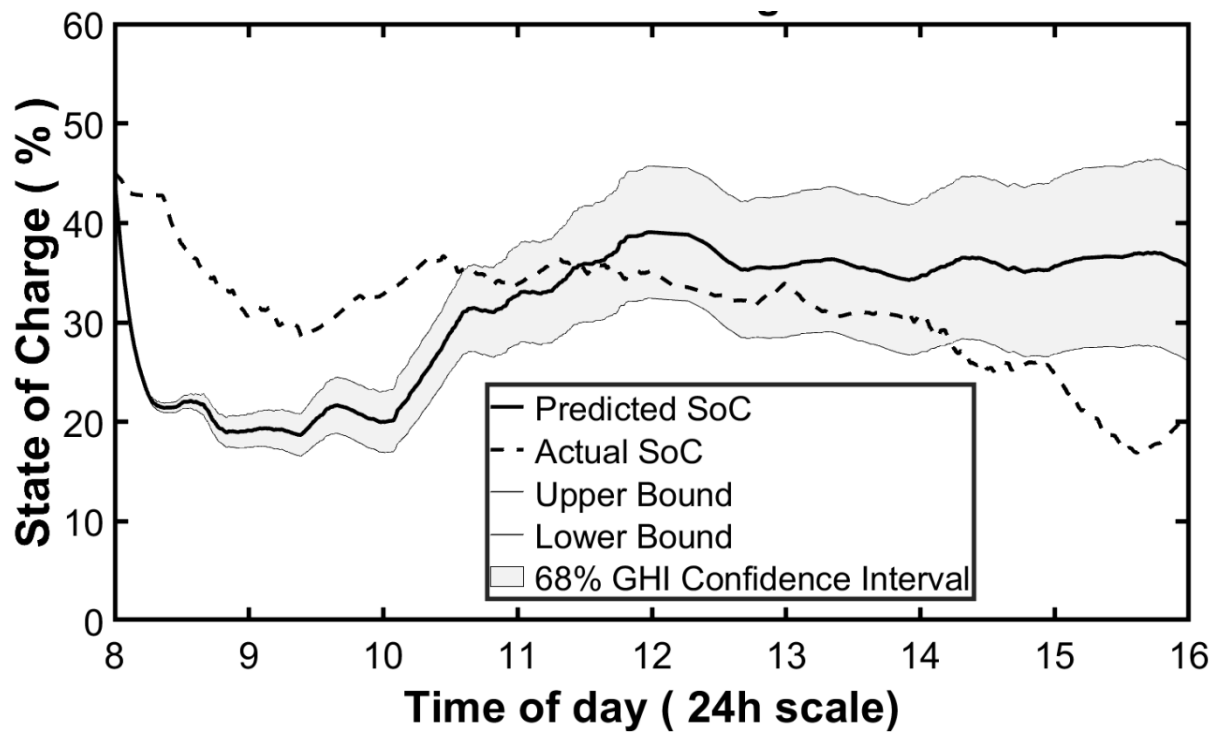


Figure 39: SSC2018 Day 7, SoC comparison

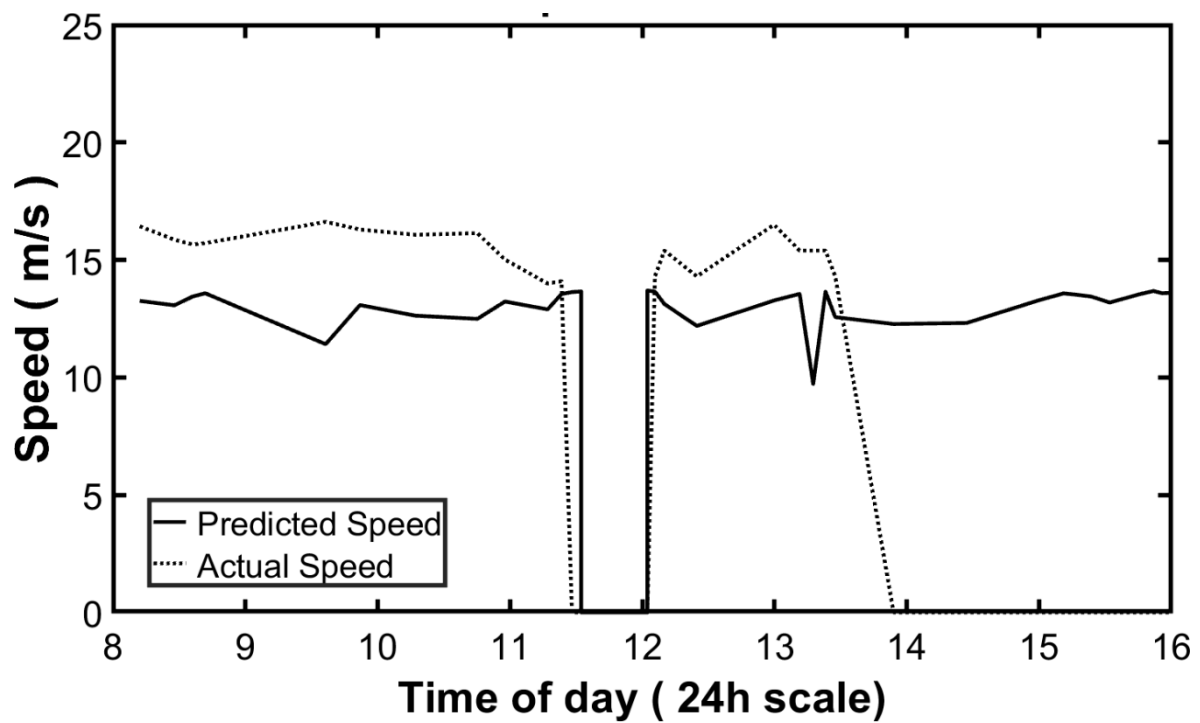


Figure 40: SSC2018 Day 4, speed profile comparison

Day 4 did, however, see significant *GHI* prediction errors (Figure 41) most likely as a result of scattered and unpredictable cloud movement (as observed on that day). This day (Day 4) experienced the largest *GHI RMSE* of 193.22 % (Table 30).

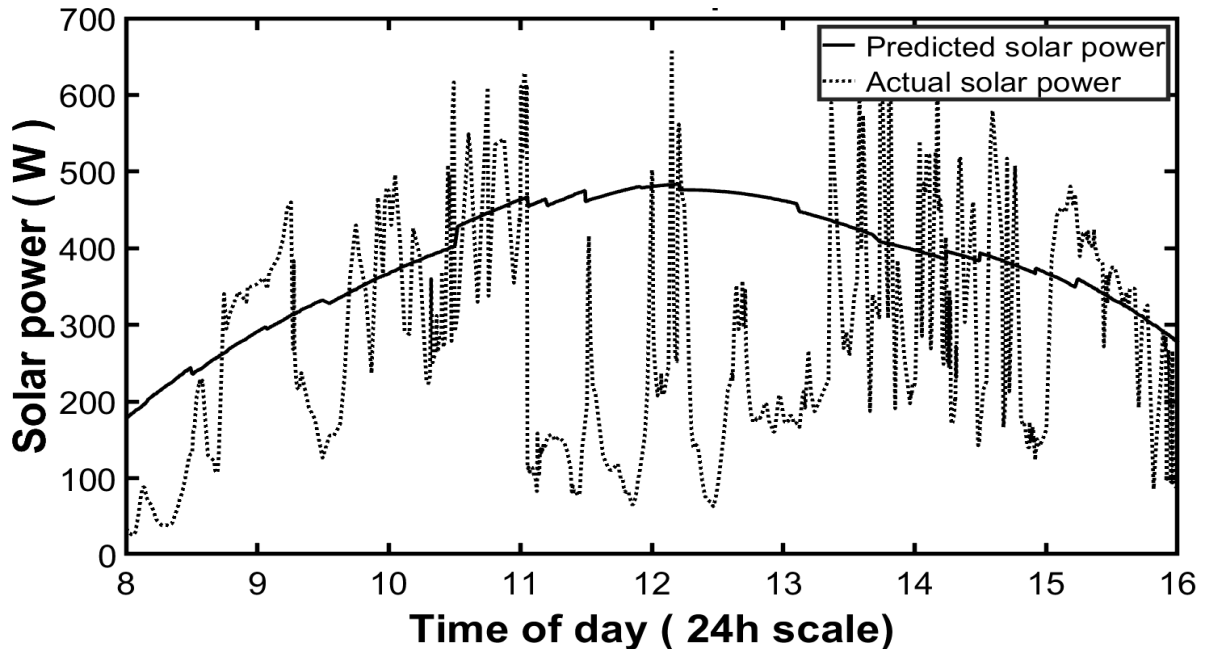


Figure 41: SSC2018 Day 4, solar power comparison

As a result, Day 4 recorded much less energy from the sun than was predicted (12 % less, Table 31) and on average, the day also experienced more wind (Figure 42) from the rear of the car than predicted. The under-prediction of the *GHI* component coupled with the poor adherence to the optimal speed profile (Figure 40) resulted in an astounding three times more energy (Table 31) than predicted being used to cover the same distance.

Similarly to Day 1 and 6, Day 4 and Day 7 had reasonably high coefficients of determination between the *SoC* and the *GHI* and speed errors, even though the adherence to the optimal speed profile is the opposite for the two sets of days.

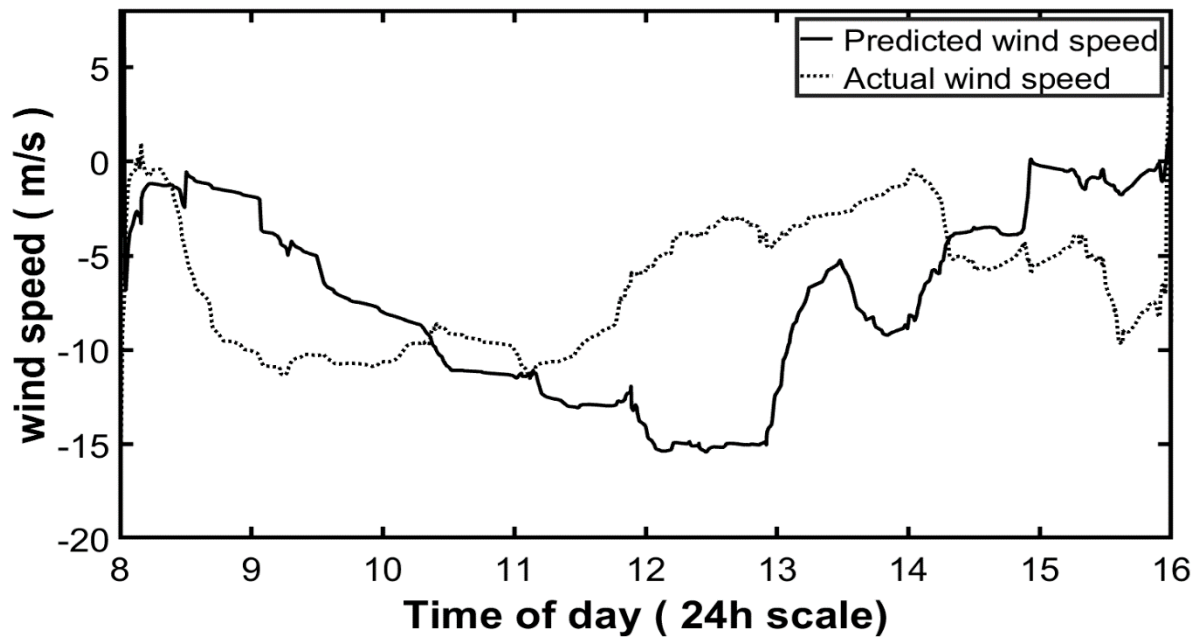


Figure 42: SSC2018 Day 4, wind comparison

Most of Day 7's metrics demonstrated low error values resulting in a high coefficient of determination between the *SoC* error and the *GHI* and speed error components, except for the speed error (62.32 % *RMSE*), which was the largest error in all eight days.

During this day on average, the wind was recorded as coming more from the rear of the car. However, the rest of the error parameters were relatively low and comparable with Days 1 and 6. By the end of this day (which was the end of the Sasol Solar Challenge 2018) 4 % less battery energy was used than had been predicted. After summing all the portions of battery energy used each day (including gained battery energy on Day 2 and 3), Sun Chaser III ended up with a battery *SoC* of about 10 % upon completion of the challenge.

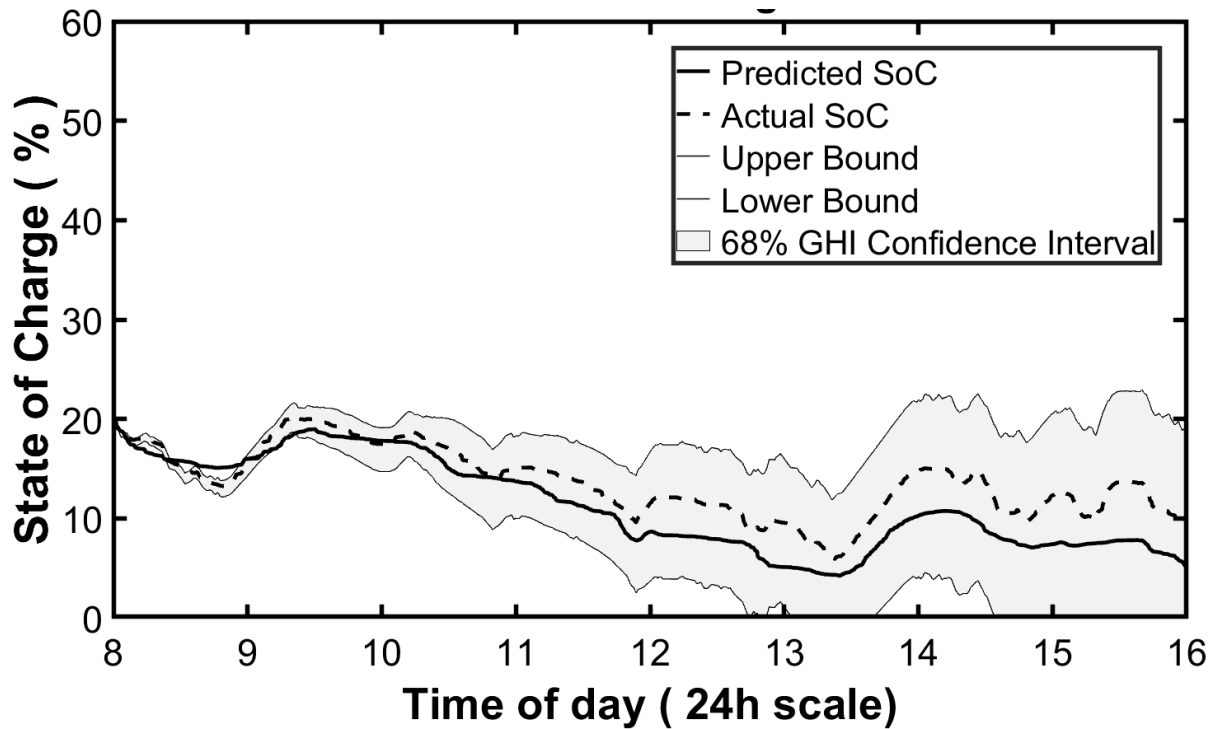


Figure 43: SSC2018 Day 8, *SoC* comparison

After evaluating the performance of the five days of usable data, it is clear that deviating from the speed profile (in other words, driving faster or slower than the optimised speed profile recommendation) is detrimental to the stored battery energy and usefulness of the simulations; likewise, when significant errors were observed among the weather forecast parameters.

On rare occasions, errors of forecasted parameters resulted in a positive effect on the battery pack. These were mostly seen in situations of more wind from the rear than predicted and in cases of *GHI* underprediction. *SoC* error coefficients of determination are observed to be the highest with the *GHI* errors and speed errors, which confirms that these parameters have the best linear relationship with the *SoC* error. Foreseeably, errors in other parameters reduce the quality of the linear relationship between the *SoC* errors and the *GHI* and speed errors.

Considering the five days of useful data, the optimisation technique was able to predict the battery *SoC* to within an absolute value of 8 %, providing the forecasts are within typical meteorological expected upper and lower bounds (referring to Day 1, 6 and 8) as well as speed *RMSE* errors below 17 % (user driving behaviour dependent). More

significant weather forecast accuracy deviations (Day 4) and speed deviations (Day 7) resulted in three to four times more energy used than expected to cover the same distance in the same time.

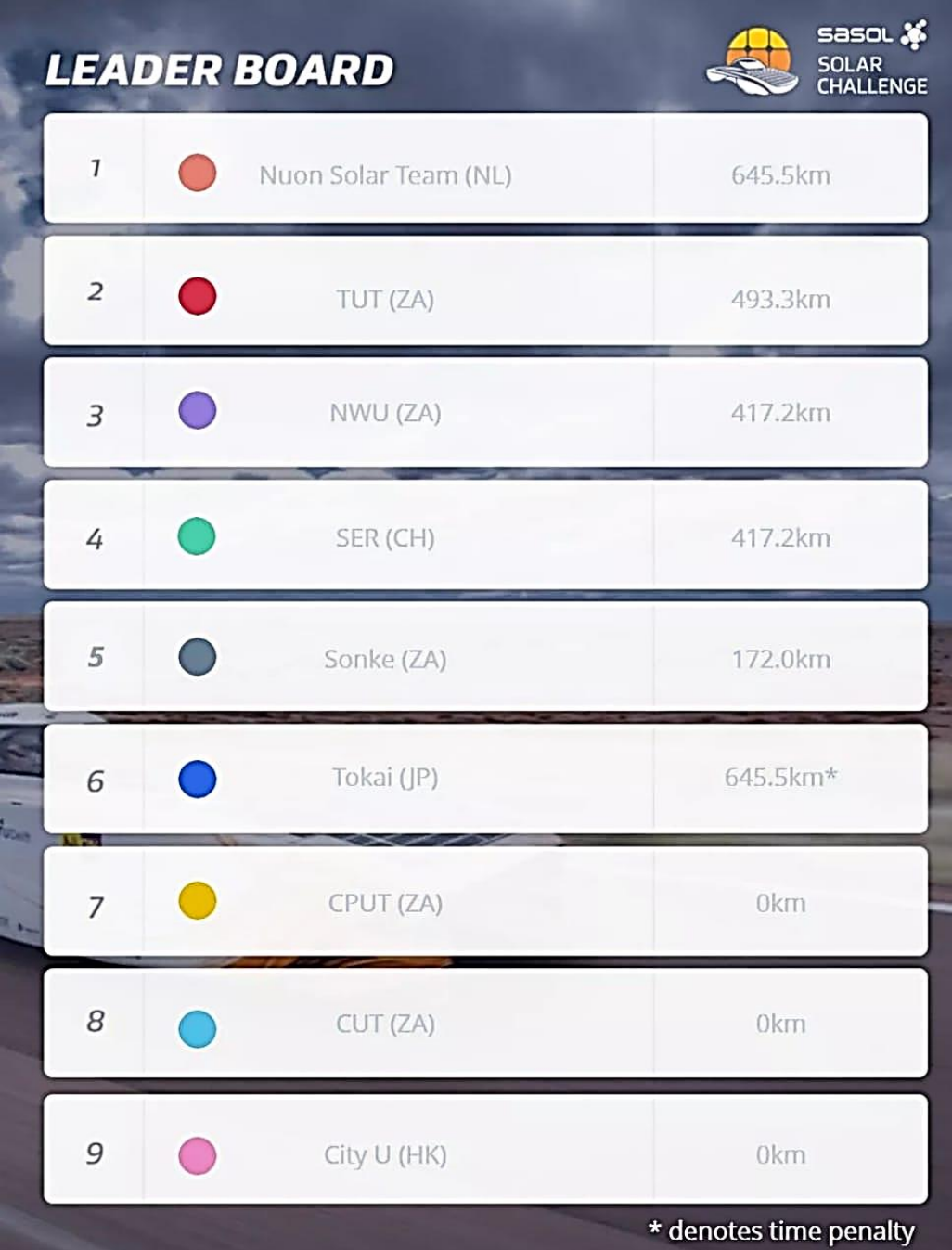
Certainly, one of the most significant results is that the average sum of the coefficients of determination for each day adds up to 0.94. This establishes that on average, 94 % of the variation in the energy simulation (State of Charge - *SoC*) error can be explained by the variables contained within the derived energy model. The remaining 6 % variation in the energy simulation error may have occurred as a result of small unmodelled vehicle dynamics (including Coriolis forces), non-linearity of the charge and discharge cycles of the battery and temperature effects.

Furthermore, the *GHI* confidence intervals proved useful in defining upper and lower *SoC* limits on days where the speed profile was adhered to (Days 1, 6 and 8), leaving the *GHI* as the primary variable that would influence the actual *SoC*. On days where the speed profile was not adhered to (Day 4 and 7), the *GHI* confidence intervals were less useful since the actual *SoC* already deviates significantly from the estimated *SoC* which the *GHI* confidence intervals are centred around.

The following section covers a more focussed examination of the first, seventh and last day of the SSC2018. This section discusses the specific route characteristics and the weather conditions on these days and the significance of these results to this work.

### Detailed case study of Day 1

The significance of this day is that TUT managed to travel the third furthest distance overall (in relation to all the participants) on this day, and the furthest in relation to the local participants. The 493 km TUT travelled on this day is an unofficial record for the furthest distance travelled in any Sasol Solar Challenge by a local team with 4 m<sup>2</sup> of silicon solar panels. Figure 44 shows the official leader board results for this day.



The image shows a digital leader board for the Sasol Solar Challenge. At the top left, the text 'LEADER BOARD' is displayed in a bold, white, italicized font. At the top right, the Sasol Solar Challenge logo is visible, featuring a stylized sun and the text 'sasol SOLAR CHALLENGE'. The leader board consists of a table with nine rows, each representing a team. Each row contains a rank number, a colored circle representing the team's color, the team name and country, and the distance travelled in km. The background of the leader board is a dark, textured image of a solar panel array.

Rank	Team	Distance (km)
1	Nuon Solar Team (NL)	645.5km
2	TUT (ZA)	493.3km
3	NWU (ZA)	417.2km
4	SER (CH)	417.2km
5	Sonke (ZA)	172.0km
6	Tokai (JP)	645.5km*
7	CPUT (ZA)	0km
8	CUT (ZA)	0km
9	City U (HK)	0km

\* denotes time penalty

Figure 44: SSC2018 Day 1, official results

The elevation profile in Figure 45 depicts the re-occurrence of three distinctive peaks, that is, the three loop sections covered on Day 1 as recommended by the optimisation simulation output.

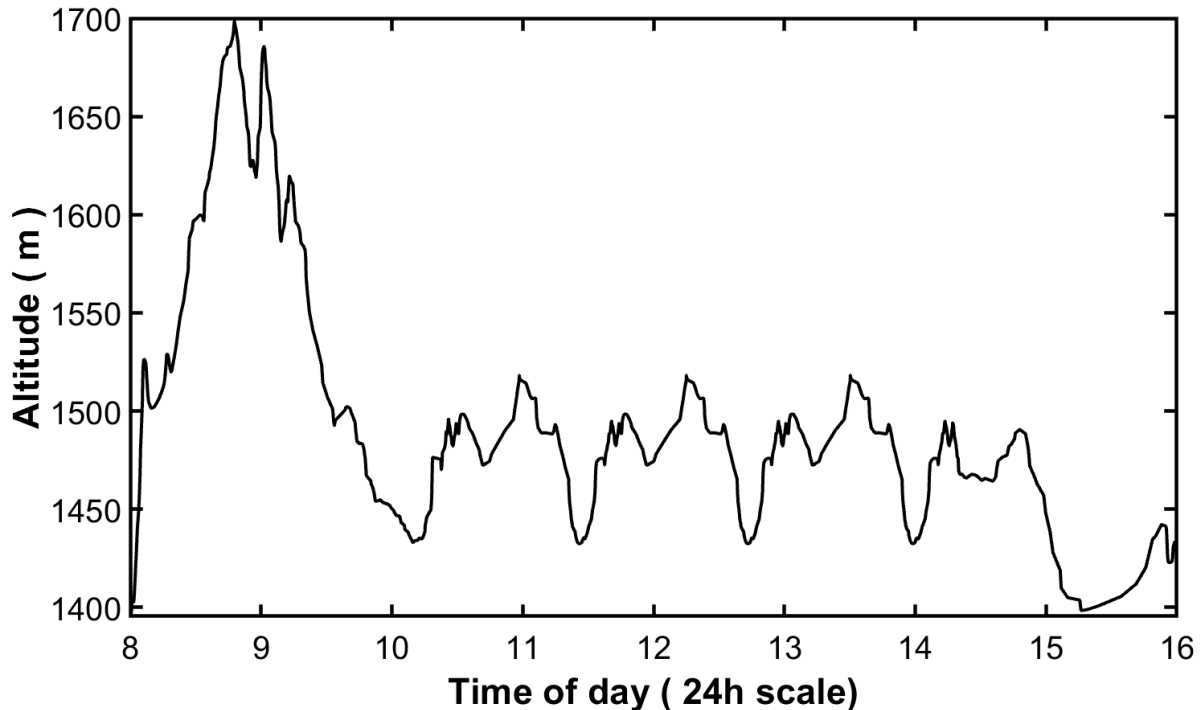


**Figure 45: SSC2018 Day 1, route elevation**

Apart from one or two hills, the road gradient was predominantly flat. The clouds on this day were initially low at about 20 % *TCC* in the morning descending until around midday, after which the cloud cover increased nearly linearly to about 70 % at 16:00. The air density for the day had a mean value of  $1 \text{ kg.m}^{-3}$  and a mean deviation of less than 5 % during the day. The accuracy of the wind predictions was fair overall compared to the recorded wind on the day except for the period 14:30 to 16:00 as depicted in Figure 36. The real recorded data of the useful solar power plot (Figure 47) contained a few high-frequency anomalies that were observed throughout the day. This was possibly due to the trees, bridges, and other significant obstacles momentarily casting shade onto the solar vehicle and onto the roof-mounted solar irradiance sensor. Overall, the useful solar power prediction, with the aid and application of the PMFs to increase accuracy, performed well, even during a day of varying cloud cover conditions.



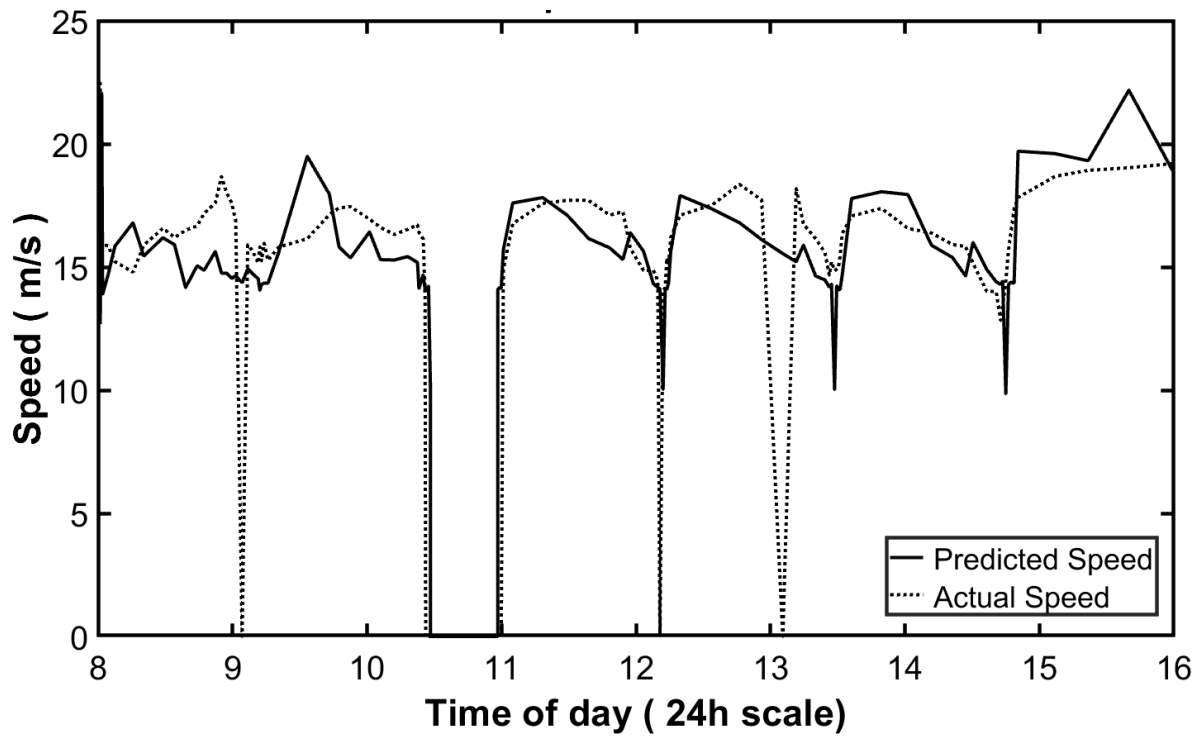


Figure 46: SSC2018 Day 1, speed profile comparison

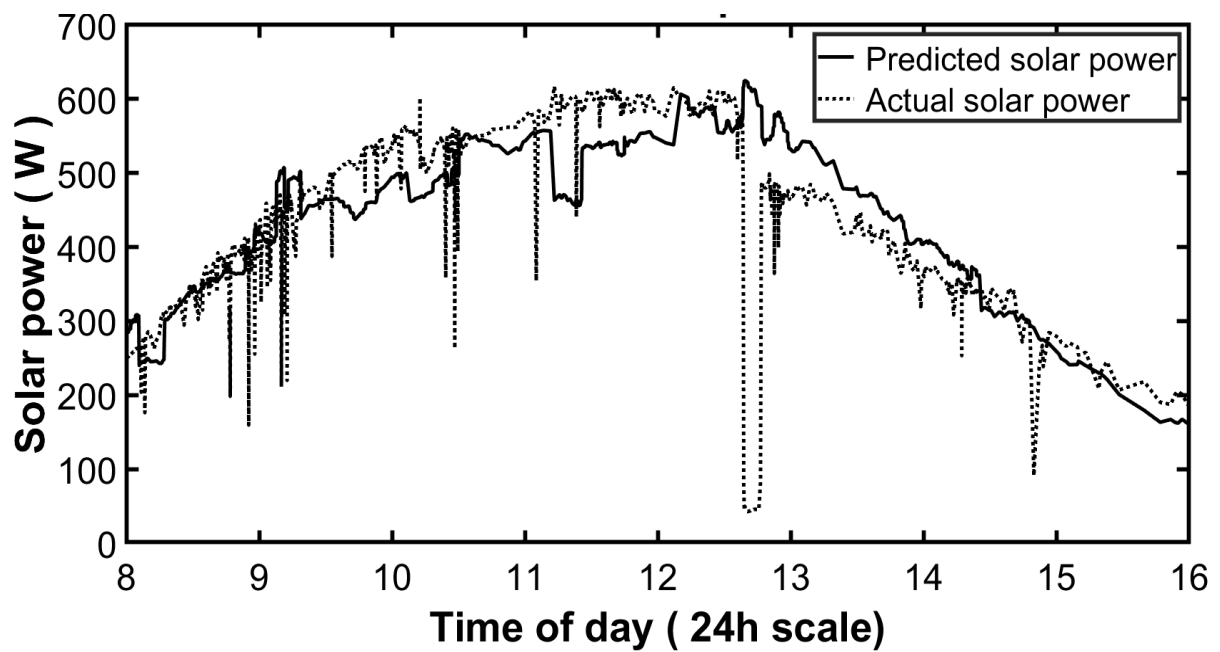


Figure 47: SSC2018 Day 1, solar power comparison

During the first day of the SSC2018, the team realised that it was somewhat impractical to follow the exact optimal speed profile suggested by the optimisation technique. Traffic conditions on national roads often compelled the driver to deviate from the optimal speed profile as illustrated in Figure 46, where the dotted line in the graph tracks the driver's actual variations in speed. However, the maximum acceleration necessary to adhere to this optimal speed profile was less than  $0.5 \text{ m.s}^{-2}$ , which is entirely safe and acceptable for the driver as well as the solar-powered electric vehicle. Thus, no extra constraints were included to remedy this behaviour. The team followed the speed recommendations as far as practically possible and chose the best average speed to try to satisfy the mean of a few consecutive speed points where it was deemed impractical to follow the optimal speed profile wholeheartedly. The mandatory control-stop occurred at around 10:30 to 11:00, which is well in line with the original prediction. A few brief stops had to be made along the route just after 09:00, 12:00, and 13:00, which had not been accounted for in the forecast. These stops were mainly due to traffic conditions and driver changes.

When examining the actual and predicted *SoC* curves in Figure 35, a reasonable correlation between the two curves could be seen up until approximately 13:00, at which point the actual *SoC* decreased more than had been predicted. This miscorrelation was most likely caused by the deviations of the various actual weather conditions from those that were predicted. In addition to this, the electric vehicle did not adhere as precisely to the speed profile as was recommended by the UI. Overall, this caused an overprediction of about 7 % *SoC* by 16:00 on Day 1 of the SSC2018. Another compelling correlation was that the three distinctive peaks seen in the curve of the optimal speed profile (Figure 46) after 11:00, were roughly inversely proportional to the peaks in the elevation profile (Figure 45). This indicates that the optimisation technique is greatly affected by the road profile as this is one of the more significant consumers of energy and subsequently, an area where energy could potentially be optimised. Fortunately, the elevation profile of the desired route is known and constant, which means that although the elevation profile is seen to affect energy usage significantly, it is effectively and robustly predictable.

### Detailed case study of day 7

At the start of this day, the Sasol Solar Challenge teams found themselves in a morning rainstorm. All local solar car teams (except TUT) opted not to drive in the rain. TUTs energy management system indicated that distance would be maximised when driving through the fully overcast rainstorm as opposed to loading the solar car on a trailer and travelling to a point further on the route where the rain had subsided.

A digital leaderboard for the Sasol Solar Challenge, Day 7. The background is a blue sky with a checkered flag pattern on the left and a photo of people on the right. The title 'LEADERBOARD' is in large white letters, with '#SASOLSOLARCHALLENGE' below it. The Sasol Solar Challenge logo is in the top right. The table has four columns: Rank, Team (with a colored circle), Day 7 Mileage Covered, and Total Mileage. Teams are listed from rank 1 to 9. Asterisks in the Day 7 mileage indicate a time penalty.

		TEAM	DAY 7 MILEAGE COVERED	TOTAL MILEAGE
1	Red circle	TUT (ZA)	308,7km	1994km
2	Green circle	SER (CH)	291,6km*	2240,5km
3	Dark blue circle	Sonke (ZA)	54,4km	544,5km
4	Pink circle	City U (HK)	35,2km	130,3km
5	Light blue circle	CUT (ZA)	22,6km	110,3km
6	Yellow circle	CPUT (ZA)	19,2km	19,2km
7	Orange circle	Nuon (NL)	532,7km*	3515km
8	Blue circle	Tokai (JP)	468,7km*	3545,7km
9	Purple circle	NWU (ZA)	325,9km*	1935,3km

\* DENOTES TIME PENALTY

Figure 48: SSC2018 Day 7, official results

On this day, TUT completed 308 km, which once again topped the leaderboard (Figure 48) among local teams. Although team NWU is seen to have 325.9 km for this day, the asterisk indicates that this distance was obtained outside of the rules of the Challenge and hence was not a valid result. Figure 49 shows the unfavourable rainy conditions of the first few hours of this day.



**Figure 49: SSC2018 Day 7, weather conditions**

None of the other local teams had any formal energy management strategies and therefore relied on their intuition for making decisions. At first, the TUT team was sceptical about the energy strategy recommendations of the UI, which suggested that maximising distance for this day meant driving through the morning rainstorm. The outcome is proof of the superiority of the optimisation technique.

Even though the TUT team opted to follow the recommendations of the optimisation technique to drive in the rain, it was deemed unsafe to travel at the optimal speeds (Figure 50) during the rain period. The road was extremely slippery, and the route had severe road grades which required additional caution. Figure 51 reveals the steep hills which the driver had to traverse in the rainstorm as well as the two-loop road sections, which are the two visible repeating patterns. It is important to note that the elevation

profile and useful solar power plots (Figure 53) are for reference only and are based on the speed profile as in Figure 50. These plots do not necessarily correlate with the real-world time of day due to the intentional speed variations imposed by the energy manager for the sake of safety.

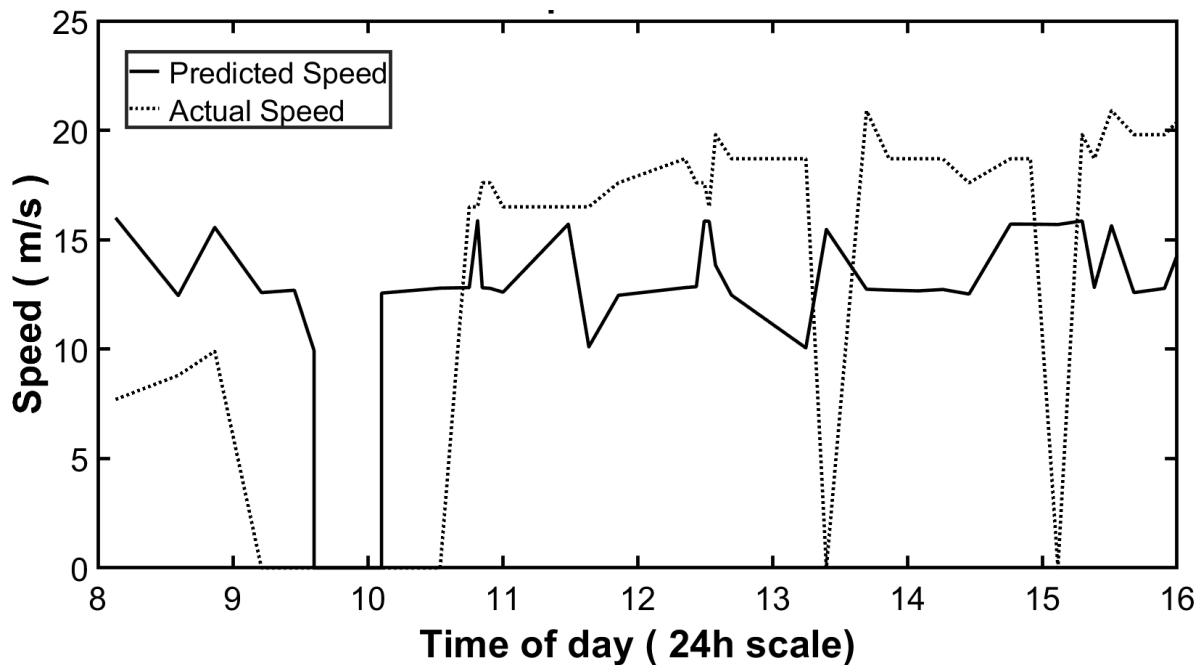


Figure 50: SSC2018 Day 7, speed profile comparison

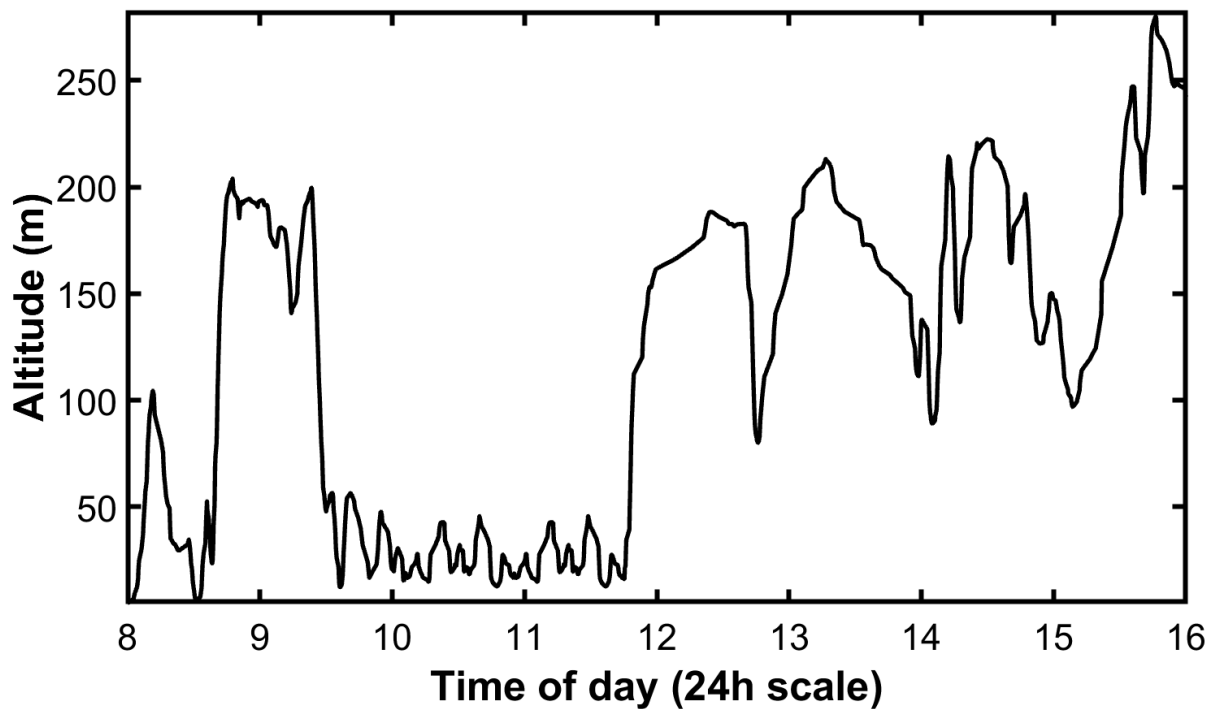


Figure 51: SSC2018 Day 7, route elevation

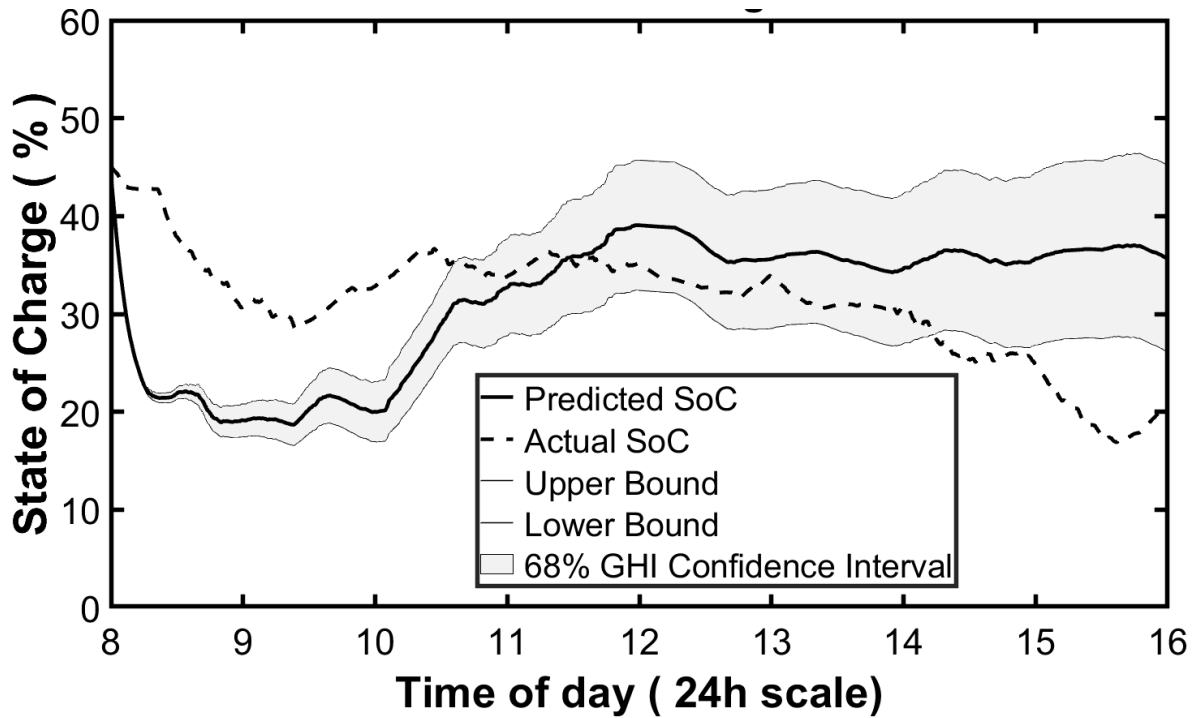


Figure 52: SSC2018 Day 7, *SoC* comparison

The morning weather conditions contributed to high driver fatigue which meant a driver change was needed at 09:30, and it was decided to take the mandatory 30-minute break at that stage too. By this time the rain started to subside and the cloud cover reduced to about 70 % *TCC*.

At around 10:30 the team once again re-entered the challenge. As a result of the slow driving during the morning, the energy manager decided to increase the optimal speed recommendations by approximately 25 % for the rest of the day. The effect of deviating from the optimal speed (Figure 50) is evident in the *SoC* plot (Figure 52). This effect is observed as an under-estimation in the morning with the crossover point at around 11:30 after which an over-estimation is observed. Hence, Day 7 has the most significant speed *RMSE* error of all the days (Table 30). The energy manager could have opted to re-calculate the optimal speed profile during the day. However, it was intentionally not done in order to be able to document the statistical and graphical significance of a case where the optimal speed profile calculation could only be executed once, prior departure in the morning.

The useful solar power plot, Figure 53, depicts the predicted solar energy curve skewed to the right as a result of the severe rain and cloud reducing the *GHI* magnitude during the morning. Overall, the *GHI* prediction was still favourable for this day, which correlates well with the statistics in Table 30.

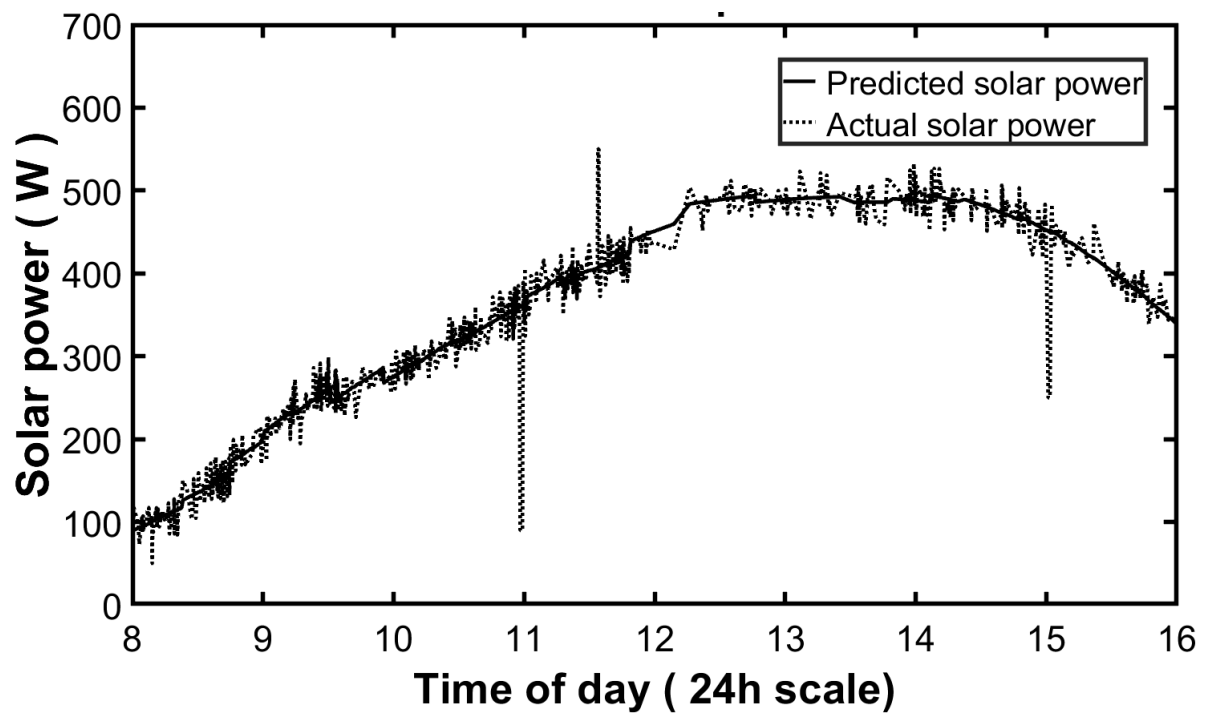
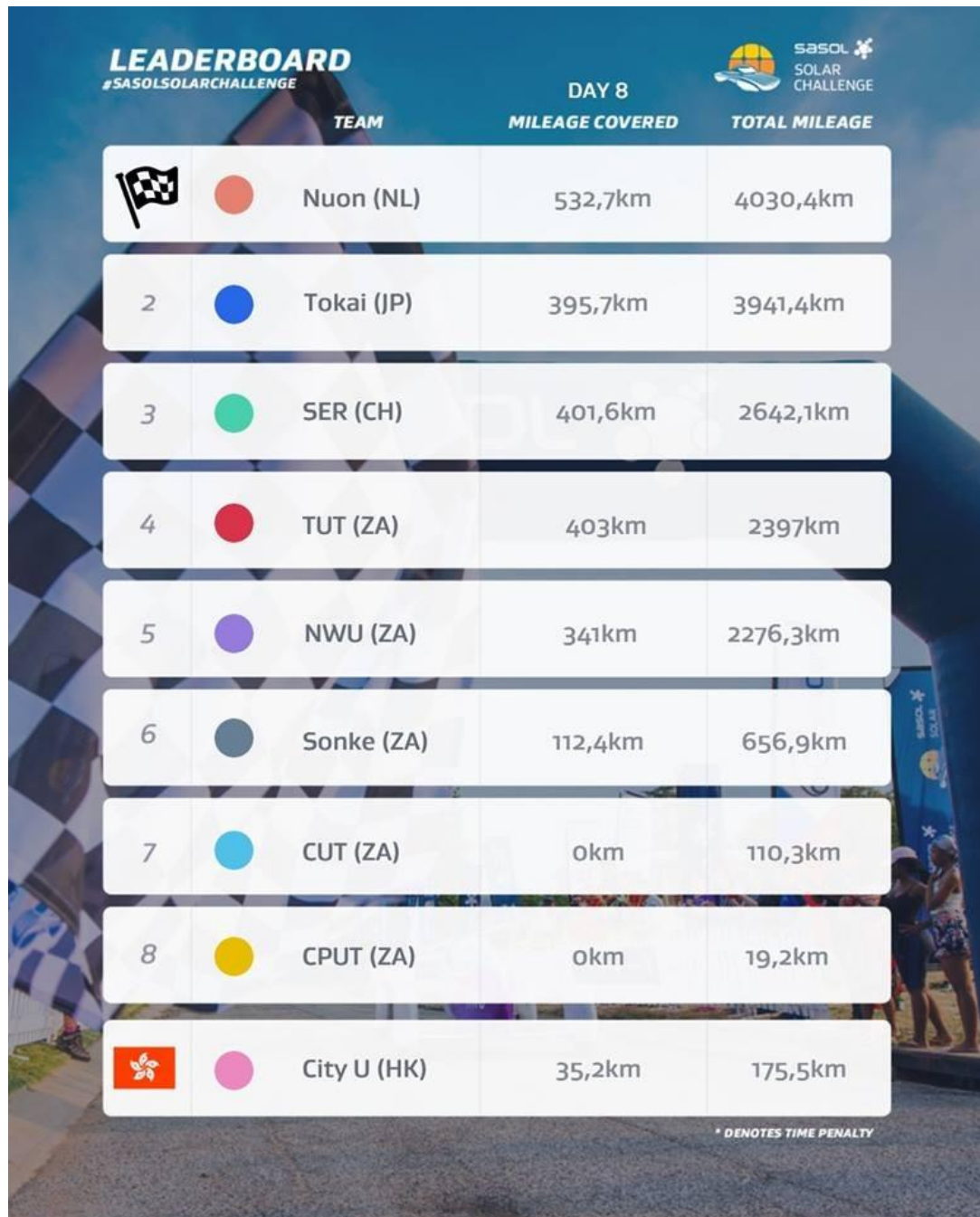











Figure 53: SSC2018 Day 7, solar power comparison

### Detailed case study of day 8

This was the final day of the SSC2018, which took teams from Swellendam to Stellenbosch. The leaderboard results are shown in Figure 54.

The image is a digital graphic of a leaderboard for the Sasol Solar Challenge 2018, Day 8. It features a blue background with a checkered pattern on the left and a photo of participants on the right. The title 'LEADERBOARD' is in large white letters, with '#SASOLSOLARCHALLENGE' below it. The 'DAY 8' title is centered above the table. The Sasol Solar Challenge logo is in the top right. The table has four columns: a rank column, a team column with a flag and colored circle, a 'MILEAGE COVERED' column, and a 'TOTAL MILEAGE' column. The teams are listed in descending order of total mileage. A small note at the bottom right states '\* DENOTES TIME PENALTY'.

	TEAM	MILEAGE COVERED	TOTAL MILEAGE
	 Nuon (NL)	532,7km	4030,4km
2	 Tokai (JP)	395,7km	3941,4km
3	 SER (CH)	401,6km	2642,1km
4	 TUT (ZA)	403km	2397km
5	 NWU (ZA)	341km	2276,3km
6	 Sonke (ZA)	112,4km	656,9km
7	 CUT (ZA)	0km	110,3km
8	 CPUT (ZA)	0km	19,2km
	 City U (HK)	35,2km	175,5km

\* DENOTES TIME PENALTY

Figure 54: SSC2018 Day 8, official results



The weather conditions for this day were in complete contrast to the previous day as seen in Figure 55 where the TUT team is seen at their mandatory 30-minute control stop at the southernmost tip of Africa, Cape Agulhas Lighthouse.



**Figure 55: SSC2018 Day 8, weather conditions**

A comparison between the magnitude and shape of the useful solar power plots of Day 7 (Figure 53) and Day 8 (Figure 56) further reveals the favourable weather conditions of Day 8. Although the weather conditions seemed ideal for solar harvesting, the route of Day 8 is notorious and known to be one of the most challenging in the Sasol Solar Challenge, due to the mountain range which is an integral part of the route (Figure 57) for this day. This route boasts the locally renowned mountain road, Sir Lowry's Pass. This pass puts even the best of cars and trucks to the test with a 450 m accent to its summit.

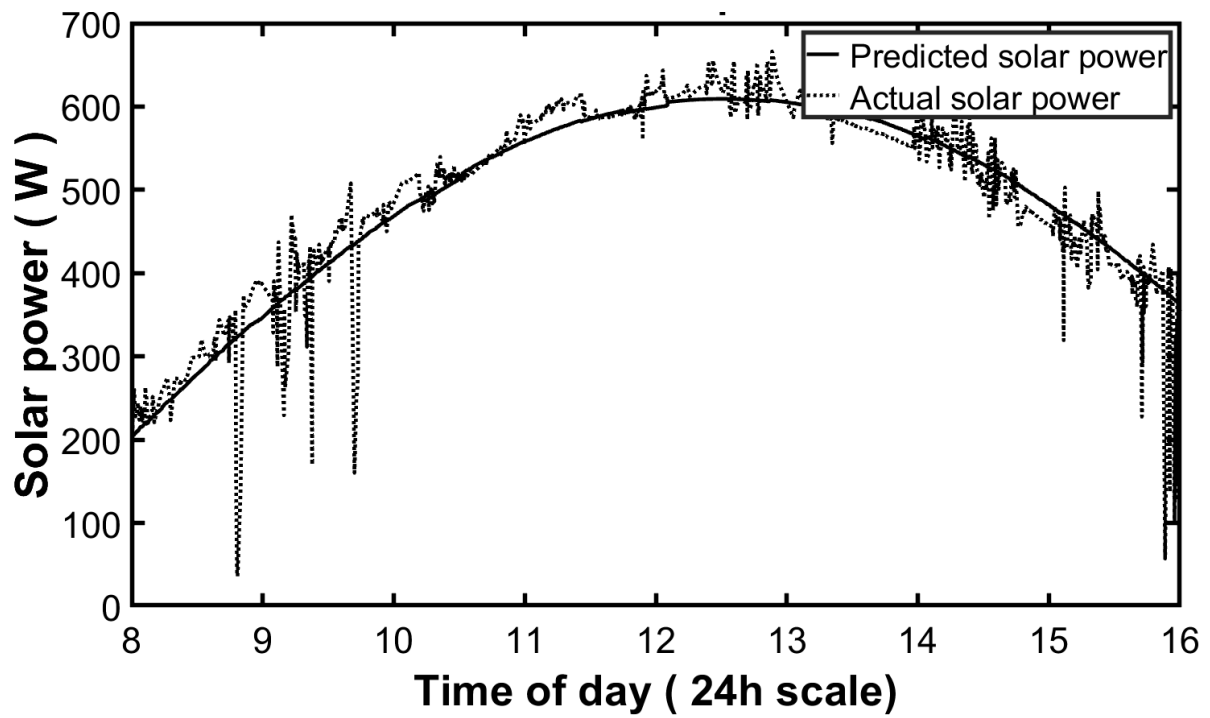


Figure 56: SSC2018 Day 8, solar power comparison

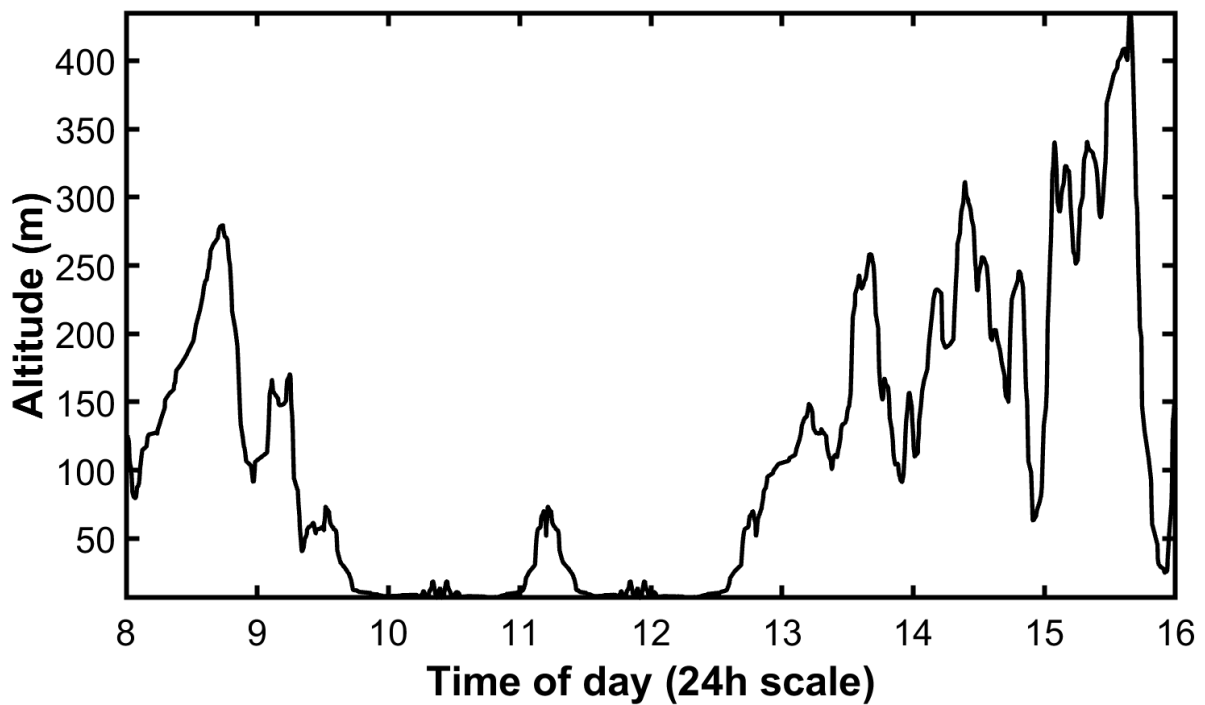


Figure 57: SSC2018 Day 8, route elevation

By the last day of the challenge, most teams would have expended a large portion of their stored energy over the previous seven days in an attempt to maximise distance. Day 8 of the Sasol Solar Challenge is by far the most stressful for any team energy manager. The additional loop section opportunity (seen from 10:00 to 12:30 in Figure 57) is situated before the mountainous region which requires careful planning to maximise distance while still being able to reserve enough energy to summit the massive hills reached from 12:30 to 15:45 in Figure 57. When observing Figure 58, the minimum value of the *SoC* was predicted to be 5 % at about 13:30. This is where the optimiser reached the battery safety-critical constraint ( $\beta$ ) as contained in Equation (35). With every significant downhill, the regenerative braking can be seen to increase the stored energy, which helps to alleviate the energy impact of the next hill.

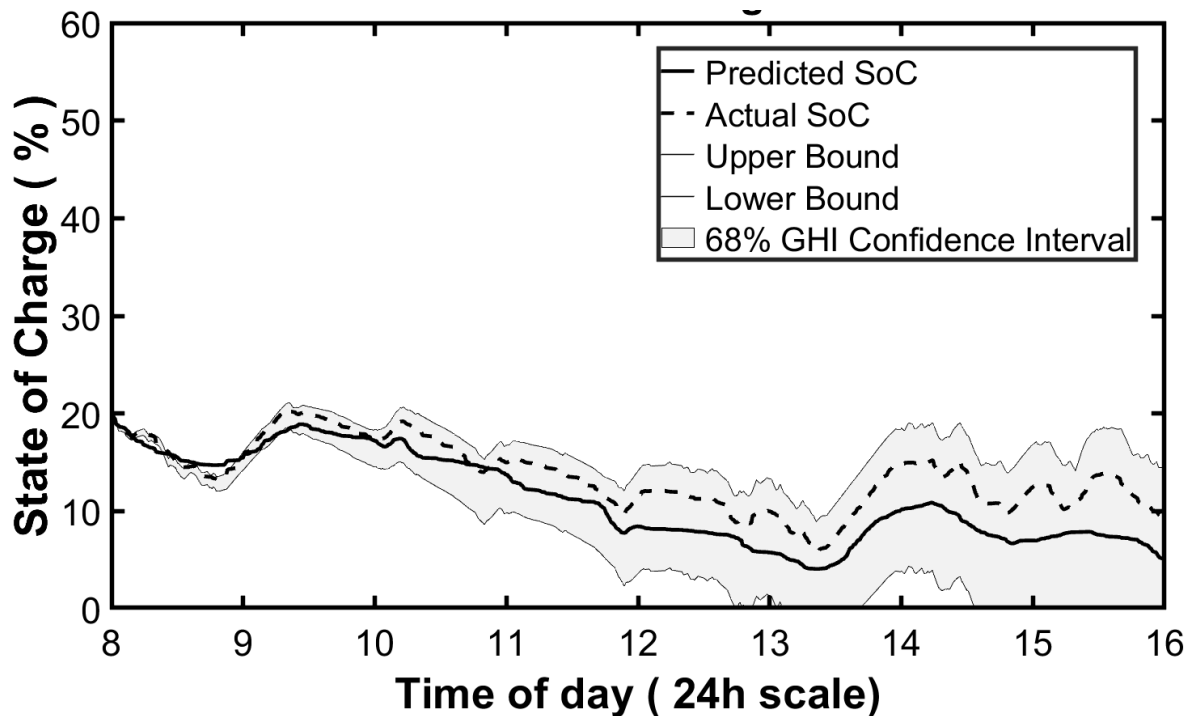


Figure 58: SSC2018 Day 8, *SoC* comparison

To an ordinary energy manager with no assistance from a formal optimisation strategy, the sunny conditions seemed like the ideal opportunity to do many additional loop road sections. This turned out to be a dangerous assumption as none of the other local teams conserved enough energy to navigate to the summit of Sir Lowry's Pass successfully, which followed the loop road sections. These intuitive energy decisions

of the other local teams, uninformed by a data-driven system to optimise energy use, ensured that TUT was the only local team that finished the final day without penalty and without having to load the solar car on a trailer, which was the case with all other local teams. The speed profile for Day 8 is not shown as it does not add significant value to this section.

## **CASE STUDY CONCLUSION**

During the Sasol Solar Challenge 2018, the optimisation technique benefitted the TUT solar car team immensely. The optimisation technique was shown to be robust on days of extreme weather conditions as well on days with complex mountain terrain. The superiority of the optimisation technique was highlighted on several occasions where the recommendations from the simulation trumped team intuition and experience-based decision-making processes. Furthermore, the optimisation technique proved that it was able to maximise the performance of Sun Chaser III and advise the energy manager on how to expend energy optimally over an eight-day horizon with accurate predictions.

Lastly, the results showed that deviating from the optimal speed profile is severely detrimental to the outcome. Therefore, it is advised that the team do whatever it takes within safe and legal limits to keep to the optimal speed profile to maximise performance.

## VII. CONCLUSIONS, RECOMMENDATIONS AND FUTURE WORK

### RESEARCH QUESTIONS

The aims and objectives of this work have been addressed by answering the research questions set out in Chapter I (Research Objective and Project Overview). The research questions of this work were addressed in the following manner:

Research Question 1 and its sub-questions, was addressed in Chapter II (Literature Review), Chapter III (Modelling), Chapter IV (Environmental Conditions) and in Chapter V (Optimisation).

The variables influencing the mathematical model of the solar car were comprehensively described in Chapter II and extended and formalised in the form of usable equations and functions in Chapter III. All the dependent (such as the *SoC*), independent (electromechanical energy model parameters) and moderating (weather conditions) variables have been identified and their relationships established. The *GHI* forecast and speed of the car was found to have the most significant effect on the simulation accuracy of the *SoC*.

It was shown that the statistical variation in the environmental variables (especially the *GHI* component) could be characterised and used to improve the forecast accuracy as well as the forecast confidence interval. This was achieved by making use of forecast bias compensation and a Gridded Model Output Statistics method.

It was found that a specific focus on the weather conditions is called for in the energy model in the South African context as is an optimisation method capable of producing an optimal speed profile (in regular intervals) in contrast to the regularly employed average speed methods. These requirements are in answer to the frequently varying road conditions (hills and mountainous regions) as well as challenging weather conditions, especially near the coastal regions.

Research Question 2, and its sub-questions, was addressed in Chapter II (Literature Review) and Chapter V (Optimisation).

Chapter II reveals that many different kinds of deterministic as well as stochastic optimisation methods can be used to optimise the speed profile. However, no literature could be identified in regard to best practice for maximising distance travelled as in the case of the Sasol Solar Challenge. Chapter V showed that low computational intensity deterministic optimisation algorithms such as SQP and DP, are highly effective in solving the optimal speed profile and loop road quantities, respectively. The South African context requires a smart optimisation structure capable of using Cloud-Based information (with weather forecasts available on-the-fly) to increase the accuracy of the energy simulations. It was shown that a bi-level optimisation technique with a SQP structure for the upper-level and a DP structure for the lower-level was effective at optimising the energy as well as the driving distance of a solar electric vehicle competing in a Sasol Solar Challenge. The bi-level optimisation technique also displayed satisfactory performance in terms of its computational ability.

Research Question 3, and its sub-questions, was addressed in Chapter II (Literature Review), Chapter III (Modelling), Chapter IV (Environmental Conditions), Chapter V (Optimisation) and Chapter VI (Case Study Results).

The early chapters of this work identified the critical vehicle and environmental conditions to be considered when robust and accurate optimisation is required. Unfortunately, no existing optimisation applications could be used for comparison as none currently exist that provide both the optimal speed profile as well as the optimal loop quantities for a Sasol Solar Challenge event. Performance metrics were used throughout this work to analyse and quantify the amount of error in the model simulations, weather forecasts and optimisation outputs (optimal speed profiles and loop road quantities).

This work has further shown how the optimisation technique could be used in near real-time to provide accurate and robust updates in regard to optimal driving speeds and strategies for maximising distance travelled.

## **SIGNIFICANCE OF THE FINDINGS**

The significance and implications of the findings in this work culminated in the SCIII team from TUT obtaining a never-before-achieved 1<sup>st</sup> place among local solar car teams and a 4<sup>th</sup> place overall at the SSC2018 international event. The key to their achievements and exceptional performance was in having an optimal speed profile as well as having access to the optimal loop road sections for each day.

Firstly, the scientific contributions of this work have resulted in four internationally recognised peer-reviewed published papers (as mentioned in Chapter I). Another outcome is a re-usable optimisation environment suitable for the SSC context to be used by future solar car teams from TUT.

Finally, the most significant contribution of this work is the presentation of a novel application of a bi-level optimisation technique. This technique is able to simultaneously optimise solar car energy usage as well as make recommendations regarding the optimal number of loop road sections to be driven each day. This is done by creating an optimal speed profile, which will maximise the total distance covered (variable distance). The application mentioned above has not as yet been formalised elsewhere at the time of this work.

## **FUTURE WORK AND RECOMMENDATIONS**

Although the mathematical energy model of the solar car proved able to provide an accurate and robust representation of the actual energy consumed while driving, refining the energy model will improve its accuracy even further:

- a) How can the aerodynamic lift and cross-winds be included in the energy model? What would be the performance benefit of including these variables in the energy model?
- b) What would the benefit be of incorporating a dynamic model of the Li-Ion battery to represent the physical phenomena occurring in the battery's cells through an equivalent electrical circuit? How would this addition of a battery model significantly affect the estimation of the *SoC*?
- c) Can exploiting phenomena such as Wake Energy Retrieval (vehicles travelling in the slipstream of another vehicle) improve energy predictions?

The coefficient of drag (a constant) and the coefficient of rolling resistance (a function) are currently being determined through extensive simulation and traditional experiments. Other techniques for finding these values also exist:

- a) How can machine learning be used to find the coefficients by only making use of recorded vehicle data? Or, how can these coefficients be found by means of an optimisation routine?

In this work, it was established that it is essential to statistically enhance the weather forecast to a specific application for improved performance. The impact on the accuracy, performance and computation time of characterising the statistical variability of all the weather variables used in the optimisation technique is of importance for future work:

- a) By what degree will statistically enhancing all weather forecast variables improve the overall performance similar to the *GHI* component in this work?
- b) How can the simulation confidence interval become more realistic by making use of all the weather variables to construct the interval bounds?

The optimisation technique expounded in this work provides adequate computational performance (measured in execution time); however, full real-time simulation updates will be advantageous to the energy manager of a solar racing team:

- a) What techniques can be used to further increase the computational efficiency of the proposed optimisation technique without making use of higher performance computer hardware?
- b) What computational improvement can be achieved by decreasing the resolution of the variables (vectors and matrices) used in the energy model? What is the break-even point between reducing the energy model variable resolution and gaining computation performance when considering its effect on the output accuracy of the simulations?



## LIST OF REFERENCES

- [1] D. Carrejo and J. Marshall, "What is mathematical modelling? Exploring prospective teachers' use of experiments to connect mathematics to the study of motion," *Mathematics Education Research Journal*, vol. 19, 06/01 2007, doi: 10.1007/BF03217449.
- [2] M. Wolfram and L. Liedewij, "Physical and Mathematical Modeling in Experimental Papers," *Elsevier Cell* 163, pp. 1577 - 1583, 2015.
- [3] X. Wu, D. Freese, A. Cabrera, and W. A. Kitch, "Electric vehicles' energy consumption measurement and estimation," *Transportation Research Part D: Transport and Environment*, vol. 34, pp. 52-67, 2015/01/01/ 2015, doi: <https://doi.org/10.1016/j.trd.2014.10.007>.
- [4] A. Damiano, C. Musio, and I. Marongiu, "Experimental validation of a dynamic energy model of a battery electric vehicle," in *2015 International Conference on Renewable Energy Research and Applications (ICRERA)*, 22-25 Nov. 2015 2015, pp. 803-808, doi: 10.1109/ICRERA.2015.7418523.
- [5] H. Aouzellag, H. Abdellaoui, K. Iffouzar, and K. Ghedamsi, "Model-based energy management strategy for hybrid electric vehicle," in *2015 4th International Conference on Electrical Engineering (ICEE)*, University of Boumerdes, 13-15 Dec. 2015 2015, pp. 1-6, doi: 10.1109/INTEE.2015.7416604.
- [6] S. Jakkidi, "Design of a solar car strategy using multi-objective optimization," University of Missouri, 2002.
- [7] K. Reeves, A. Montazeri, and C. J. Taylor, "Model development and energy management control for hybrid electric race vehicles," in *2016 UKACC 11th International Conference on Control (CONTROL)*, 31 Aug.-2 Sept. 2016 2016, pp. 1-6, doi: 10.1109/CONTROL.2016.7737651.
- [8] S. Schoeman and J. Carroll, "A combined energy system model for solar racers," in *AFRICON 2013*, South Africa, 2013, pp. 1-5, doi: 10.1109/AFRCON.2013.6757600.
- [9] Q. Yan, B. Zhang, and M. Kezunovic, "Optimization of electric vehicle movement for efficient energy consumption," in *2014 North American Power Symposium (NAPS)*, 7-9 Sept. 2014 2014, pp. 1-6, doi: 10.1109/NAPS.2014.6965467.

- [10] D. S. K. Sarrafan, K. M. Muttaqi & G. Town, "Accurate range estimation for an electric vehicle including changing environmental conditions and traction system efficiency," *IET Electrical Systems in Transportation*, vol. 7, no. 2, pp. 117-124, 2017.
- [11] M. W. Levin, M. Duell, and S. T. Waller, "Effect of Road Grade on Networkwide Vehicle Energy Consumption and Ecorouting," *Transportation Research Record*, vol. 2427, no. 1, pp. 26-33, 2014/01/01 2014, doi: 10.3141/2427-03.
- [12] N. H. T. S. Administration, "NHTSA Tire Fuel Efficiency Consumer Information Program Development: Phase 2 – Effects of Tire Rolling Resistance Levels on Traction, Treadwear, and Vehicle Fuel Economy," 2009.
- [13] B. Wiegand, "Estimation of the Rolling Resistance of Tires," *SAE Technical Paper 2016-01-0445*, 2016, doi: 10.4271/2016-01-0445.
- [14] I. Preda, D. Covaciu, and G. Ciolan, *Coast Down Test – Theoretical and Experimental Approach*. Transilvania University of Brasov, Romania, 2010.
- [15] C. Oosthuizen, B. v. Wyk, and Y. Hamam, "Modelling and simulation of the South African designed Sun Chaser II solar vehicle," in *2017 IEEE AFRICON*, 18-20 Sept. 2017 2017, pp. 1149-1154, doi: 10.1109/AFRCON.2017.8095644.
- [16] L. G. Anderson, "Rolling Resistance Modelling," PhD, Department of Science, Systems and Models,, Roskilde University, Denmark, 2015.
- [17] A. Suyabodha, "A Relationship between Tyre Pressure and Rolling Resistance Force under Different Vehicle Speed " presented at the ICMAA 2017, Malacca, Malaysia, 2017.
- [18] V. Sirenko and U. Rohatgi, "Methods of Reducing Vehicle Aerodynamic Drag," in *ASME 2012 Summer Heat Transfer Conference*, Puerto Rico, USA, 07/08 2012, doi: 10.1115/FEDSM2012-72491.
- [19] O. Isvan, "Wind speed, wind yaw and the aerodynamic drag acting on a bicycle and rider," *Journal of Science and Cycling; Vol 4, No 1 (2015)*, 06/29/ 2015. [Online]. Available: <http://www.jsc-journal.com/ojs/index.php?journal=JSC&page=article&op=view&path%5B%5D=168>.
- [20] T. Lajos, "Basics of vehicle aerodynamics," ed, 2002.
- [21] S. Fareeq, "AERODYNAMIC EVALUATION OF RACING WINGS OF A FORMULA CAR," University of Herdfordshire, United Kingdom, 2015.

- [22] J. Colman *et al.*, "Lift and drag coefficients behaviour at low Reynolds number in an airfoil with Gurney flap submitted to a turbulent flow: Part 1," *Latin American Applied Research As. – Argentina*, vol. 38, pp. 195-200, 07/01 2008.
- [23] G. Doig and C. Beves, "Aerodynamic design and development of the Sunswift IV solar racing car," *International Journal of Vehicle Design*, vol. 66, p. 143, 01/01 2014, doi: 10.1504/IJVD.2014.064550.
- [24] M. Anderson, "Churning losses and efficiency in gearboxes," Licentiate of Engineering in Machine Design, Department of Machine Design, KTH Royal Institute of Technology, SWEDEN, 2014.
- [25] C. Schlegel, A. Hosl, and S. Diel, "Detailed Loss Modelling of Vehicle Gearboxes," in *Proceedings 7th Modelica Conference*, Italy, 2009.
- [26] A. Irimescu, L. Mihon, and G. Pădure, "Automotive transmission efficiency measurement using a chassis dynamometer," *International Journal of Automotive Technology*, vol. 12, pp. 555-559, 08/01 2011, doi: 10.1007/s12239-011-0065-1.
- [27] B. O. S. Varga, A.; Mariasiu, F., "Prediction of Electric Vehicle Range: A Comprehensive Review of Current Issues and Challenges," *Energies*, vol. 12, no. 5, p. 946, 2019.
- [28] R. MILLIGAN, "CRITICAL EVALUATION OF THE BATTERY ELECTRIC VEHICLE FOR SUSTAINABLE MOBILITY," DOCTOR of PHILOSOPHY, School of Engineering and the Built Environment, Edinburgh Napier University, Edinburgh, 2016.
- [29] M. N. Hashemnia and B. Asaei, "Comparative study of using different electric motors in the electric vehicles," in *2008 18th International Conference on Electrical Machines*, Portugal, 2008, pp. 1-5, doi: 10.1109/ICELMACH.2008.4800157.
- [30] T. Rudnicki, R. Czerwinski, D. Polok, and A. Sikora, "Performance analysis of a PMSM drive with torque and speed control," in *2015 MIXDES - 22nd International Conference "Mixed Design of Integrated Circuits & Systems"*, Poland, 2015, pp. 562-566, doi: 10.1109/MIXDES.2015.7208586.
- [31] D. Suyambazhahan, "Experimental Study of Regenerative brakes System used in an Automobile Engine," in *38th National Conference on Fluid Mechanics and Fluid Power*, Bhopal, 2011.

- [32] S. Mandal, M. R. I. Sarker, M. S. Rahman, and M. Beg, "An analysis of braking energy regeneration in electric vehicles," *International Journal of Renewable Energy Research*, vol. 7, 03/26 2017.
- [33] G. Wager, J. Whale, and T. Braunl, "Performance evaluation of regenerative braking systems," *Proceedings of the Institution of Mechanical Engineers, Part D: Journal of Automobile Engineering*, p. 095440701772865, 11/17 2017, doi: 10.1177/0954407017728651.
- [34] W. Chanpeng and P. Hachanont, "Design of Efficient In-Wheel Motor for Electric Vehicles," *Energy Procedia*, vol. 56, pp. 525-531, 2014/01/01/ 2014, doi: <https://doi.org/10.1016/j.egypro.2014.07.188>.
- [35] T. A. Huynh and M. F. Hsieh, "Performance Analysis of Permanent Magnet Motors for Electric Vehicles (EV) Traction Considering Driving Cycles," *Energies*, vol. 11, p. 1385, 2018.
- [36] L. Shiyong, T. Lemley, and G. Keohane, "A COMPARISON STUDY OF THE COMMUTATION METHODS FOR THE THREE-PHASE PERMANENT MAGNET BRUSHLESS DC MOTOR," in *Electrical Manufacturing Technical Conference 2009: Electrical Manufacturing and Coil Winding Expo*, Nashville, TN, United States, 2009, pp. 49-55.
- [37] U. S. D. o. Energy, "DETERMINING ELECTRIC MOTOR LOAD AND EFFICIENCY," United States of America, 1997.
- [38] A. Doyle and T. Muneer, "Energy consumption and modelling of the climate control system in the electric vehicle," *Energy Exploration & Exploitation*, vol. 37, no. 1, pp. 519-543, 2019/01/01 2018, doi: 10.1177/0144598718806458.
- [39] T. Huybrechts, Y. Vanommeslaeghe, D. Blontrock, G. Van Barel, and P. Hellinckx, *Automatic Reverse Engineering of CAN Bus Data Using Machine Learning Techniques*. 2018, pp. 751-761.
- [40] Y. Miao, P. Hynan, A. Jouanne, and A. Yokochi, "Current Li-Ion Battery Technologies in Electric Vehicles and Opportunities for Advancements," *Energies*, vol. 12, no. 1074, 2019.
- [41] C. Iclodean, B. Varga, N. Burnete, D. Cimerdean, and B. Jurchiș, "Comparison of Different Battery Types for Electric Vehicles," *IOP Conference Series: Materials Science and Engineering*, vol. 252, p. 012058, 10/01 2017, doi: 10.1088/1757-899X/252/1/012058.

- [42] A. Nyman, I. Semko, and H. Ekstrom, "Modeling the Lithium-Ion Battery," 2013.
- [43] A. Blakers, N. Zin, K. R. McIntosh, and K. Fong, "High Efficiency Silicon Solar Cells," *Energy Procedia*, vol. 33, pp. 1-10, 2013/01/01/ 2013, doi: <https://doi.org/10.1016/j.egypro.2013.05.033>.
- [44] J. Luceno-Sanchez, A. Diez-Pascual, and R. Capilla, "Materials for Photovoltaics: State of Art and Recent Developments," *International Journal of Molecular Sciences*, vol. 20, no. 976, 2019.
- [45] E. Trottemant, "Nuna II Breaks All Records to Win the World Solar Challenge!," in *ESTEC*, ed. Netherlands: Education Office, 2003.
- [46] M. Lybech, "Modelling of the Variation of Air Density with Altitude through Pressure, Humidity and Temperature," EMD International A/S, Denmark, 2005.
- [47] L. Massidda and M. Marrocu, "Quantile Regression Post-Processing of Weather Forecast for Short-Term Solar Power Probabilistic Forecasting," *Energies*, vol. 11, 2018.
- [48] T. Mahachi, "Energy yield analysis and evaluation of solar irradiance models for a utility scale solar PV plant in South Africa," Thesis: MEng (E & E), Department of Electrical and Electronic Engineering, University of Stellenbosch, South Africa, 2016.
- [49] D. Matuszko, "Influence of the extent and genera of cloud cover on solar radiation intensity," *International Journal of Climatology*, vol. 32, pp. 2403-2414, 12/01 2012, doi: 10.1002/joc.2432.
- [50] H. Sangrody, M. Sarailoo, N. Zhou, N. Tran, M. Motalleb, and E. Foruzan, "Weather forecasting error in solar energy forecasting," *IET Renewable Power Generation*, vol. 11, no. 10, pp. 1274-1280, 2017, doi: 10.1049/iet-rpg.2016.1043.
- [51] S. Warren, R. Eastman, and C. Hahn, "A Survey of Changes in Cloud Cover and Cloud Types over Land from Surface Observations, 1971 96," *Journal of Climate - J CLIMATE*, vol. 20, 02/01 2007, doi: 10.1175/JCLI4031.1.
- [52] K. Waluś and Z. Olszewski, "Analysis Of Tire-road Contact Under Winter Conditions," *Proceedings of the World Congress on Engineering 2011, WCE 2011*, vol. 3, pp. 2381-2384, 07/01 2011.
- [53] N. G. Zacharof and G. Fontaras, "Review of in use factors affecting the fuel consumption and CO2 emissions of passenger cars," European Union, 2016.

- [54] R. Thitipatanapong and T. Luangnarutai, "Effects of A Vehicle's Driver Behavior to The Fuel Economy," in *International Conference on Automotive Engineering*, Bangkok, 2011.
- [55] K. L. Chan *et al.*, "Evaluation of ECMWF-IFS (version 41R1) operational model forecasts of aerosol transport by using ceilometer network measurements," *Geosci. Model Dev.*, vol. 11, no. 9, pp. 3807-3831, 2018, doi: 10.5194/gmd-11-3807-2018.
- [56] G. White, F. Yang, and V. Tallapragda, "The Development and Success of NCEP's Global Forecast System," National Oceanic and Atmospheric Administration, USA, 2018.
- [57] V. Radar. "Top Meteorology Companies." <https://www.ventureradar.com/keyword/Meteorology> (accessed 4 September, 2019).
- [58] A. Agüera-Pérez, J. C. Palomares-Salas, J. J. González de la Rosa, and O. Florencias-Oliveros, "Weather forecasts for microgrid energy management: Review, discussion and recommendations," *Applied Energy*, vol. 228, pp. 265-278, 2018/10/15 2018, doi: <https://doi.org/10.1016/j.apenergy.2018.06.087>.
- [59] P. Mathiesen and J. Kleissl, "EVALUATION OF NUMERICAL WEATHER PREDICTION FOR SOLAR FORECASTING," Department of Mechanical and Aerospace Engineering, University of California, California, 2012.
- [60] P. Pinson and R. Hagedorn, "Verification of the ECMWF ensemble forecasts of wind speed against observations," ECMWF, 2011, vol. 19.
- [61] E. ToolBox. "Air - Density, Specific Weight and Thermal Expansion Coefficient at Varying Temperature and Constant Pressures." [https://www.engineeringtoolbox.com/air-density-specific-weight-d\\_600.html?vA=30&units=C#](https://www.engineeringtoolbox.com/air-density-specific-weight-d_600.html?vA=30&units=C#) (accessed September, 2019).
- [62] A. Nespoli *et al.*, "Day-Ahead Photovoltaic Forecasting: A Comparison of the Most Effective Techniques," *Energies*, vol. 12, no. 9, p. 1621, 2019, doi: 10.3390/en12091621.
- [63] D. P. Ruth, B. Glahn, V. Dagostaro, and K. Gilbert, "The Performance of MOS in the Digital Age," *Weather and Forecasting*, vol. 24, no. 2, pp. 504-519, 2009, doi: 10.1175/2008waf2222158.1.

- [64] Y. Shin and C. Yi, "Statistical Downscaling of Urban-scale Air Temperatures Using an Analog Model Output Statistics Technique," *Atmosphere*, vol. 10, no. 8, p. 427, 2019, doi: 10.3390/atmos10080427.
- [65] A. v. Vuuren. "EXPLORE THE SASOL SOLAR CHALLENGE." <http://www.solarchallenge.org.za/solar-challenge/overview> (accessed.
- [66] P. Pudney and P. Howlett, "Critical Speed Control of a Solar Car," *Optimization and Engineering*, vol. 3, pp. 97–107, 2002, doi: <https://doi.org/10.1023/A:1020907101234>.
- [67] A. Scheidegger, "Energy Management Optimization for a Solar Vehicle," Masters, Ecole Polytechnique Federale De Lausanne, France, 2006.
- [68] Z. TAha, R. Passarella, and J. Sah, "A Review on Energy Management system of Solar Car," in *Proceedings of the 9th Asia Pasific Industrial Engineering & Management Systems Conference*, Bali, Indonesia, 2008.
- [69] E. Yesil, A. Onol, and A. Icke, "Strategy Optimization of a Solar Car for a Long-distance Race using Big Bang – Big Crunch Optimization," presented at the 14th IEEE International Symposium on Computational Intelligence and Informatics, 2013.
- [70] E. Guerrero Merino and M. A. Duarte-Mermoud, "Online energy management for a solar car using pseudospectral methods for optimal control," *Optimal Control Applications and Methods*, vol. 37, no. 3, pp. 537-555, 2016/05/01 2016, doi: 10.1002/oca.2210.
- [71] M. Elshafei, A. Al-Qutub, and A. A. Saif, "Solar car optimization for the World Solar Challenge," in *2016 13th International Multi-Conference on Systems, Signals & Devices (SSD)*, 21-24 March 2016 2016, pp. 751-756, doi: 10.1109/SSD.2016.7473675.
- [72] X. Shao *et al.*, "Solar irradiance forecasting by machine learning for solar car races," in *2016 IEEE International Conference on Big Data (Big Data)*, 5-8 Dec. 2016 2016, pp. 2209-2216, doi: 10.1109/BigData.2016.7840851.
- [73] M. Lv *et al.*, "Speed planning for solar-powered electric vehicles," presented at the Proceedings of the Seventh International Conference on Future Energy Systems - e-Energy '16, Canada, 2016.
- [74] S. Rohkämper, M. Hellwig, and W. Ritschel, "Energy optimization for electric vehicles using dynamic programming," in *2017 International Conference on*



- Research and Education in Mechatronics (REM)*, 14-15 Sept. 2017 2017, pp. 1-5, doi: 10.1109/REM.2017.8075252.
- [75] X. Wu, X. He, G. Yu, A. Harmandayan, and Y. Wang, "Energy-Optimal Speed Control for Electric Vehicles on Signalized Arterials," *IEEE Transactions on Intelligent Transportation Systems*, vol. 16, pp. 2786-2796, 04/29 2015, doi: 10.1109/TITS.2015.2422778.
- [76] A. Karlsson, "Cooling methods for electrical machines," Master Programme in Electrical Engineering, Electrical Engineering, UPPSALA UNIVERSITY, Sweden, 2014.
- [77] A. Razak, Y. M. Irwan, W. Z. Leow, M. Irwanto, I. Safwati, and M. Zhafarina, "Investigation of the Effect Temperature on Photovoltaic (PV) Panel Output Performance," *International Journal on Advanced Science, Engineering and Information Technology*, vol. 6, no. 5, 2016, doi: 10.18517/ijaseit.6.5.938.
- [78] T. W. Schlatter and D. V. Baker. "Notes on polynomial approximation by the NOAA/ERL/PROFS program office." <https://icoads.noaa.gov/software/other/profs> (accessed.
- [79] J. B. Brooks *et al.*, "SAURAN: A new resource for solar radiometric data in Southern Africa," *Journal of Energy in Southern Africa*, vol. 26, no. 1, February 2015 2015.
- [80] K. Das, "A Brief Review of Tests for Normality," *American Journal of Theoretical and Applied Statistics*, vol. 5, p. 5, 01/01 2016, doi: 10.11648/j.ajtas.20160501.12.
- [81] L. DeCarlo, "On the Meaning and Use of Kurtosis " *Psychological Methods*, vol. 2, no. 3, pp. 292-307, 1997.
- [82] P. G. Kosmopoulos, S. Kazadzis, K. Lagouvardos, V. Kotroni, and A. Bais, "Solar energy prediction and verification using operational model forecasts and ground-based solar measurements," *Energy*, vol. 93, pp. 1918-1930, 2015, doi: 10.1016/j.energy.2015.10.054.
- [83] C. Oosthuizen, B. Van Wyk, Y. Hamam, D. Desai, Y. Alayli, and R. Lot, "Solar Electric Vehicle Energy Optimization for the Sasol Solar Challenge 2018," *IEEE Access*, vol. 7, pp. 175143-175158, 2019, doi: 10.1109/access.2019.2957056.



- [84] S. Dempe, V. Kalashnikov, G. A. Pérez-Valdés, and N. Kalashnykova, *Bilevel Programming Problems: Theory, Algorithms and Applications to Energy Networks*. Berlin: Springer, 2015.
- [85] M. A. Erdogdu, L. Mackey, and O. Shamir, "Global Non-convex Optimization with Discretized Diffusions," in *32nd Conference on Neural Information Processing Systems (NeurIPS 2018)*, Montréal, Canada, 2018.
- [86] R. G. Jeroslow, "The polynomial hierarchy and a simple model for competitive analysis," *Mathematical Programming*, vol. 32, no. 2, pp. 146-164, 1985/06/01 1985, doi: 10.1007/BF01586088.
- [87] Mathworks. "Constrained Nonlinear Optimization Algorithms." <https://www.mathworks.com/help/optim/ug/constrained-nonlinear-optimization-algorithms.html#bsgqpl4> (accessed 2019).
- [88] R. E. Bellman, *Dynamic Programming*. Princeton: Princeton University Press, 2010.

## **ANNEXURE A: CODE VARIABLES**

# Annexure A

Variable name	Symbol	Function or description	Units	Resolution
<b>General</b>				
Time and date	-	Used by the weather forecast API and rest of UI	-	-
Start time of day	-	Used by the weather forecast API and rest of UI	-	-
Finish time of day	-	Used by the weather forecast API and rest of UI	-	-
<b>Mathematical energy model</b>				
Coefficient of aerodynamic drag	$C_d$	Used by the energy model	-	-
Coefficient of rolling resistance	$C_r$	Used by the energy model	-	-
Car and driver mass	$m$	Used by the energy model	kg	-
Car frontal area	$A_{car}$	Used by the energy model	m <sup>2</sup>	-
Car wheel diameter	-	Used by the energy model	m	-
Solar array size	$A_{pv}$	Used by the energy model	m <sup>2</sup>	-
Sun to battery efficiency	$\eta_{elec}$	Used by the energy model	-	-
Battery capacity	$e_{cap}$	Used by the energy model	Wh	-
Air density	$\rho$	Used by the energy model	Kg/m <sup>3</sup>	-
Electric motor efficiency	$\eta_{motor}$	Polynomial function, used by the energy model	-	-
<b>Route information</b>				
Distance 1	-	Distance matrix containing day route distances up to the mandatory 30 minute stop	m	50m
Distance loop	-	Distance matrix for the loop road of that day	m	50m

## Annexure A

Distance 3	-	Distance matrix containing day route distances from the mandatory 30 minute stop to the terminus of that day	m	50m
Latitude/Longitude 1	-	Lat/Lon matrix containing day route location information up to the mandatory 30 minute stop	DMM for North and East	50m
Latitude/Longitude loop	-	Lat/Lon matrix for the loop road of that day	DMM for North and East	50m
Latitude/Longitude 1	-	Lat/Lon matrix containing day route location information from the mandatory 30 minute stop to the terminus of that day	DMM for North and East	50m
Elevation 1	-	Elevation matrix containing day route elevations up to the mandatory 30 minute stop	m	50m
Elevation loop	-	Elevation matrix for the loop road of that day	m	50m
Elevation 3	-	Elevation matrix containing day route elevations from the mandatory 30 minute stop to the terminus of that day	m	50m
Bearing or heading 1	-	Bearing matrix containing day route bearings up to the mandatory 30 minute stop	compass directions, 0° to 359°	50m
Bearing or heading loop	-	Bearing matrix for the loop road of that day	compass directions, 0° to 359°	50m
Bearing or heading 3	-	Bearing matrix containing day route Calculation from the mandatory 30 minute	compass directions, 0° to 359°	50m

## Annexure A

		stop to the terminus of that day		
Current GPS location	-	Current GPS location measured by mobile weather station	Lat/Lon	5m
<b>Route weather</b>				
Solar irradiance	<i>GHI</i>	Requested via the Meteomatics AG API	w/m <sup>2</sup>	15 minutes
Wind to N	-	Requested via the Meteomatics AG API	m/s	15 minutes
Wind to E	-	Requested via the Meteomatics AG API	m/s	15 minutes
Total Cloud Cover	<i>TCC</i>	Requested via the Meteomatics AG API	%	15 minutes
Temperature: dew point	-	Requested via the Meteomatics AG API	°C	15 minutes
Temperature: surface air	-	Requested via the Meteomatics AG API	°C	15 minutes
Air pressure	-	Requested via the Meteomatics AG API	hPa	15 minutes
Rain probability	-	Requested via the Meteomatics AG API	%	15 minutes
Rain amount	-	Requested via the Meteomatics AG API	mm	15 minutes

## **ANNEXURE B: CODE SPECIFICATIONS**

## **MATLAB®**

During the development of the code for this research work, the following MATLAB® toolboxes were utilised.

- a. communication\_toolbox
- b. curve\_fitting\_toolbox
- c. optimization\_toolbox
- d. signal\_blocks
- e. signal\_toolbox
- f. statistics\_toolbox

## **Code length and variables used**

- a. Main UI (I, II & III): ≈450 memory locations & ≈3000 MATLAB® lines of code
- b. Lower-level: ≈80 memory locations & ≈250 MATLAB® lines of code
- c. Upper-level: ≈200 memory locations & ≈600 MATLAB® lines of code
- d. Weather API: ≈40 memory locations & ≈150 MATLAB® lines of code

## **Computation time specifications**

For reference purposes, the laptop used to execute the code en-route had the following specifications: HP ZBook 15u G3 (Intel Core i7-6500U), 16 GB DDR4 with 256 SSD, AMD FirePro W4190M (2GB GDDR5) GPU, Windows 10 Enterprise (x64).

- a. Full computation of all eight days: ≈1200 seconds
- b. Computation of one day: average ≈150 seconds